1976

Atomic and Molecular Rydberg States: a Correlative Approach.

Hung-tai Wang
Louisiana State University and Agricultural & Mechanical College

ATOMIC AND MOLECULAR RYDBERG STATES: A CORRELATIVE APPROACH

A Dissertation

Submitted to the Graduate Faculty of the
Louisiana State University and
Agricultural and Mechanical College
in partial fulfillment of the
requirements for the degree of
Doctor of Philosophy

in

The Department of Chemistry

by
Hung-tai Wang
B.S., Tunghai University, Taiwan, 1969
August 1976

DEDICATION

To my wife and my parents

ACKNOWLEDGEMENTS

The author wishes to express his sincere appreciation to Professor Séan P. McGlynn for his guidance and inspiration during the course of this investigation. He also wishes to express his gratitude to Professors J. Callaway and A. R. P. Rau for their advice and helpful discussions. He is very grateful to present and past members of Professor McGlynn's Research Group: Dr. Petr Hochmann, Dr. Walter S. Felps, Dr. Klaus Wittle, Dr. John D. Scott, Mrs. Anne Wahlborg, Mr. Thomas P. Carsey, Mr. David Dougherty, Mr. Swapan Chattopadhyay and Mr. Gary L. Findley for their assistance and suggestions to this work.

Financial assistance pertinent to the preparation of this dissertation from the "Dr. Charles E. Coates Memorial Fund of Louisiana State University Foundation donated by George H. Coates", is gratefully acknowledged. Research was supported by the U. S. Energy Research and Development Administration -- Division of Biomedical and Environmental Research -- Physics and Technological Program.

Finally, the author wishes to thank Mrs. Martha Prather for the efficient typing of the manuscript.

TABLE OF CONTENTS

LIST OF TABLES

TABLE Page

CHAPTER ONE

LIST OF FIGURES

CHAPTER FOUR

ABSTRACT

A correlative approach to atomic and molecular Rydberg states has been formulated. This approach is based on effective quantum number regularities. The usual interpretation of the effective quantum number n* (i.e., as the difference between an aufbau principal quantum number n and the quantum defect u) has been abandoned in order to extend the definition of n* into the realm of valence- and inner-shell orbitals.

Characteristic differences of n* are capable of describing the general behavior of atomic energy levels in the form of an "average atom" and of measuring the deviation from hydrogen-like behavior. The precursor concept, isoelectronic sequences and fine structures have been investigated in the context of n*.

For molecules, differences of n* provide a foundation for studies of substituent effects, chemical shifts, and valence-shell splittings. Regularities in n* have been observed for the Rydberg states, but only when the degree of bonding and molecular geometry is taken into consideration.

The series behavior of atomic and molecular Rydberg states contains information about non-hydrogenic potentials, particularly their sign and relative range of effectiveness.

Assignments for CH_3I, HI and H_2O are presented in order to exemplify the correlative attitude. Reported data on monocarbonyls and albylethylenes have been used in order to demonstrate the validity of n* correlations. The lowest-energy Rydberg states of H_2, transbutadiene and benzene are discussed using the criterion of n* differences.

Suggestions for future work for atoms and molecules are discussed.

INTRODUCTION

The elucidation of the electronic structure of atoms and molecules is essential to the understanding of their chemical and physical properties. The classification of atomic and molecular spectra provides the foundation for this enterprise. For example, the periodic table was initially constructed on the basis of the chemical properties of the atoms. However, it was quantum mechanics combined with spectroscopy which provided the detailed knowledge of shell structures and which finally rationalized periodic behavior.

Most studies in atomic spectroscopy have centered on rather isolated topics (e.g., some particular atoms of interest; several configurations of a specific atom; or even some levels of a certain configuration). Such studies, while providing important and very detailed information, forego any overview of the relatedness among atoms in regard to either columnar or row behavior. Recently, however, there has been a renaissance[1-7] in such correlative studies, particularly with respect to row behavior, and some interesting shell-structure dependencies[1,2,5-7] have been observed. Unfortunately, this renewed interest did not extend to the columnar behavior of atoms within periodic groups. The columnar properties, pertaining as they do to chemically

similar atoms, are of particular interest to chemists: The results of such studies can easily be extended into the molecular domain.

Molecular spectroscopists usually group molecules into categories on the basis of their possession of "related chromophores". The "related chromophores" can be individual elements from some column of the periodic table or they can be polyatomic functionals. In fact, under certain conditions, the presence of a common chromophore in any group of molecules dictates spectral similarities: The individual electronic structures are merely slightly modified versions of that of the chromophore.

The columnar behavior of a periodic group, besides its usefulness to molecular spectroscopy, should also be of interest in itself: Correlations of this sort may well suggest a new model, one which might provide insight to the general understanding of atomic spectra. Finally, the extension of such schemes to the molecular situation should induce both theoretical advancement as well as simplify the empirical analysis of the electronic structures of complicated molecules.

It is the goal of this work to find pertinent atomic and molecular correlations and to rationalize them within a theoretical framework. Some applications of the molecular correlation algorithms serve both as a test of the correlative attitude itself and as the source of its

rationalization.

The plan of this dissertation is as follows:

-----The basic correlative attitude for atoms will be developed in Chapter One and the theoretical implications of the empirical observations will be discussed fully.

-----The second chapter will attempt the extension of the atomic results into the molecular realm. Definitions of "chromophore" and "substituent", and some empirical observations concerning them, will be provided. Deviations of the molecular behavior from that of the atomic case will be rationalized, in part anyway, on the basis of symmetry decrement and molecular geometry. The presence of potential terms with a higher-order dependency on the radial coordinate than that of the r^{-1} Coulomb attraction may also account for certain kinds of deviations.

-----Chapter Three consists of a collection of molecular data. The specific data for each different group of molecules will be discussed briefly. These data and discussions support the correlative attitude and, in addition, furnish some insight into the physical meaning of the results.

-----The fourth chapter offers a detailed analysis of the electronic spectrum of the water molecule. This study of the water molecule focuses on the typical difficulties one encounters while dealing with molecular cases. The distinction between valence and Rydberg states, the dependence of the nature of the various excited electronic

states on the molecular geometry, and the similarity between the water molecule and some related molecules are a few of the examples which will be elaborated.

-----The final chapter, the conclusion, consists of a summary of the existing work and an outline for future research.

REFERENCES

1. A. R. P. Rau and U. Fano, Phys. Rev. 167 (1968) 7.
2. S. T. Manson, Phys. Rev. 182 (1969) 97.
3. U. Fano and W. C. Martin, in "Topics in Modern Physics", edited by W. F. Britten and H. Odabasi, Colorado Associated U.P., Boulder, 1971, p. 147.
4. J. L. Dehmer, Phys. Rev. A 7 (1973) 4.
5. G. T. Condo, Phys. Rev. Lett. 33 (1974) 126.
6. J. L. Dehmer, M. Inokuti and R. P. Saxon, Phys. Rev. A 12 (1975) 102.
7. U. Fano, C. E. Theodosiou and J. L. Dehmer, Rev. Mod. Phys., to be published.

CHAPTER ONE

ATOMIC RYDBERG STATES

INTRODUCTION

Early in 1885, Balmer[1] discovered an equation which described the energies of the lines of the "Balmer series" of the hydrogen atom

$$\nu = R_H \left[\frac{1}{n_1^2} - \frac{1}{n_2^2} \right] \tag{1}$$

where n_1 and n_2 are positive integers with $n_2 > n_1$, where $n_1 = 2$, and where R_H is the hydrogen-atom version of the Rydberg constant. The Rydberg constant is

$$R = \frac{109737.31}{1 + \frac{m_e}{M}} \text{ cm}^{-1} \tag{2}$$

where m_e is the mass of an electron and M is the mass of the nucleus. Besides this regularity of energies, the intensities of the lines of the Balmer series were also observed to decrease regularly with increasing n_2, approaching a specific limit as $n_2 \to \infty$.

Later on, Rydberg[2] found that a similar equation was applicable to certain series of lines in the spectra of neutral Al, Na, K, Tl, etc. This equation is

$$\nu = \nu_\infty - \frac{R}{(n^*)^2} \tag{3}$$

with

$$n^* \equiv n-u$$

where ν_∞ is the energy of the series limit, n^* is the effective quantum number, n is the principal quantum number, and u is the quantum defect (which is roughly independent of n within a given series). It is now known that the Rydberg equation, Eq. 3, applies to the spectrum of virtually every element in the periodic table.

According to the Rydberg-Ritz combination principle,[3] the energy of any spectral line can be expressed as

$$\nu = T_i - T_j \quad (\text{in } cm^{-1}) \tag{4}$$

where T_i and T_j are the absolute binding energies of the spectroscopic terms i and j. If we choose T_i to be the term value of the ground state, Eq. (4) becomes

$$\nu = IP - T_j \tag{5}$$

where IP is the negative of the binding energy of the ground state, and T_j is the term value of the spectral line j. Providing that we write

$$T_j = \frac{R}{(n_j)^2} \tag{6}$$

Eq. (5) is seen to be the Rydberg formula of Eq. (3). Thus, we can frame the whole spectrum of energy terms of an atom into a network of series all of which have a zero of energy defined as that of the ground state, and all of which converge to specific limits which we define as the various ionization potentials.

For isoelectronic sequences of neutral atoms, the Rydberg formula is usually written as

$$\nu_j = IP - \frac{RQ^2}{(n_j^*)^2} \qquad (7)$$

where Q is the net charge on the core (e.g., Q=1 for a neutral atom). Eq. (7) is the most general form of the Rydberg formula.

The central problems of atomic spectroscopy can be supposed to evolve from the classification and identification of Rydberg series, although the Rydberg formula is primarily used only for empirical purposes.

The remarkable behavior of the quantum defect u has been rarely studied. Quantum defect theory[4-7] represents a notable exception to this situation. It links the quantum defect to the phase shift of scattering theory. Another attempt at utilization of the quantum defect led to the devisement[8] of "quantum defect orbitals".

We propose to investigate the entirety of the periodic table, with emphasis on columnar behavior. We will base our arguments on the Rydberg formula and we will emphasize the primacy of the effective quantum number, n^*. We will compare n^* with u in their abilities to correlate spectra of different atoms. At the same time, we will attempt to extend the realm of applicability of the Rydberg formula beyond its presently accepted confines. Our discussion will be empirical and phenomenological.

The lack of any theoretical-cum-computational effort is not dictated by choice but rather by the fact that our empirical results dictate an entirely new approach. To our knowledge, no existing theoretical model can provide a satisfactory rationalization of our results. We will offer some outlines for such a model, albeit very naive ones and, at the same time, we will try to use the existing theories to rationalize certain parts of our results.

I. BACKGROUND

The spectra of the neutral alkali metals constitute the simplest cases of Rydberg series. Their ground state configurations consist of a single s valence electron outside of a closed-shell core. It is possible to view this type of ground state as a "Rydberg state". The Rydberg formula Eq. (7) with Q = 1, can be written as

$$\nu_j = IP - \frac{R}{(n_j^*)^2}$$

$$= \frac{R}{(n_o^*)^2} - \frac{R}{(n_j^*)^2} \quad , \quad j = 1,2,3,... \tag{8}$$

where we treat the quantity IP as the term value of the ground state and then convert it into an effective quantum number n_o^*

$$IP \equiv T_o \equiv \frac{R}{(n_o^*)^2}$$

or

$$n_o^* \equiv \left(\frac{R}{T_o}\right)^{1/2} \tag{9}$$

The indices j and zero refer to the j'th Rydberg state and the zeroth Rydberg state (i.e., the ground state), respectively. This numbering convention for the ground

and Rydberg states is relative in that it disregards the inner-shell structure of the atom and simply labels the ground state as the zeroth state and the succeeding members of each Rydberg series, in terms of increasing energy as the first, second, third, etc. Rydberg member of that series. The current numbering convention is based on the aufbau principal quantum number n.

The effective quantum numbers n_j^* and n_o^* are related to their aufbau principal quantum number counterparts via the relations

$$n_j^* = n_j - u_j$$

$$n_o^* = n_o - u_o \tag{10}$$

where n_j and n_o are the aufbau principal quantum numbers of the j'th member of a certain Rydberg series and of the ground state, respectively; and u_j and u_o are the quantum defects of the j'th member and of the outermost s electron of the ground state, respectively. The Rydberg formula may now be written as

$$\nu_j = \frac{R}{(n_o - u_o)^2} - \frac{R}{(n_j - u_j)^2} \tag{11}$$

The major difference between Eq. (11) and Eq. (7) is that the ionization potential, IP, has been converted into n_o^*

where $n_o^* \equiv n_o - u_o$.

All columnar groups other than the alkali metal group are discussed within the context of the standard Rydberg formula

$$\nu_j = IP - \frac{R}{(n_j - u_j)^2} \tag{12}$$

where the quantity IP is retained and is not converted into $n_o^* = n_o - u_o$.

In either case, a Rydberg series comprises the transition energies, ν_j, which are expressed as the differences between T_o (or IP) and

$$T_j = \frac{R}{(n_j - u_j)^2} \tag{13}$$

where n_j suffers only integral increments and u_j is roughly constant. In the limit $n_j \to \infty$, $\nu_j \to T_o$ (or IP).

The quantum defect u_j is known to be weakly dependent on the transition energy (i.e., on n_j). It is also strongly dependent on the azimuthal quantum number, ℓ: Rydberg states with different ℓ values possess quite different quantum defects. Indeed, within any one specific configuration, say (core)$n_j\ell$, the different terms possess quite different quantum defects. Furthermore, the energy levels of each term possess different u_j's. In other words, the Rydberg formula in Eq. (12) pertains not only

to the various terms but also to the levels which result from each term (i.e., to the fine structure).

The magnitude of the quantum defect, u_j, is usually attributed to a "deviation from hydrogenic behavior". This deviation, in turn, can be attributed to many effects: penetration, exchange, polarization, etc. The net result of these effects is an n_j^* which is different from the hydrogenic n_j by the amount u_j.

The quantum defect u_j can also be connected with the phase shift[9]

$$\delta_j \equiv \pi u_j \tag{14}$$

where δ_j corresponds to the phase shift of the wave function of an electron which is scattered by a non-hydrogenic core and which eventually ends up in the j'th Rydberg state of the combined core/electron system. The phase of the wave function shifts from the hydrogenic value as the core becomes non-hydrogenic.

The magnitude of u_j as a function of ℓ is of considerable interest. It can be stated both theoretically[10] and empirically that larger ℓ values correspond to smaller u_j values and <u>vice versa</u>. Thus, s Rydberg states possess

the largest quantum defects, p Rydberg states have the next largest, and d,f, ... Rydberg states exhibit successively smaller u_j's. As an empirical fact, the quantum defects for d, f, g, ... Rydberg states are usually close to either zero or an integer. Their effective quantum numbers, in turn, are very similar to hydrogenic values (i.e., to integers). Rau and Fano[11] discovered that for high ℓ states, the centrifugal force, $\frac{\ell(\ell+1)}{r^2}$, can effectively block the electron from penetrating into the inner part of the core, thus creating a hydrogen-like situation.

It is also known[12] that cores with the same valence-shell configuration but different inner-shell structures exhibit phase shifts δ_j which increase by $\sim\pi$ as the number of inner shells increases by unity. Thus, within a column of the periodic table, the j'th member of a similarly-designated Rydberg series for successive elements in this column will have phase shifts δ_j $\sim(\delta_j+\pi), \sim(\delta_j+2\pi), \ldots$ In other words, the corresponding quantum defects will be u_j, $\sim(u_j+1)$, $\sim(u_j+2), \ldots$; and the aufbau principal quantum numbers will be n_j, n_j+1, n_j+2, ... Consequently, we find

$$\begin{aligned} n_j^* &= n_j - u_j \\ &\cong (n_j+1)-(u_j+1) \\ &\cong (n_j+2)-(u_j+2) \quad \text{etc.} \end{aligned} \tag{15}$$

Thus, for all elements of the same periodic group, the corresponding j'th Rydberg members will possess almost identical n_j^*'s even though their u_j's are quite different.

This approximate constancy of effective quantum numbers for corresponding Rydberg states of atoms in the same columnar periodic group has been a center of interest for some time.[10] Rau and Fano explained the constancy of d,f,...,etc. high ℓ Rydberg states in terms of the centrifugal barrier. For s and p Rydberg states, however, no interpretation is available. Our investigations will focus on effective quantum numbers and some attention will be devoted to this near-constancy.

II. THE EFFECTIVE QUANTUM NUMBER

Fano et al.[13] recently computed the quantum defects of s and p Rydberg series as functions of atomic number Z by utilizing the Herman-Skillman (HS) potential.[14] The quantum defects they obtained refer to zero binding energy; that is, they are asymptotic quantum defects and thus are not energy dependent. However, since the HS potential does not include any terms which could induce an LS splitting, the resulting quantum defects refer to s and p configurations and not to the spectroscopic terms. We denote these asymptotic values by $\bar{u}_s$ and $\bar{u}_p$, and convert them into the effective quantum numbers of the lowest s and p Rydberg states, $\bar{n}^*_{1s}$ and $\bar{n}^*_{1p}$, respectively, via the relationship

$$\bar{n}^*_{1s} = n_{1s} - \bar{u}_s$$

$$\bar{n}^*_{1p} = n_{1p} - \bar{u}_p \qquad (16)$$

The resulting values of $\bar{n}^*_{1s}$ and $\bar{n}^*_{1p}$ are plotted against Z in Figure 1. They exhibit distinct shell structures. The most striking feature of Figure 1 is the parallelism of the $\bar{n}^*_{1s}$ and $\bar{n}^*_{1p}$ plots: The difference between the two plots, in fact, is virtually constant throughout the whole periodic system. It is implied, therefore, that the

Figure 1. Effective quantum numbers $\bar{n}^*_{1p}$, $\bar{n}^*_{1s}$ and n^*_o are plotted against atomic number. $\bar{n}^*_{1p}$ and $\bar{n}^*_{1s}$ are calculated values from Fano et al.[13] n^*_o's are term centers obtained from Moore.[15]

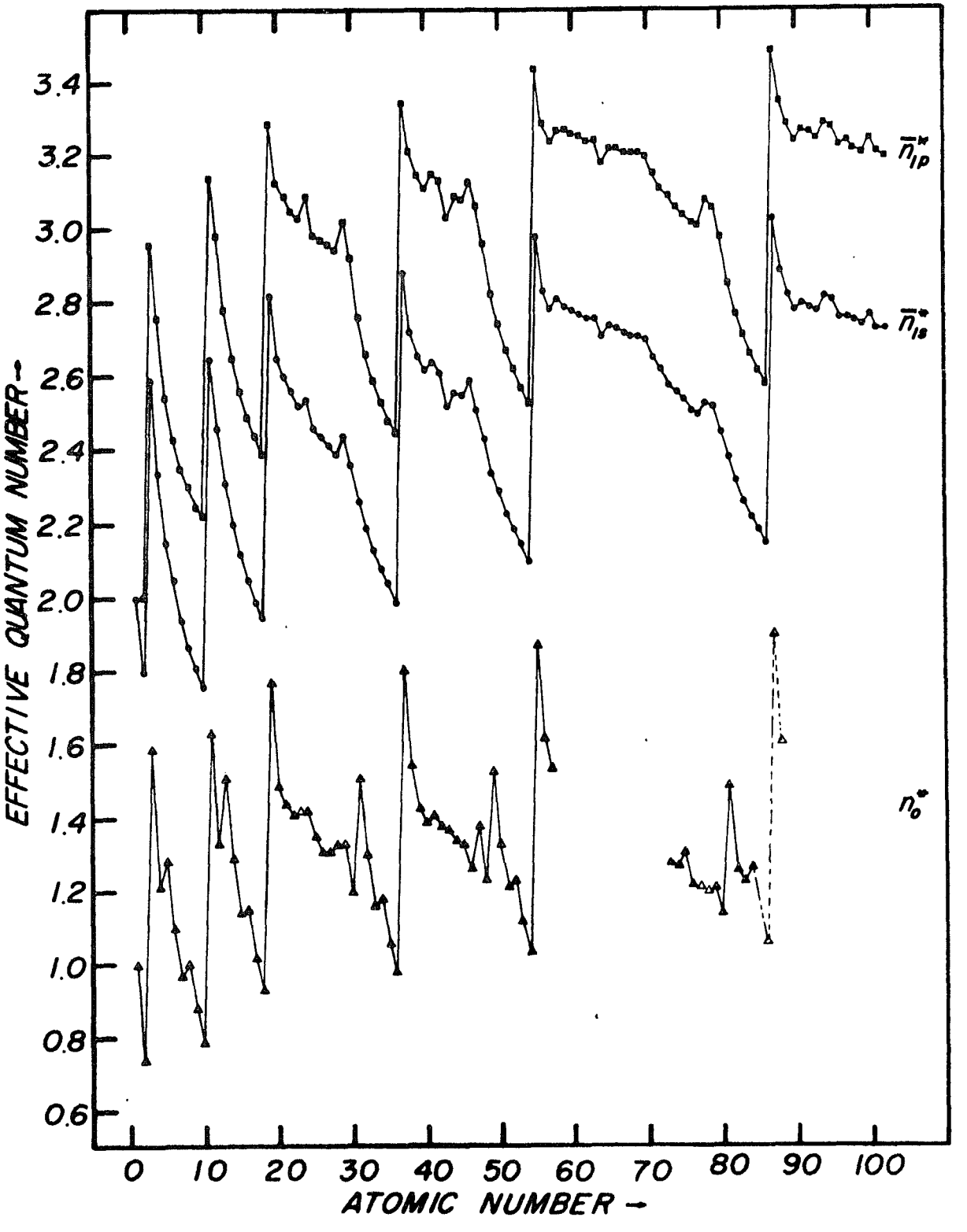
EFFECTIVE QUANTUM NUMBER →
3.4
3.2
3.0
2.8
2.6
2.4
2.2
2.0
1.8
1.6
1.4
1.2
1.0
0.8
0.6
0
10
20
30
40
50
60
70
80
90
100
ATOMIC NUMBER →
$\bar{n}^*_{1p}$
$\bar{n}^*_{1s}$
n^*_0

effective quantum numbers (or the quantum defects) of the s and p series are essentially identical except for a constant difference. For d, f, and higher ℓ Rydberg series, the presence of the centrifugal barrier tends to confine their effective quantum numbers to fixed ranges which exhibit only a slight spread about some integer value.

In Figure 1, we have also plotted n_o^* against Z. From Eq. (9), we have

$$n_o^* = \sqrt{\frac{R}{IP}} \tag{17}$$

where IP is the lowest ionization potential.[15] As noted earlier, we usually restrict such procedures to the alkali metals. If we do the same for other atoms, we run into certain difficulties in interpreting their corresponding u_o's. We will bypass this controversy for the moment and examine the n_o^* plot of Figure 1.

A. The Effective Quantum Number n_o^*

The plot of n_o^* in Figure 1 employs the ionization potential of the outermost valence electron of each atom regardless of the electron being s, p, d or f. On the other hand, the plots of $\bar{n}_{1s}^*$ and $\bar{n}_{1p}^*$ are for the s and p first Rydberg states, respectively. Nevertheless, for n_o^*'s of s and p valence orbitals, we can match corresponding

parts of the n_o^* curve to that of $\bar{n}_{1s}^*$ and $\bar{n}_{1p}^*$ when comparing them.

Except for some sub-shell structure, the n_o^* curve follows the general trend of $\bar{n}_{1s}^*$ and $\bar{n}_{1p}^*$ curves very closely. Specifically, the sudden rise after each closed-shell system and the subsequent drop toward the next closed-shell atom are very obvious. To emphasize this similarity, we have normalized the n_o^* values of the inert gases to zero and, hence, express n_o^* of subsequent s and p sub-shells as the increment relative to the subjacent inert gas value. The result is shown in Figure 2. The same procedure has been applied to $\bar{n}_{1s}^*$, the result is shown in Figure 3. The close resemblance between Figures 2 and 3 indicates that n_o^* is governed by factors similar to those which govern $\bar{n}_{1s}^*$ and, thus, $\bar{n}_{1p}^*$.

It is emphasized that the ionization potentials used in obtaining the n_o^* values are term energies, rather than the configuration energies used in the case of $\bar{n}_{1s}^*$ and $\bar{n}_{1p}^*$. This difference affects only some open-shell systems. The s sub-shell systems (i.e., the alkali metal and alkaline earths) and Group VIII (i.e., the inert gases) are not affected at all. For the other p sub-shell systems, the difference merely amounts to a smoothing of the plot between Groups III and VII, as evidenced by the dotted lines of Figure 2. It should be noted, in both Figures 2 and 3, that the second

row elements Al, Si, P, S and Cl have highly irregular n_o^* and $\bar{n}_{ls}^*$ values compared to the first, third, fourth and fifth row elements.

Several interesting results are evident in Figure 2. First, by gauging the closed-shell configurations to the same n_o^* basis, the whole array of s and p sub-shell elements constructed by adding extra electrons to the inert-gas cores are also normalized into a very similar pattern. With the major exception of the second row elements, all elements belonging to the same period group possess n_o^* values which are larger than those for the subjacent inert-gas by approximately the same amount. A similar situation exists in Figure 3 for the $\bar{n}_{ls}^*$ values. Second, the increase in n_o^* caused by placing one extra-valence s electron outside of the inert gas core is essentially the same for all alkali metals. The difference between n_o^* of an alkali metal and the subjacent inert gas is

$$dn_o^* = 0.835 \pm 0.008 \tag{18}$$

The same type of difference for $\bar{n}_{ls}^*$ is

$$d\bar{n}_{ls}^* = 0.87 \pm 0.04 \tag{19}$$

The near equality of dn_o^* and $d\bar{n}_{ls}^*$ is striking. This

Figure 2. n_o^* for Groups I, II, III, IV, V, VI and VII, expressed as increments from n_o^* of the subjacent inert gases, is plotted against its relative position with the subjacent inert gases. Dotted lines connect configuration centers for $n_o p^i$ with i = 1,2,3,4, and 5.

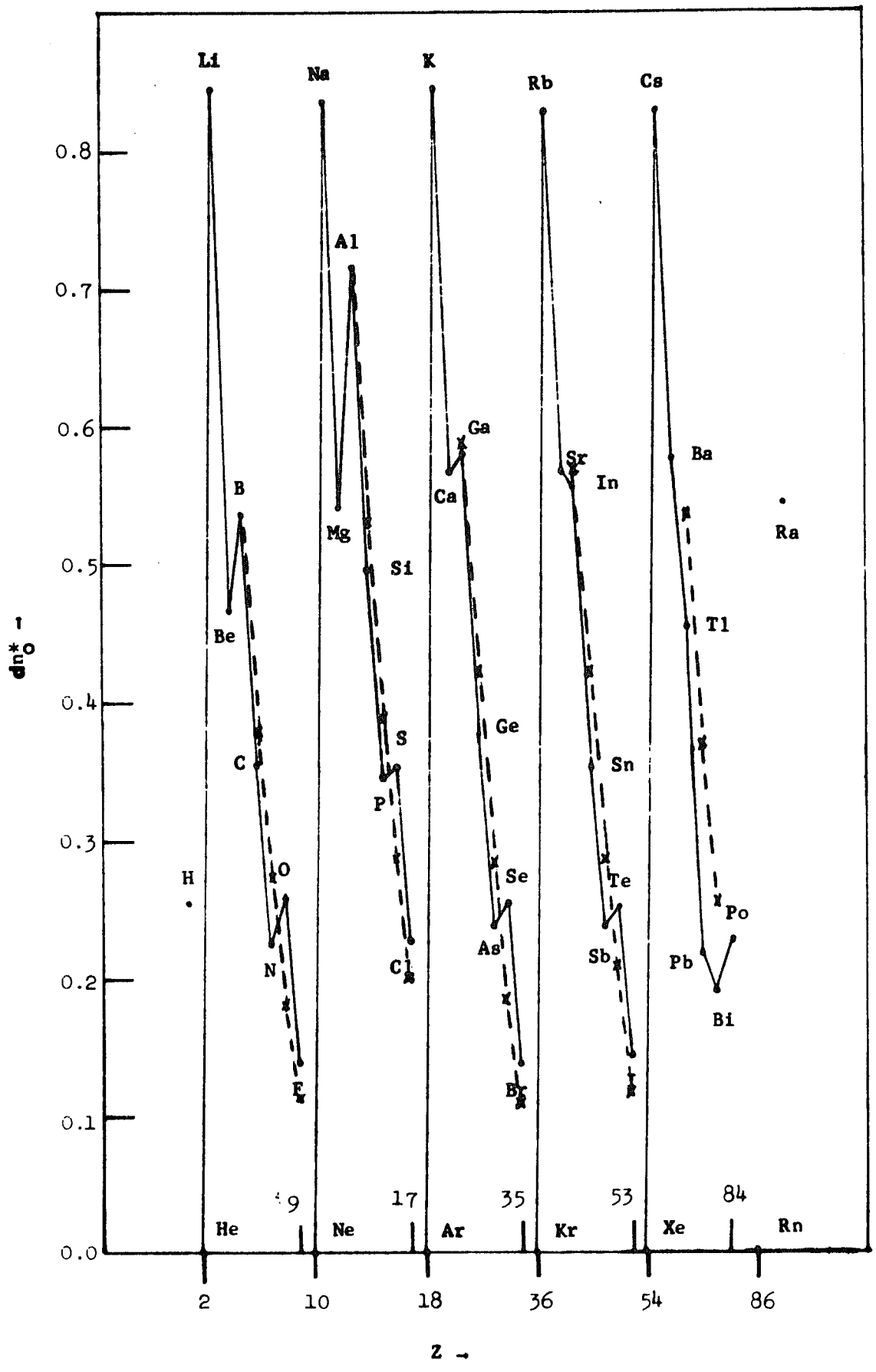
Li
Na
K
Rb
Cs
Al
Mg
Ga
Ca
Sr
In
Ba
Ra
B
Si
Be
Tl
S
Ge
C
Sn
P
Se
O
Te
H
Po
As
Sb
Pb
N
Cl
Bi
F
Br
He
Ne
Ar
Kr
Xe
Rn
0.0
0.1
0.2
0.3
0.4
0.5
0.6
0.7
0.8
2
10
18
36
54
86
9
17
35
53
84
Z →

Figure 3. $\bar{n}^*_{1s}$ for Groups I, II, III, IV, V, VI and VII, expressed as increments from $\bar{n}^*_{1s}$ of the subjacent inert gases, is plotted against its relative position with the subjacent inert gases.

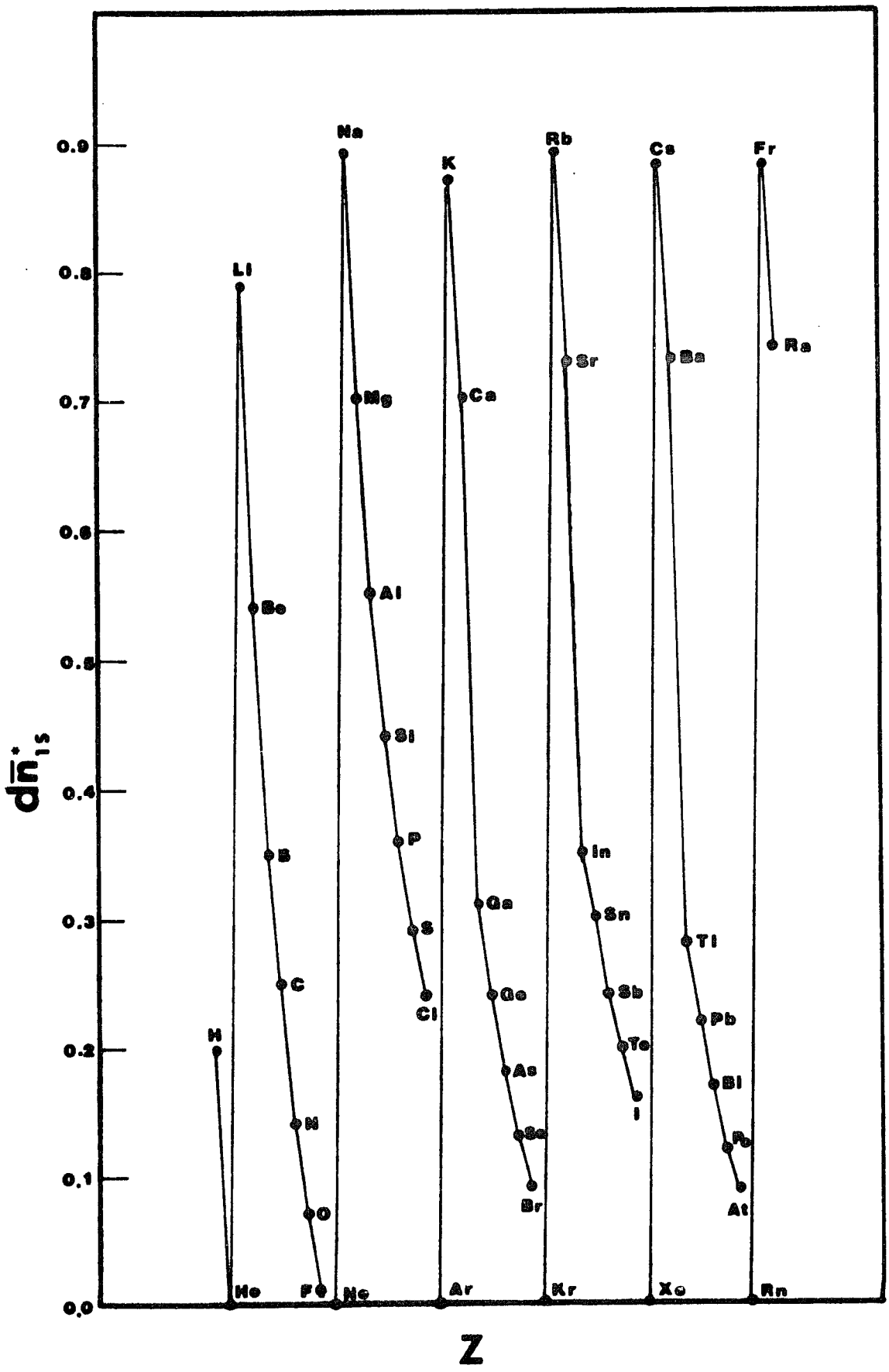
0.9
0.8
0.7
0.6
0.5
0.4
0.3
0.2
0.1
0.0
$d\bar{n}^{+}_{1s}$
Z
H
Li
Be
B
C
N
O
F
Ne
Na
Mg
Al
Si
P
S
Cl
Ar
K
Ca
Ga
Ge
As
Se
Br
Kr
Rb
Sr
In
Sn
Sb
Te
I
Xe
Cs
Ba
Tl
Pb
Bi
Po
At
Rn
Fr
Ra
He

observation has demonstrated that the meaning of the effective quantum number for both Rydberg and ground states are in some ways identical.

B. The Difference Between n_o^* and $\bar{n}_{1s}^*$, $\bar{n}_{1p}^*$

It has been established that dn_o^* between Groups I and VIII is constant at 0.835 even though the individual values of n_o^* cover a rather wide range. Specifically, consider the following n_o^* data:

Group I	Li	Na	K	Rb	Cs	spread
n_o^*	1.588	1.627	1.770	1.805	1.869	0.281
Group VIII	**He**	**Ne**	**Ar**	**Kr**	**Xe**	
n_o^*	0.744	0.794	0.927	0.978	1.041	0.297
dn_o^*	0.844	0.833	0.843	0.827	0.828	(20)

Since Group I differs from VIII in that the former has an extra s valence electron outside the closed-shell of the latter, the constancy of dn_o^* implies that differences in inner-shell structure do not influence dn_o^*. The ability to eliminate any dependency on the inner-shell structure differences is particularly valuable because it enables us

to concentrate on the characteristic columnar behavior.

The quantity $d\bar{n}^*_{1s}$, the value of which is ~0.87, can be considered in a similar way. The quantity $\bar{n}^*_{1s}$ for group I is the effective quantum number for the first excited s Rydberg state of group I while, for Group VIII, it is the effective quantum number for the first s Rydberg configuration obtained by exciting the outermost p electron into the nearest empty shell. For Group I, the core is closed-shell but, for Group VIII, it is open shell (i.e., p^5). Since the ground state of Group I elements is essentially a lowest-energy Rydberg state, the first excited s Rydberg state can be supposed to be the next member of the s series. Consequently, the difference between the effective quantum numbers, n^*_o and $\bar{n}^*_{1s}$, should be and is found to be ~1.00. This fact, combined with $dn^*_o = n^*_o$ (Group I) - n^*_o (Group VIII) = 0.835 and $d\bar{n}^*_{1s} = \bar{n}^*_{1s}$ (Group I) - $\bar{n}^*_{1s}$ (Group VIII) = 0.87, implies that $\bar{n}^*_{1s}$ (Group VIII) - n^*_o (Group VIII) $\cong$ 1.00. This finding is quite important: It supports the assertion that the ground state of any Group VIII element can be considered on the same footing as a "normal" Rydberg state. Thus, we can separate a quantum defect, u_o, from n^*_o just as we can a $\bar{u}_{1s}$ from $\bar{n}^*_{1s}$. If we follow the usual interpretation of quantum defect values and suppose that they constitute a measure of the deviation from hydrogen-like behavior caused by penetration, exchange, polarization, etc., the

concept of a u_o is difficult to accept. As a result, we choose n^*, instead of u, as the parameter to use in measuring the deviation from hydrogen-like behavior for "non-Rydberg" states.

The constancy of dn_o^* and $d\bar{n}_{1s}^*$ leads to the quantity Δn_{1s}^* which is defined as

$$\Delta n_{1s}^* \equiv n_{1s}^* - n_o^* \tag{21}$$

where n_{1s}^* and n_o^* refer to the same element. As noted above, for Group VIII, it is found that

$$\Delta \bar{n}_{1s}^* = \bar{n}_{1s}^* - n_o^* \cong 1.00 \ . \tag{22}$$

Keep in mind that the quantities $\bar{n}_{1s}^*$ are taken from Fano et al.[13] and these authors employed a model HS potential. As it turns out, these calculated values are systematically off from the experimental values by 0.1. This is shown numerically in the following:

	He	Ne	Ar	Kr	Xe	Rn
$\bar{n}^*_{1s}$ (Fano et al.)	1.80	1.76	1.95	1.99	2.10	2.15
n^*_{1s} (experimental)	1.74	1.69	1.86	1.91	1.99	--
$\Delta\bar{n}^*_{1s}$ (Fano et al.)	1.06	0.97	1.02	1.01	1.06	1.09
Δn^*_{1s} (experimental)	1.00	0.90	0.93	0.93	0.95	--

The experimental n^*_{1s} quantity is obtained by using the energy independent u_s at high n and the definition

$$n^*_{1s} \equiv n_{1s} - u_s \ . \tag{23}$$

We use this extrapolated n^*_{1s} rather than the authentic value simply because $\bar{n}^*_{1s}$ was obtained similarly.[13] The average Δn^*_{1s} is ~0.94 for He, Ne, Ar, Kr and Xe, and ~0.93 if He is excluded.

The constancy of Δn^*_{1s} exists not only for the configurations shown above but also for individual terms. Furthermore, Δn^*_{2s}, Δn^*_{3s} ,..., Δn^*_{js}, etc., which we define as

$$\begin{aligned} \Delta n^*_{2s} &= (n_{2s} - u_{2s}) - n^*_o \\ \Delta n^*_{3s} &= (n_{3s} - u_{3s}) - n^*_o \\ &\vdots \\ \Delta n^*_{js} &= (n_{js} - u_{js}) - n^*_o \end{aligned} \tag{24}$$

will differ from each other by near-integers since u_{2s}, u_{3s},..., u_{js} are essentially identical. These facts are exemplified in Figures 4 and 5. We define

$$\Delta n^*_{js} = m + \Delta n^*_s \tag{25}$$

where Δn^*_s is modulo 1 or the decimal part of Δn^*_{js} and m is the integer part of Δn^*_{js}. Similarly, we can use the same label m to designate the n^*_{js} which corresponds to Δn^*_{js} in Eq. (25).

Figure 4 shows the results for the s Rydberg series

$$n_o p^6,\ {}^1S_o \rightarrow n_o p^5\ n_j s[3/2]^o,\ J = 2\ ;\ \text{core}\ {}^2P^o_{1\frac{1}{2}} \tag{26}$$

of the inert gases. [We employ the jℓ-coupling notation of Racah (see Ref. 15)]. The plot for n^*_{js} dramatizes the characteristic behavior exhibited by Δn^*_{js}. While n^*_{js} covers a range of ~0.3, Δn^*_{js} exhibits a spread of only ~0.03. Figure 5 is the enlarged version of Δn^*_{js} for another Rydberg series of s terms which happens to be slightly perturbed.

The behavioral characteristics of Δn^*_{js} for both configurations and terms deserves further attention. It is the quantity Δn^*_{js} which we choose to displace the quantum defect as a measure of deviations from hydrogenic behavior. Since we intend to discuss fine

Figure 4. n^*_{js} and Δn^*_{js} are plotted against index m [see Eq. (25) in text] for the $n_o p^6 \rightarrow n_o p^5\ n_j s\,[\frac{3}{2}]^o$, J=2; core($^2P^o_{3/2}$) transition of Ne, Ar, Kr and Xe. The jℓ-coupling notation by Racah is employed here.[15]

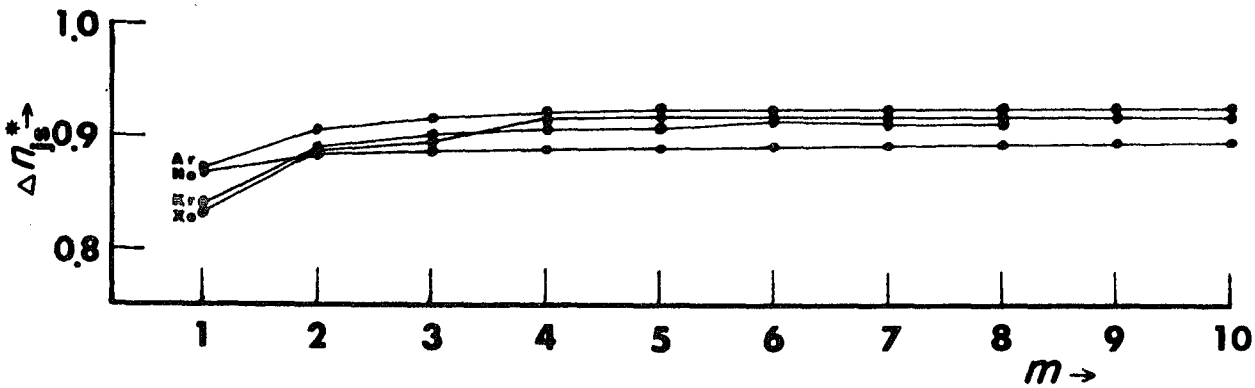
1.0
0.9
0.8
$\Delta\eta^{*\uparrow}_{jm}$
Ar
Ne
Kr
Xe
1
2
3
4
5
6
7
8
9
10
m →

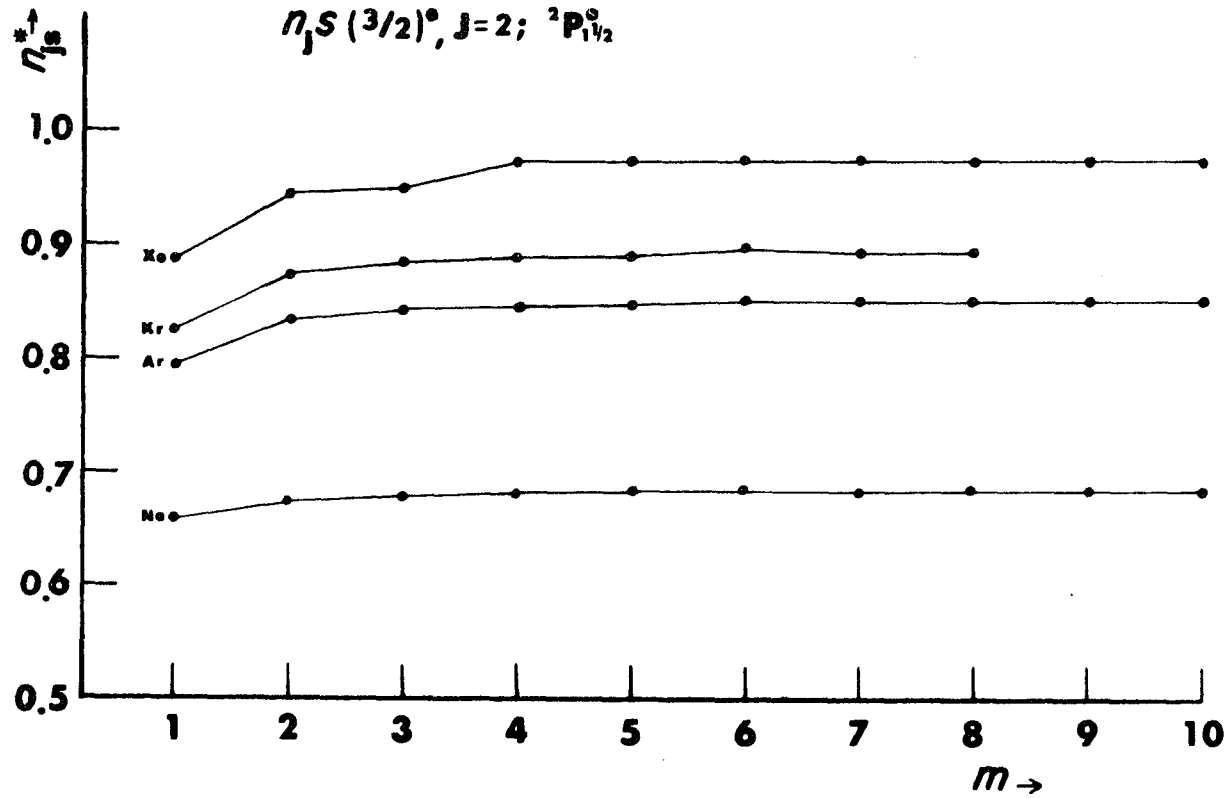
$\eta^{*\uparrow}_{jm}$
$\eta_j S\,(3/2)^\circ$, J = 2; $^2P^\circ_{1\frac{1}{2}}$
1.0
0.9
0.8
0.7
0.6
0.5
Xe
Kr
Ar
Ne
1
2
3
4
5
6
7
8
9
10
m →

Figure 5. Plot of Δn^*_{js} vs. m similar to Figure 4 (see figure caption of Figure 4). The n^*_{ls} values are for the transition of Ne, Ar, Kr and Xe: $n_o p^6 \rightarrow n_o p^5\ n_j s[\frac{3}{2}]^o$, J=1; core($^2P^o_{3/2}$) , which arises from the same term as the transition shown in Figure 4.

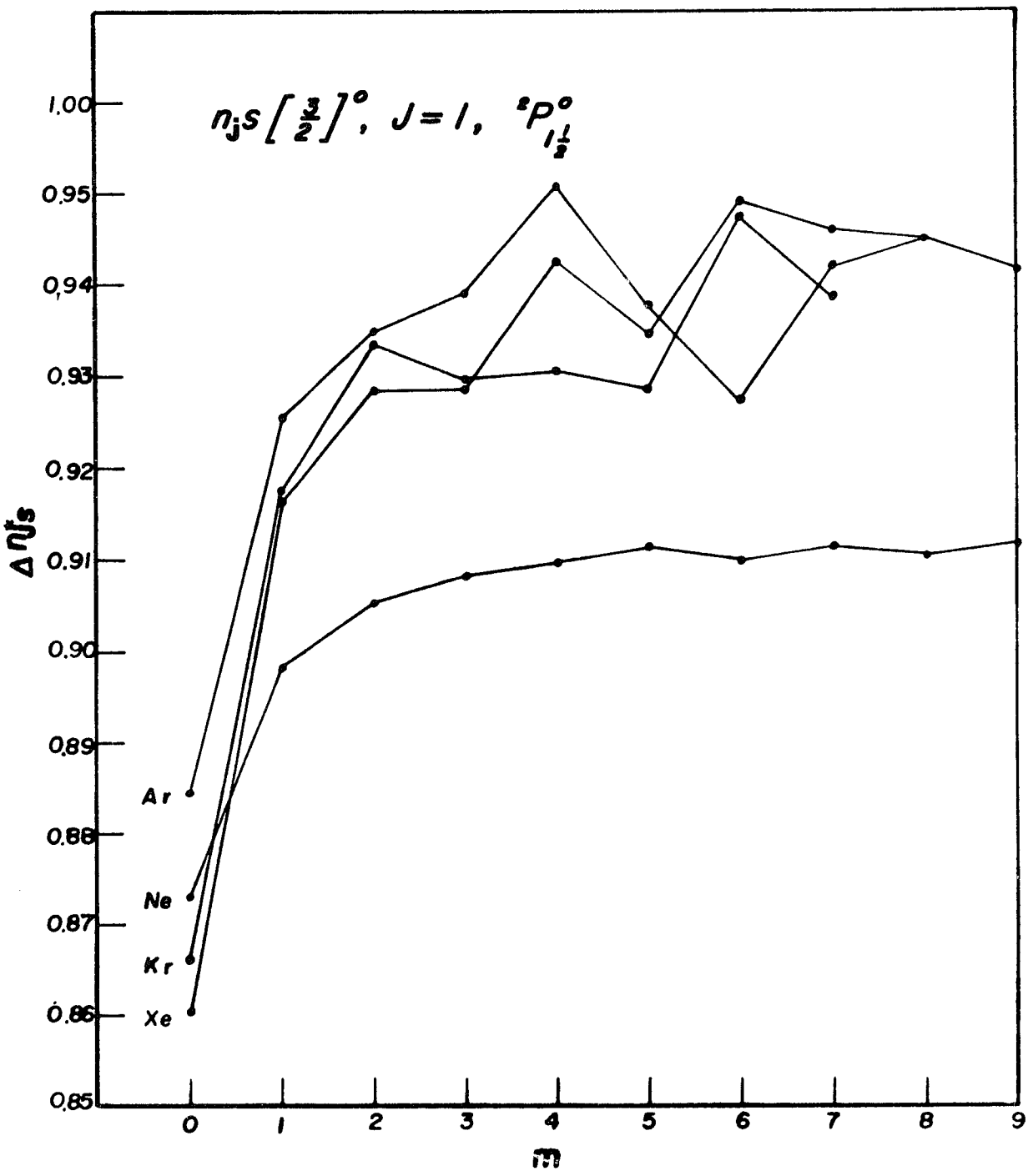
$n_j s\left[\frac{3}{2}\right]^o$, $J=1$, $^2P^o_{1\frac{1}{2}}$
1.00
0.95
0.94
0.93
0.92
0.91
0.90
0.89
0.88
0.87
0.86
0.85
$\Delta n_j s$
Ar
Ne
Kr
Xe
0
1
2
3
4
5
6
7
8
9
m

structure in a later section, we confine ourselves, for the remainder of this section, to considerations of configurations.

The parallelism between $\bar{n}^*_{1s}$ and $\bar{n}^*_{1p}$ of Figure 1 suggests that $\Delta\bar{n}^*_{1p}$, like $\Delta\bar{n}^*_{1s}$, should also be a constant for atoms from the same periodic group. Indeed, close inspection of Figure 1 discloses that $\Delta\bar{n}^*_{1s}$ and $\Delta\bar{n}^*_{1p}$ are effective constants for each periodic group but that they do differ from group to group. Thus, from the observation of the constancy of dn^*_o and $d\bar{n}^*_{1s}$, we have deduced similar results for $\Delta\bar{n}^*_{1s}$ and $\Delta\bar{n}^*_{1p}$. The ability of the latter to describe deviations from hydrogen-like behavior will be elaborated in Section III. However, we do wish to emphasize that the use of the calculated $\bar{n}^*_{1s}$ and $\bar{n}^*_{1p}$ quantities or the experimental n^*_{1s} and n^*_{1p} quantities makes little difference insofar as general trends are concerned since the former differ systematically from the latter by ~0.1. Therefore, we will no longer differentiate them notationally unless such be absolutely necessary.

The characteristic columnar behavior of the effective quantum numbers and their differences should be important both theoretically and experimentally. As will be demonstrated later, this finding has far-reaching implications for both atomic and molecular spectrocopy.

In the meantime, the results concerning dn^*_o and dn^*_{1s} prompts us to investigate inner-shell levels.

C. The Effective Quantum Numbers for Inner-Shell Levels

Once we remove the constraint which restricts the concept of an effective quantum number to Rydberg states, we can intrude into the inner-shell domain. This intrusion is implied by the manner in which we have defined n_o^* for the group VIII elements. The fact that $dn_o^* \simeq dn_{1s}^*$ [see Eqs. (18) and (19)] and that Δn_{1s}^* is constant for the inert-gases prompts the following question: Since Δn_{1s}^* for the inert gases represents the difference between the $n_o p^6$ ground state and the $n_o p^5 n_1 s$ configuration, can we infer a similar difference between n_{-1p}^* and n_{os}^* for the alkali metals if n_{-1p}^* refers to that p sub-shell of the closed-shell core which is subjacent to the valence $n_o s$ sub-shell? The answer is contained in the following data:

	Na	K	Rb	Cs	Spread
n_{os}^*	1.65	1.82	1.87	1.94	0.29
n_{-1p}^*	0.66	0.87	0.97	1.05	0.39
Δn_{-1p}^*	0.99	0.95	0.90	0.89	0.10

The quantity n_{os}^* is the extrapolated experimental value which utilizes the asymptotic u_s and [see Eq. (23)] and

$$n_{os}^* \equiv n_o - u_s \ . \tag{27}$$

The n^*_{-1p} values are obtained from ionization potential data.[16] The constancy of

$$\Delta n^*_{-1p} = n^*_{os} - n^*_{-1p} , \tag{28}$$

although not as good as in Group VIII, is quite evident. The average value of Δn^*_{-1p} for the alkali metals is ~0.93, which is identical to that for the inert gases [i.e., ~0.93 (excluding He)]. This congruence encourages us to examine inner-shell effective quantum numbers in their entirety. Before doing so, however, it is necessary to define a nomenclature for extra-, infra- and intra valence-shell terms. We choose the valence shell as the standard and refer all the extra and infra-shell terms to the principal quantum number n_o of the valence shell. The reason for this will become evident later. Consider the example of Kr with the ground state configuration:

$$\text{K: } 1s^2 2s^2 2p^6 3s^2 3p^6 4s^2 3d^{10} 4p^6$$

Since the valence shell is the $4p^6$ sub-shell, we denote 4p by $n_o p$ and its effective quantum number by n^*_{op}. Then, for example, we find

$$
\begin{aligned}
3d &\rightarrow n_{-1}d \quad \text{and} \quad n^{*}_{-1d} \\
3p &\rightarrow n_{-1}p \quad \text{and} \quad n^{*}_{-1p} \\
2p &\rightarrow n_{-2}p \quad \text{and} \quad n^{*}_{-2p} \\
4s &\rightarrow n_{o}s \quad \text{and} \quad n^{*}_{os} \\
1s &\rightarrow n_{3}s \quad \text{and} \quad n^{*}_{-3s}
\end{aligned} \tag{29}
$$

Conversely, for Rydberg states, we find

$$
\begin{aligned}
4d &\rightarrow n_{o}d \quad \text{and} \quad n^{*}_{od} \\
5d &\rightarrow n_{1}d \quad \text{and} \quad n^{*}_{1d} \\
5p &\rightarrow n_{1}p \quad \text{and} \quad n^{*}_{1p} \\
5s &\rightarrow n_{1}s \quad \text{and} \quad n^{*}_{1s} \\
6d &\rightarrow n_{2}d \quad \text{and} \quad n^{*}_{2d} \\
6p &\rightarrow n_{2}p \quad \text{and} \quad n^{*}_{2p} \\
6s &\rightarrow n_{2}s \quad \text{and} \quad n^{*}_{2s} \\
&\text{etc.}
\end{aligned} \tag{30}
$$

The differences between effective quantum numbers are now redefined only between orbitals of the same ℓ; i.e.,

$$
\Delta n^{*}_{j\ell} = |n^{*}_{j\ell} - n^{*}_{o\ell}| \quad , \quad j = \pm 1, \pm 2, \ldots \tag{31}
$$

The differences between two effective quantum numbers, neither of which is n_o^*, are expressed as follows: The difference between n_{-1}s and n_{-2}s is simply written as

$$n^*_{-1s} - n^*_{-2s} \cdot \tag{32}$$

It should also be mentioned that the distinction between s, p, d, ... for any one shell will be dropped when it is the whole shell rather than some specific sub-shell of it which is of interest. That is, we write n_o, $n_{\pm 1}$, $n_{\pm 2}$,... for such cases.

The inner-shell n^*'s are defined in the same manner as those for both valence and Rydberg states, namely as

$$n_j^* \equiv \sqrt{\frac{RQ^2}{IP_j}}$$

where IP_j is the j'th inner-shell ionization potential. In other words, we define inner-shell binding energies as

$$T_j \equiv IP_j = \frac{RQ^2}{(n_j^*)^2} \tag{33}$$

instead of the usual

$$T_j \equiv \frac{R(Z-\sigma)^2}{n_j^2} \tag{34}$$

where Z is the atomic number, σ is a screening constant and n_j is the principal quantum number.[10] This disregard of normal practices is justified by the data and the discussion which follows. Equation (33) for inner-shell orbitals has been proposed by Mulliken.[18] While indicating the possibility of using the inner-shell n^* as an index to Rydberg series, he regarded such n^*'s as having only a formal significance.

The inner-shell ionization potentials are taken from Siegbahn et al.[16,17] and the valence-shell and Rydberg state data are taken from Moore.[15] The results for Groups I, II, III, VII and VIII are given in Table 1 to 5. We assign He to Group II because it does not possess a p inner-shell as do the other inert gases.

There are several points of interest in Tables 1 to 5. The n^* of the valence shell terms is roughly constant for each element of a given periodic group: The total spread is less than 1 even though n_o changes considerably. Specifically, the spreads of n_o^* for Groups I, II, III, VII and VIII are 0.869, 0.861, 0.298, 0.450 and 0.318 while the corresponding changes in n_o are 5, 6, 4, 4 and 4. Furthermore, n_o^* varies between ~0.8 to ~1.9, whereas n_o varies between 1 and 7. This constancy, as mentioned earlier, has been a subject of concern for a long time. The n^*'s for the extra-shell, or Rydberg, terms increase from n_o^* by nearly integral steps, as is implied by the Rydberg formula. For inner-shell

TABLE 1A

Effective Quantum Numbers for Alkali Metals[a,b]

Atom	1s	2s	3s	4s	5s	6s	7s	
H	1.000	(2.000)	(3.000)					
Li	0.497	1.588	(2.596)	(3.598)				
Na	0.113	0.465	1.627	(2.643)	(3.647)			
K	0.061	0.190	0.633	1.770	(2.801)	(3.810)		
Rb	0.030	0.082	0.206	0.673	1.805	(2.845)	(3.856)	
Cs	0.019	0.049	0.106	0.243	0.769	1.869	(2.920)	(3.934)
Fr	0.012	0.027	0.054[d]	0.109[d]	0.241[d]	0.633[d]	--[c]	--[c]

Atom	2p	3p	4p	5p	6p	7p	8p
H	(2.000)	(3.000)	(4.000)				
Li	(1.959)	(2.956)	(3.954)				
Na	0.662	(2.117)	(3.133)	(4.138)			
K	0.215	0.869	(2.234)	(3.265)	(4.275)		
Rb	0.086	0.237	0.974	(2.290)	(3.325)	(4.340)	
Cs	0.052	0.115	0.287	1.050	(2.350)	(3.395)	(4.410)
Fr	0.029	0.060[d]	0.126	0.301[d]	0.952[d]	--[c]	--[c]

a) All values refer to configuration centers. Orbitals are assigned by aufbau numbering.
b) Underlined values refer to outermost sub-shell of valence electrons.[15] Numbers in parentheses refer to Rydberg states.[15,16] Unmarked values refer to inner-shell orbitals.
c) Unreported.
d) Interpolated values from Ref. 16.

TABLE 1B

Effective Quantum Numbers for Alkali Metals[a,b]

Atom	n^*_{-6s}	n^*_{-5s}	n^*_{-4s}	n^*_{-3s}	n^*_{-2s}	n^*_{-1s}	n^*_{0s}	n^*_{1s}	n^*_{2s}
H							1.000	(2.000)	(3.000)
Li						0.497	1.588	(2.596)	(3.598)
Na					0.113	0.465	1.627	(2.643)	(3.647)
K				0.061	0.190	0.633	1.770	(2.801)	(3.810)
Rb			0.030	0.082	0.206	0.673	1.805	(2.845)	(3.856)
Cs		0.019	0.049	0.106	0.243	0.769	1.869	(2.920)	(3.934)
Fr	0.012	0.027	0.054	0.109	0.241	0.633	--	--	--

Atom		n^*_{-5p}	n^*_{-4p}	n^*_{-3p}	n^*_{-2p}	n^*_{-1p}	n^*_{0p}	n^*_{1p}	n^*_{2p}
H								(2.000)	(3.000)
Li							(1.959)	(2.956)	(3.954)
Na						0.662	(2.117)	(3.133)	(4.138)
K					0.215	0.869	(2.234)	(3.265)	(4.275)
Rb				0.086	0.237	0.974	(2.290)	(3.325)	(4.340)
Cs			0.052	0.115	0.287	1.050	(2.350)	(3.395)	(4.410)
Fr		0.029	0.060	0.126	0.301	0.952	--	--	--

a) For nomenclature of effective quantum numbers, see text.
b) For other symbols, see footnotes to Table 1A.

TABLE 2A

Effective Quantum Numbers for Alkaline Earths[a,b]

Atom	1s	2s	3s	4s	5s	6s	7s	8s
He	0.744	(1.726)	(2.735)					
Be	0.350	1.208	(2.210)					
Mg	0.102	0.391	1.334	(2.348)				
Ca	0.058	0.176	0.556	1.492	(2.517)			
Sr	0.029	0.078	0.195	0.598	1.546	(2.579)		
Ba	0.019	0.048	0.103	0.232	0.583	1.616	(2.673)	
Ra	0.011	0.027	0.053[d]	0.106[d]	0.231	0.556	1.605	----[c]

Atom	2p	3p	4p	5p	6p	7p
He	(1.955)	(2.953)				
Be	(1.511)					
Mg	0.512	(1.734)				
Ca	0.198	0.723	(1.853)			
Sr	0.083	0.224	0.825	(1.930)		
Ba	0.050	0.112	0.273	0.937	(1.990)	
Ra	0.029	0.059	0.121	0.287	0.846	(2.060)

a), b), c), d), see footnotes to Table 1A

TABLE 2B

Effective Quantum Numbers for Alkaline Earths[a]

Atom	n^*_{-6s}	n^*_{-5s}	n^*_{-4s}	n^*_{-3s}	n^*_{-2s}	n^*_{-1s}	n^*_{0s}	n^*_{1s}
He							0.744	(1.726)
Be						0.350	1.208	(2.210)
Mg					0.102	0.391	1.334	(2.348)
Ca				0.058	0.176	0.556	1.492	(2.517)
Sr			0.029	0.078	0.195	0.598	1.546	(2.579)
Ba		0.019	0.048	0.103	0.232	0.583	1.616	(2.673)
Ra	0.011	0.027	0.053	0.106	0.231	0.556	1.605	--

Atom	n^*_{-5p}	n^*_{-4p}	n^*_{-3p}	n^*_{-2p}	n^*_{-1p}	n^*_{0p}	n^*_{1p}
He							(1.955)
Be						(1.511)	(2.615)
Mg					0.512	(1.734)	(2.857)
Ca				0.198	0.723	(1.853)	(3.094)
Sr			0.083	0.224	0.825	(1.930)	(3.029)
Ba		0.050	0.112	0.273	0.937	(1.990)	(3.200)
Ra	0.029	0.059	0.121	0.287	0.846	(2.060)	(3.217)

a) For symbols and nomenclature, see footnote to Table 1B.

TABLE 3A

Effective Quantum Numbers for Group III Elements[a,b]

Atom	1s	2s	3s	4s	5s	6s	7s	8s
B	0.269	--[c]	(2.020)	(3.034)				
Al	0.093	0.340	--	(2.188)	(3.219)			
Ga	0.036	0.102	0.293	--	(2.157)	(3.188)		
In	0.022	0.057	0.128	0.334	--	(2.219)	(3.253)	
Tl	0.013	0.030	0.061	0.127	0.315	--	(2.195)	(3.230)

Atom	2p	3p	4p	5p	6p	7p	8p
B	1.280	--					
Al	0.431	1.509	(2.670)				
Ga	0.110	0.362	1.515	(2.681)			
In	0.060	0.142	0.420	1.558	(2.736)		
Tl	0.032	0.067	0.146	0.407	1.578	(2.757)	

a), b), c), d), see footnotes to Table 1A.

TABLE 3B

Effective Quantum Numbers for Group III Elements[a]

Atom	n^*_{-5s}	n^*_{-4s}	n^*_{-3s}	n^*_{-2s}	n^*_{-1s}	n^*_{0s}	n^*_{1s}	n^*_{2s}
B					0.269	--	(2.020)	(3.034)
Al				0.093	0.340	--	(2.188)	(3.219)
Ga			0.036	0.102	0.293	--	(2.157)	(3.188)
In		0.022	0.057	0.128	0.334	--	(2.219)	(3.253)
Tl	0.013	0.030	0.061	0.127	0.315	--	(2.195)	(3.230)

Atom		n^*_{-4p}	n^*_{-3p}	n^*_{-2p}	n^*_{-1p}	n^*_{0p}	n^*_{1p}
B						1.280	--
Al					0.431	1.509	(2.670)
Ga				0.110	0.362	1.515	(2.681)
In			0.060	0.142	0.420	1.558	(2.736)
Tl		0.032	0.067	0.146	0.407	1.578	(2.757)

a) For symbols and nomenclature, see footnotes to Table 1B.

TABLE 4A

Effective Quantum Numbers for Halogens[a,b]

Atom	1s	2s	3s	4s	5s	6s	7s
F	0.141	0.663	(1.710)				
Cl	0.069	0.224	0.869	(1.832)			
Br	0.032	0.087	0.230	0.710	(1.826)		
I	0.020	0.051	0.113	0.270	0.986	(1.843)	
At	0.012	0.028	0.056[d]	0.114[d]	0.264[d]	0.869[d]	--[c]

Atom	2p	3p	4p	5p	6p	7p
F	0.854	(2.168)				
Cl	0.260	0.996	(2.286)			
Br	0.093	0.272	1.051	(2.343)		
I	0.054	0.124	0.333	1.102	(2.420)	
At	0.030	0.062	0.132	0.332[d]	1.304[d]	--

a), b), c), d), see footnotes to Table 1A

TABLE 4B

Effective Quantum Numbers for Halogens[a]

Atom	n^*_{-5s}	n^*_{-4s}	n^*_{-3s}	n^*_{-2s}	n^*_{-1s}	n^*_{0s}	n^*_{1s}
F					0.141	0.663	(1.710)
Cl				0.069	0.224	0.869	(1.832)
Br			0.032	0.087	0.230	0.710	(1.826)
I		0.020	0.051	0.113	0.270	0.986	(1.843)
At	0.012	0.028	0.056	0.114	0.264	0.869	--

Atom	n^*_{-4p}	n^*_{-3p}	n^*_{-2p}	n^*_{-1p}	n^*_{0p}	n^*_{1p}
F					0.854	(2.168)
Cl				0.260	0.996	(2.286)
Br			0.093	0.272	1.051	(2.343)
I		0.054	0.124	0.333	1.102	(2.420)
At	0.030	0.062	0.132	0.332	1.304	

a) For symbols and nomenclature, see footnotes to Table 1B.

TABLE 5A

Effective Quantum Numbers for Inert Gases[a,b]

Atom	1s	2s	3s	4s	5s	6s	7s	8s
Ne	0.124	0.530[e]	(0.666)	(2.683)				
Ar	0.065	0.204	0.682[e]	(1.807)	(2.842)			
Kr	0.031	0.084	0.216[d]	0.703[e]	(1.835)	(2.886)		
Xe	0.020	0.050	0.109[d]	0.253[d]	0.763[e]	(1.889)	(2.955)	
Rn	0.012	0.027	0.055[d]	0.111[d]	0.252[d]	0.723[d]	(1.872)	--[c]

Atom	2p	3p	4p	5p	6p	7p	8p
Ne	0.794	(2.138)	(3.157)				
Ar	0.234	0.927	(2.267)	(3.300)			
Kr	0.090	0.250	0.978	(2.319)	(3.358)		
Xe	0.053	0.119	0.304	1.041	(2.343)	--[c]	
Rn	0.030	0.060	0.129	0.312[d]	1.112	(2.410)	--[c]

a), b), c), d), See footnotes to Table 1A.

e) These values are taken from Ref. 17.

TABLE 5B

Effective Quantum Numbers for Inert Gases[a]

Atom	n^*_{-5s}	n^*_{-4s}	n^*_{-3s}	n^*_{-2s}	n^*_{-1s}	n^*_{0s}	n^*_{1s}	n^*_{2s}
Ne					0.125	0.530	(1.666)	(2.683)
Ar				0.065	0.204	0.682	(1.807)	(2.842)
Kr			0.031	0.084	0.216	0.703	(1.835)	(2.886)
Xe		0.020	0.050	0.109	0.253	0.763	(1.889)	(2.955)
Rn	0.012	0.027	0.055	0.111	0.252	0.723	(1.872)	--

Atom		n^*_{-4p}	n^*_{-3p}	n^*_{-2p}	n^*_{-1p}	n^*_{0p}	n^*_{1p}	n^*_{2p}
Ne						0.794	(2.138)	(3.157)
Ar					0.234	0.927	(2.267)	(3.300)
Kr				0.090	0.250	0.978	(2.319)	(3.358)
Xe			0.053	0.119	0.304	1.041	(2.343)	--
Rn		0.030	0.060	0.129	0.312	1.112	(2.410)	--

a) For symbols and nomenclature, see footnotes to Table 1B.

terms, the effective quantum numbers grow smaller for the deeper layers, precisely as the binding energies grow larger. The choice of the valence-shell as the standard was based on this fact and on several other considerations: First, the Rydberg series are most easily observed in the excitation of valence-shell electrons and it is this type data which is most complete. Second, the excitation of inner-shell electrons into Rydberg states may create many complicated effects which sometimes undermine the validity of the frozen-core approximation. Third, the striking regularities in Δn^*_{1s} and Δn^*_{1p} may be supposed to codify the average columnar behavior; hence, it would appear appropriate to induce (or attempt to induce) regularities within the same framework. And, fourth, this choice of reference happens to be particularly effective.

The most interesting feature of Tables 1 to 5 is the constant change in effective quantum numbers which occurs on going from one shell to the next, regardless of whether one or both of the shells are extra-, intra- or infra-valence-shell. This is demonstrated in Tables 6-10. The alignment of sub-shells relative to the reference valence-shell is the key to the apparent regularities (see also Tables 1B to 5B).

The data for inner-shell ionization potentials[16] are sometimes unreliable. One source of error lies in the use of interpolation procedures.[16] Another is the experimental

TABLE 6

Differences Between n^*_j's for Alkali Metals

Atom	$n^*_{5s}-n^*_{6s}$	$n^*_{4s}-n^*_{5s}$	$n^*_{3s}-n^*_{4s}$	$n^*_{2s}-n^*_{3s}$	$n^*_{1s}-n^*_{2s}$	Δn^*_{1s}	Δn^*_{1s}	$n^*_{2s}-n^*_{1s}$
H							1.000	1.000
Li						1.091	1.008	1.002
Na					0.352	1.162	1.016	1.004
K				0.129	0.442	1.137	1.031	1.009
Rb			0.052	1.124	0.467	1.132	1.040	1.011
Cs		0.030	0.057	0.137	0.526	1.100	1.051	1.014
Fr	0.015	0.027	0.055	0.132	0.392	--	--	--

Atom		$n^*_{4p}-n^*_{5p}$	$n^*_{3p}-n^*_{4p}$	$n^*_{2p}-n^*_{3p}$	$n^*_{1p}-n^*_{2p}$	Δn^*_{1p}	Δn^*_{1p}	$n^*_{2p}-n^*_{1p}$
H								1.000
Li							0.997	0.998
Na						1.455	1.016	1.005
K					0.645	1.365	1.031	1.010
Rb				0.151	0.737	1.316	1.035	1.015
Cs			0.063	0.172	0.763	1.300	1.045	1.015
Fr		0.031	0.066	0.175	0.651	--	--	--

TABLE 7

Differences Between n^*_j's for Alkaline Earths

Atom	$n^*_{5s}-n^*_{6s}$	$n^*_{4s}-n^*_{5s}$	$n^*_{3s}-n^*_{4s}$	$n^*_{2s}-n^*_{3s}$	$n^*_{1s}-n^*_{2s}$	Δn^*_{1s}	Δn^*_{1s}
He							0.982
Be						0.858	1.002
Mg					0.289	0.943	1.014
Ca				0.118	0.380	0.936	1.025
Sr			0.049	0.117	0.403	0.948	1.033
Ba		0.029	0.055	0.129	0.351	1.033	1.057
Ra	0.016	0.026	0.053	0.125	0.325	1.049	--

Atom		$n^*_{4p}-n^*_{5p}$	$n^*_{3p}-n^*_{4p}$	$n^*_{2p}-n^*_{3p}$	$n^*_{1p}-n^*_{2p}$	Δn^*_{1p}	Δn^*_{1p}
He							
Be							1.104
Mg						1.222	1.123
Ca					0.525	1.130	1.241
Sr				0.141	0.601	1.105	1.099
Ba			0.062	0.161	0.664	1.053	1.210
Ra		0.030	0.062	0.166	0.559	1.214	1.157

TABLE 8

Difference Between n^*_j's For Group III Elements

Atom	$n^*_{4s}-n^*_{5s}$	$n^*_{3s}-n^*_{4s}$	$n^*_{2s}-n^*_{3s}$	$n^*_{1s}-n^*_{2s}$	Δn^*_{1s}	Δn^*_{1s}	$n^*_{2s}-n^*_{1s}$
B							1.014
Al				0.247	--	--	1.031
Ga			0.066	0.191	--	--	1.031
In		0.035	0.071	0.206	--	--	1.034
Tl	0.013	0.031	0.066	0.188	--	--	1.035

Atom		$n^*_{3p}-n^*_{4p}$	$n^*_{2p}-n^*_{3p}$	$n^*_{1p}-n^*_{2p}$	Δn^*_{1p}	Δn^*_{1p}	
B						--	
Al					1.078	1.161	
Ga				0.252	1.153	1.166	
In			0.082	0.278	1.138	1.178	
Tl		0.035	0.079	0.261	1.171	1.179	

TABLE 9

Difference Between n^*_j's for Halogens

Atom	$n^*_{4s}-n^*_{5s}$	$n^*_{3s}-n^*_{4s}$	$n^*_{2s}-n^*_{3s}$	$n^*_{1s}-n^*_{2s}$	Δn^*_{1s}	Δn^*_{1s}
F					0.522	1.047
Cl				0.155	0.645	0.963
Br			0.055	0.143	0.480	1.116
I		0.031	0.062	0.157	0.716	0.857
At	0.016	0.028	0.058	0.150	0.605	--

Atom		$n^*_{3p}-n^*_{4p}$	$n^*_{2p}-n^*_{3p}$	$n^*_{1p}-n^*_{2p}$	Δn^*_{1p}	Δn^*_{1p}
F						1.314
Cl					0.736	1.290
Br				0.179	0.779	1.292
I			0.070	0.209	0.769	1.318
At		0.032	0.070	0.200	0.972	--

TABLE 10

Difference Between n^*_j's for Inert Gases

Atom	$n^*_{4s}-n^*_{5s}$	$n^*_{3s}-n^*_{4s}$	$n^*_{2s}-n^*_{3s}$	$n^*_{1s}-n^*_{2s}$	Δn^*_{1s}	Δn^*_{1s}	$n^*_{2s}-n^*_{1s}$
Ne					0.405	1.136	1.017
Ar				0.139	0.478	1.125	1.035
Kr			0.053	0.132	0.487	1.132	1.051
Xe		0.030	0.059	0.144	0.510	1.126	1.066
Rn	0.015	0.028	0.056	0.141	0.471	1.149	--

Atom		$n^*_{3p}-n^*_{4p}$	$n^*_{2p}-n^*_{3p}$	$n^*_{1p}-n^*_{2p}$	Δn^*_{1p}	Δn^*_{1p}	$n^*_{2p}-n^*_{1p}$
Ne						1.344	1.019
Ar					0.693	1.340	1.033
Kr				0.160	0.728	1.341	1.039
Xe			0.066	0.185	0.737	1.302	--
Rn		0.030	0.069	0.183	0.800	1.300	--

inaccuracy. For the valence-shell values, where highly accurate results are available,[15] there exists a discrepancy of ~3 to 4 eV between Siegbahn's results[16] and those of Moore.[15] In any case, we use Moore's data[15] for both valence and extra-valence shell values. For the deeper inner-shell values, the inaccuracy intrinsic to Siegbahn's data[16] is not troublesome because the number of significant figures cited exceeds three (i.e., the number used for most of the inner-shells in Tables 1 to 10). However, for intra-valence-shell and the subjacent inner-shell, significant error can result from the use of Siegbahn's data.[16] Thus, for the n_o and n_{-1} shells, we rely on the "whole column" behavior and discount the importance of erratic values. The most reliable values for intra-valence-shell ionization potentials are those of n^*_{os} for the inert gases[17] (excluding Rn). Since the values of n^*_{1s} taken from Moore[15] are also highly reliable, the column of $\Delta n^*_{1s} = n^*_{1s} - n^*_{os}$ provides an average which can be used as a standard for other groups. This is exemplified for Groups I and VII in Table 11. While $n^*_{1s} - n^*_{-1s}$ for Groups VII and VIII and $n^*_{os} - n^*_{-2s}$ for Group I are essentially identical, the Δn^*_{1s} values for the halogens and the Δn^*_{-1s} values for the alkali metals are quite irregular compared to the accurate Δn^*_{1s} values for inert gases. We can conclude that the n^*_{-1s} values for alkali metals and n^*_{os} values for halogens are unreliable. Thus, we can estimate

TABLE 11

Comparison Among Groups I, VII and VIII[a]

Atom	$n^*_{0s}-n^*_{-2s}$	Atom	$n^*_{1s}-n^*_{-1s}$	Atom	$n^*_{1s}-n^*_{-1s}$
Na	1.514	F	1.569	Ne	1.541
K	1.579	Cl	1.608	Ar	1.603
Rb	1.599	Br	1.596	Kr	1.619
Cs	1.626	I	1.573	Xe	1.636
Fr	--	At	--	Rn	1.620

Atom	$n^*_{-1s}-n^*_{-2s}$	Δn^*_{-1s}	Atom	Δn^*_{-1s}	Δn^*_{1s}	Atom	Δn^*_{-1s}	Δn^*_{1s}
Na	0.352	1.162	F	0.522	1.047	Ne	0.405	1.136
K	0.442	1.137	Cl	0.645	0.963	Ar	0.478	1.125
Rb	0.467	1.132	Br	0.480	1.116	Kr	0.487	1.132
Cs	0.526	1.100	I	0.716	0.857	Xe	0.510	1.126
Fr	0.392	--	At	0.605	--	Rn	0.471	1.149

a) The mismatch match between Group I and Groups VII and VIII is due to the fact that alkali metals have their valence s electron corresponding to the n_{1s} for halogens and inert gases.

the ionization potentials. In Table 12, we collect the average differences between various shells for Groups I, II, III, VII and VIII. The reason for the apparent deviation of Groups II and III is not clear to us. The only comment we can make is that, after the 4th row, the d and f sub-shells start filling, which may account for the irregularity emerging from the n_{-1} shell and building up to n_o and n_1 shells.

One important aspect of Table 12 is the mismatch enforced on Groups I and II by shifting their columns to the right by one step. This shift is validated both by the empirical data and is justified by our treatment of the valence shell s electron of these two groups as Rydberg states.

As mentioned earlier, the experimental data for the n_o intra-valence-shell (or n_{-1} inner-shell for Group I) are not reliable; hence, differences involving either n^*_{os} or n^*_{op} (n^*_{-1s} and n^*_{-1p} for Group I) are unreliable also. However, this difficulty can be evaded by using $n^*_{1s}-n^*_{-1s}$ and $n^*_{1p}-n^*_{-1p}$ instead. (For Group I, they are $n^*_{os}-n^*_{-2s}$ and $n^*_{op}-n^*_{2p}$). The average results for these differences are presented below:

Group	$n^*_{1s}-n^*_{-1s}$	$n^*_{1p}-n^*_{-1p}$
I	1.577	2.058
VII	1.590	2.065
VIII	1.604	2.065

TABLE 12

Average Differences Between n^*_j's

Group	$(n^*_{4s}-n^*_{5s})$	$(n^*_{3s}-n^*_{4s})$	$(n^*_{2s}-n^*_{3s})$	$(n^*_{1s}-n^*_{2s})$	Δn^*_{1s}	Δn^*_{1s}	$(n^*_{2s}-n^*_{1s})$
I[a]	0.015	0.029	0.055	0.130	0.447[b]	1.130[c]	1.034[c]
	0.016	0.028	0.052	0.122	0.350	0.961	1.032[d]
III	0.013	0.033	0.068	0.208	--	--	1.029
VII	0.016	0.029	0.058	0.151	0.594	0.996	--
VIII	0.015	0.029	0.056	0.139	0.474	1.130	1.042

Group	$(n^*_{3p}-n^*_{4p})$	$(n^*_{2p}-n^*_{3p})$	$(n^*_{1p}-n^*_{2p})$	Δn^*_{1p}	Δn^*_{1p}	$(n^*_{2p}-n^*_{1p})$
I[a]	0.031	0.065	0.166	0.699	1.359	1.032[c]
II[a]	0.030	0.062	0.156	0.587	1.145	1.166[d]
III	0.035	0.080	0.264	1.135	1.171	--
VII	0.032	0.070	0.196	0.761[e]	1.304	1.030
VIII	0.030	0.067	0.176	0.740	1.325	

a) Alkali metals and alkaline earths are shifted to the right by one column in order to compare them with the relevant columns of other groups.
b) This average does not include Fr.
c) This average does not include Li.
c) This average does not include Be.
d) This average does not include At.

The agreement is excellent. We are justified in taking averages of all the differences of effective quantum numbers for Groups I, VII and VIII and in regarding these averages as typifying the behavior of these groups. The results are given in Table 13.

The average quantities in Table 13 are of importance because, by their use, we can estimate n^*_{1s}, n^*_{2s}, n^*_{1p}, n^*_{2p}, etc. from the knowledge of the number of inner-shells and the value n^*_{js} or n^*_{jp} for the deepest inner-shell. In other words, the experimentally measured K- and L-shell ionization potentials combined with the position of the atom in the periodic table is adequate for the generation of all the other (i.e., inner-, valence- and extra-shell) binding energies of this element. The K- and L-shell ionization potentials are also used as standards in experimental measurements.[16] They usually contain three or more significant figures, which is highly desirable for the predictions of outer-shell values. To demonstrate, let us look at the example of inert gases. From Tables 5A, 12, and 13, we can build the whole spectrum of inert gases starting from the effective quantum numbers for the 1s and 2p levels. This is shown in Table 14. Note that the predictability for the Rydberg states is excellent. An error of ~0.05 is quite severe for inner-shell values but not so bad for extra-shell values.

TABLE 13

Average Differences for Groups I, VII and VIII

	$n^*_{-4}-n^*_{-5}$	$n^*_{-3}-n^*_{-4}$	$n^*_{-2}-n^*_{-3}$	$n^*_{-1}-n^*_{-2}$	$n^*_{1}-n^*_{-1}$	$n^*_{2}-n^*_{1}$
s shells	0.015	0.029	0.056	0.140	1.590	1.038
p shells		0.031	0.065	0.179	2.063	1.031

TABLE 14

Estimations of Effective Quantum Numbers for Inert Gases[a]

	Ne	Ar	Kr	Xe	Rn
1s	(0.125)	(0.065)	(0.031)	(0.020)	(0.012)
2s	0.572	0.205	0.087	0.049	0.027
	(0.530)	(0.204)	(0.084)	(0.050)	(0.027)
3s	1.715	0.652	0.227	0.105	0.056
	(1.666)	(0.682)	(0.216)	(0.109)	(0.055)
4s	2.753	1.782	0.674	0.245	0.112
	(2.683)	(1.807)	(0.703)	(0.253)	(0.111)
5s		2.820	1.804	0.692	0.252
		(2.842)	(1.835)	(0.763)	(0.252)
6s			2.842	1.822	0.699
			(2.886)	(1.889)	(0.723)
7s				2.860	1.829
				(2.955)	(1.872)
8s					2.867

	Ne	Ar	Kr	Xe	Rn
2p	(0.794)	(0.234)	(0.090)	(0.053)	(0.030)
3p	2.153	0.933	0.256	0.118	0.061
	(2.138)	(0.927)	(0.250)	(0.119)	(0.060)
4p	3.185	2.292	0.955	0.284	0.126
	(3.157)	(2.267)	(0.978)	(0.304)	(0.129)
5p		3.324	2.314	0.983	0.292
		(3.300)	(2.319)	(1.041)	(0.312)
6p			3.346	2.342	0.991
			(3.358)	(2.343)	(1.112)
7p				3.374	2.350
					(2.410)
8p					3.382

a) Values in parentheses are experimental. Others are estimated.

The implications of Table 14 will be elaborated in Section III. In the meantime, we wish to emphasize several points. (i) We have chosen to compare s-shells with s-shells and p-shells with their own kind. However, comparisons between s- and p-shells are also feasible and, indeed, these comparisons also show regularities (e.g., the $\bar{n}^*_{ls}$ and $\bar{n}^*_{lp}$ behavior). (ii) We will concentrate on the alkali metals and inert gases in all ensuing discussions. These two groups are related in two ways: They differ from each other by one electron (e.g., Ar and K); and they also differ from each other by a whole periodic row (e.g., K and Kr). (iii) Although the elements of other groups (e.g., Groups II and III) may deviate from the average behavior of Groups I and VIII, we expect that the deviations will fall smoothly from Group III to Group VIII. As exemplified by Figure 1, the major change in n^*_{js} and n^*_{jp} occurs after the filling of each row, whereupon they gradually converge on those of the next inert gas.

The values of $n^*_{js}-n^*_{(j-1)s}$ [or $n^*_{jp}-n_{(j-1)p}$] are essentially identical for Groups I, VII and VIII. The largest deviation from these values occurs in Groups II and III. Due to the smooth decrease of n^*_{js} and n^*_{jp} on going from Group III to Group VIII, the differences of effective quantum numbers of Groups IV, V, VI and VII approach the inert gas values, as evidenced by the

similarity between the halogens and the inert gases. Thus, we can take Groups I and VIII as representatives of the Groups which they encompass without losing the generality of characteristic columnar behavior.

III. PRECURSORS AND DEVIATIONS FROM HYDROGEN-LIKE BEHAVIOR

A precursor to a Rydberg orbital $n_i\ell$, with ℓ=s,p, d,f,..., is defined as $n_j\ell$ where $j<i$ and the ℓ's are identical. Precursors can be divided into real and virtual types. For alkali metals, the real precursors are those $n_j\ell$'s for which $j<0$, and the virtual precursors are those for which $0\leq j<i$. For example, for the 3s→5s excitation, the 5s orbital of Na has inner-shell 1s, 2s real precursors, whereas the valence-shell 3s and the extra-shell 4s are the virtual precursors. However, for the 3s-5s excitation the 5s Rydberg orbital of Mg has 1s, 2s and 3s as real precursors, whereas 4s is the only virtual precursor.

Orbitals with real precursors are penetrating orbitals. Thus, they exhibit deviations from hydrogen-like behavior which is gauged by the quantum defect, u. Orbitals with no real precursors are non-penetrating and hydrogen-like, and possess near-integer effective quantum numbers. These conclusions are illustrated in Table 1A. For Li, the 1s orbital serves as the real precursor and consequently the 2s, 3s,... states all have non-integer effective quantum numbers. But, for 2p, 3p,... states, there is no real precursor and their effective quantum numbers are 1.959, 2.956,..., which are nearly integers

As mentioned earlier, the extraction of the quantum defect from δ or n^* is both ambiguituous and controversial. The link with the

phase shift of scattering theory is given by[4,9]

$$\tan \delta = \tan \pi u \tag{35}$$

with solutions

$$\delta + k\pi = \pi u \ , \quad k = 0,1,2,... \tag{36}$$

or alternatively,

$$\delta = \pi(u+k) \ , \quad k = 0,1,2,... \tag{37}$$

Thus, with every phase shift δ, we can associate an infinite numbers of quantum defects, each of which differs from the other by an integer number. This happenstance makes for ambiguity in the division of an effective quantum number into integer and non-integer parts. For example, the alkali metals of Table 1A have almost identical values of n^*_{1s}, yet convention specifies that we divide them into corresponding aufbau principal numbers and quantum defects as follows

$$\begin{aligned}
&\text{Li:} \quad 2.596 = 3 - 0.404 \\
&\text{Na:} \quad 2.643 = 4 - 1.307 \\
&\text{K:} \quad 2.801 = 5 - 2.199 \\
&\text{Rb:} \quad 2.845 = 6 - 3.155 \\
&\text{Cs:} \quad 2.920 = 7 - 4.080 \ .
\end{aligned} \tag{38}$$

The quantum defects of neighbors differ by ~1. Consequently, one is tempted to forego the aufbau numbering completely and to substitute it by a relative system, for example,

$$\begin{aligned} &\text{Li:} \quad 2.596 = 1 + 1.596 \\ &\text{Na:} \quad 2.643 = 1 + 1.643 \\ &\text{K:} \quad 2.801 = 1 + 1.801 \\ &\text{Rb:} \quad 2.845 = 1 + 1.845 \\ &\text{Cs:} \quad 2.920 = 1 + 1.920 \end{aligned} \tag{39}$$

where 1 is the serial index of the first s Rydberg state and the remainder is the relative quantum defect. However, ample empirical evidence for the aufbau numbering exists; this evidence will be discussed in Section IV. This evidence is so strong that we feel compelled to reject the relative numbering system. Our use of the valence-shell as a reference serves merely to align the various shells according to the constancy of their corresponding n*'s. This choice renders no support to the scheme of Eq. (39). Actually, the proper alignment of shells shows a regularity in n* which discredits the primacy of any kind of "quantum defect", whether aufbau, relative, or otherwise.

The interpretation of the quantum defect as a measure of penetration into the core is meaningful only for extra-

valence-shell orbitals. For valence-shell and inner-shell orbitals, there is no sense in extracting information about penetration from their effective quantum numbers. In this connection, it is of interest to examine the inert gases further. Inspection of the following data indicates

	n_{os}	n_{1s}
Atom	$n^*_{os}=n_o-u_{os}$	$n^*_{1s}=n_1-u_{1s}$
Ne	0.530=2-1.470	1.666=3-1.334
Ar	0.682=3-2.318	1.807=4-2.193
Kx	0.703=4-3.279	1.835=5-3.165
Xe	0.763=5-4.237	1.889=6-4.111
Rn	0.723=6-5.277	1.872=7-5.128

that u_s for the valence s sub-shell is almost identical to that for the extra-valence s shell. The former values, of course, have no physical meaning because the valence s shell lies within the valence p sub-shell whose outer edge provides a rough estimate of the core size.

We now intend to describe an alternative description of non-hydrogen-like behavior. In order to do so, we must first develope the concept of a periodic table based on effective quantum number differences.

A. The Aufbau Principle and the Average Atom

The Aufbau Principle usually refers to the successive filling of electrons into the various shells of the periodic table. As indicated earlier, and is supported by the data in Tables 12, 13 and 14, we can generate the electronic spectra of elements in the periodic table by using the known characteristic differences of n*'s. The shell increments shown in Table 13 work for the s and p sub-shells of Group I, VII and VIII only. Somewhat different increments can be obtained for other groups and for d, f,... sub-shells as well. However, the data of Table 13 should be sufficient for illustration.

The concept of real and virtual precursors simplifies the construction of the electronic spectrum. From the position of an element in the periodic table, we can determine the number of real and virtual precursors for a given $n_j \ell$ with ℓ = s or p. Then, based on the K- or L-shell ionization potential, the binding energies of higher shells can be determined very simply. For instance, from Tables 12 and 13 the first real precursor for an s shell will increase the effective quantum number of the shell in question by ~1.13, the second by ~0.46, etc. A similar situation exists for p sub-shells. The virtual precursors increase the effective quantum numbers by ~1.00 in both cases.

Besides serving as spectral generators, the differences in n* also define the "average atom". An "average atom" represents some general facet of the electronic structure of the groups of atoms. Its electronic spectrum, which is composed of levels separated by the shell increments, has its zero point at the K-shell. We can get information about the binding energies of any specific atom from the "average atom" electronic structure by submersion the K-shell n^*_{js} under it. Then the n^*_{jp}'s can be constructed by utilizing the constancy in $n^*_{jp}-n^*_{js}$. The accuracy of the predicted binding energies increases with increasing n_j. In other words, the predictability is highest for Rydberg states which, fortunately, represent our main interest.

Similar rules can be developed for LS split terms and their fine structures. This will be discussed in Section V.

B. Deviations from Hydrogen-Like Behavior

For hydrogen-like atoms, the change of effective (principal) quantum numbers from shell to shell is unity. Deviations from unity occur when more than one electron appears. For example, the He 1s shell has $n^*_{os} = 0.744$ instead of 1.00 (Table 2A). The next shell has $n^*_{1s} = 1.726$; thus, $\Delta n^*_{1s} = 0.982$, which differs from unity by only 0.018. According to our criterion, which is based

on differences between effective quantum numbers, the deviation from the hydrogen-like case is very slight for the 2s level. One might say that the 2s electron recapitulates the deviation of the 1s shell. In the case of Li (Table 1A), we find $n^*_{os} = 1.588$, which deviates from the hydrogenic value of 2.000 by 0.412. We attribute the deviation to the presence of the 1s core for which $n^*_{-1s} = 0.497$. Since $\Delta n^*_{-1s} = 1.091$, which is very close to the hydrogenic difference of unity, the 2s electron again recapitulates the deviation of the 1s core. The deviation of the 1s shell from hydrogen-like behavior is of two types: One is due to the presence of the extra 1s electron and to some extent, the presence of the outer 2s electron. For atoms with both s and p inner-shells, there will be a split of the effective quantum numbers, n^*_{js} and n^*_{jp}, within the same inner-shell. This latter source of deviation should also be recapitulated by successive inner-, valence-, or extra-shell orbitals with the same s or p designation.

Our building procedure can now be rationalized as follows: The innermost shell possesses the initial deviation and this deviation is recapitulated by the next shell (which may also exhibit its own deviation). These combined deviations are recapitulated by the next higher shell and so on. This accumulation of deviations is expressed as the differences between successive effective

quantum numbers. The near-integer increments in n* for successive Rydberg states indicates that no contribution to the deviation from hydrogen-like quantum numbers arises from the virtual precursors. Instead, the deviations derive solely from the real precursors in the valence- and inner-shells. Once we enter the extra-valence shell domain, the deviation stays the same regardless of quantum number (or serial index). Thus, we have the usual description for this constant deviation: the "quantum defect".

This measure of deviations from hydrogen-like behavior represents a more general and unified attitude since it treats the inner-, valence- and extra-shells on the same footing. The effective quantum number for a Rydberg state can now be viewed as the result of successive deviations inflicted in the inner-shells. The more real precursors a Rydberg state has, the more shell increments it takes to construct its effective quantum number and, consequently, the larger its value (see Table 1B, for example).

It is interesting to consider "doubly-excited" states in which two electrons are excited from valence- or inner-shells into Rydberg orbitals. Under this situation, we find for the higher energy Rydberg orbital a real precursor in the lower Rydberg orbital. Although we have not

investigated the data, we remark that the accummulated deviations possessed by the lower Rydberg precursor will be recapitulated by the higher one in much the same fashion as the "singly excited" case described above.

Another phenomenon of interest is the "(Z+1)-analogy,"[19,20] which states that the energy levels of a system which has a core electron excited will be very similar to those of another species with an extra unit of positive nuclear charge and a full core. The frozen-core approximation is implicit in this "analogy". Within the frozen-core approximation, however, we have already shown for Groups I, VII and VIII that the energy levels can be constructed using identical shell increments. For example, the elements F, Ne and Na, possess exactly the same number of real s and p precursors (if we regard the 3s electron in Na as a Rydberg electron). Thus, starting from the individual K-shell effective quantum numbers of Tables 1A, 4A and 5A, we can construct the energy levels for these three elements by using the shell increments from Table 13. Note that the difference in the K-shell effective quantum numbers is less than ~0.03. Hence, the effective quantum numbers for these three elements will be identical within ~0.03. Within the confines of the frozen-core approximation, exciting a 1s electron into a Rydberg state does not influence the energy level structure. Thus, there is nothing strange about the fact that the energy levels of

one element are similar to those of the next element. The major difference originates in the effective quantum numbers of the K-shell and, since these are very similar, for adjacent elements, the result is similar energy level schemes for the Rydberg states. Thus, the "(Z+1)-analogy" is neither mysterious nor unexpected.

IV. ISOELECTRONIC SEQUENCES AND AUFBAU NUMBERING

The dispute over the different ways of dividing seemingly identical effective quantum numbers of equivalent Rydberg states (namely the aufbau and the relative numbering systems) can be settled by the following empirical study.

For an isoelectronic sequence, defined as the collection of atoms or cations with the same number of electrons but different nuclear charges, the Rydberg formula can be written as

$$\nu_j = IP - \frac{RQ^2}{(n_j^*)^2} \qquad (7)$$

where Q is the net charge on the core (Q=1 for neutral atoms, Q=2 for singly charged positive ions, etc.). As Q grows larger along an isoelectronic sequence, the system becomes more hydrogen-like: The increase of the positive nuclear charge eventually makes the Coulombic field, $-Ze^2/r$, dominate over all other potential terms in the Hamiltonian. Consequently, n_j^* approaches the hydrogenic values or, equivalently, the aufbau principal quantum numbers. This is true not only for Rydberg states but also for the valence states, as evidenced by Table 15.

The data of Table 15 exhibit convergence towards a hydrogen-like situation at high Q. For example, in Table 15A, $n_o^* = 1.280$ for B I, but approaches 2.000 at high Q

TABLE 15A

Effective Quantum Numbers for Isoelectronic Sequences[a]

Boron $2s^2 2p \rightarrow 2s^2 n\ell$

			$3s\ ^2S$		$3p\ ^2P$		$3d\ ^2D$	
Atom	Q	n^*_0	n^*_{1s}	Δn^*_{1s}	n^*_{1p}	Δn^*_{1p}	n^*_{1d}	Δn^*_{1d}
B	1	1.280	2.020	0.740	--[b]	--	3.003	1.723
C	2	1.494	2.341	0.847	2.600	1.106	2.931	1.437
N	3	1.607	2.474	0.867	2.686	1.079	2.926	1.319
O	4	1.677	2.565	0.888	2.738	1.061	2.928	1.251
F	5	1.726	2.630	0.904	2.776	1.050	2.933	1.207
Ne	6	1.761	2.677	0.916	2.781	1.020	2.938	1.177
Na	7	1.788	2.713	0.925	2.826	1.038	2.942	1.154
Mg	8	1.809	2.741	0.932	--	--	2.945	1.136
Al	9	1.827	2.765	0.938	--	--	2.950	1.123
Si	10	1.841	--	--	--	--	2.954	1.113
P	11	1.853	2.800	0.947	--	--	2.956	1.103
	.							
	.							
	.							
	c	2.000	3.000	1.000	3.000	1.000	3.000	1.000

a) Data are for term centers. Corresponding energies are from Ref. 15.

b) Unreported values.

c) Hydrogenic values.

TABLE 15B

Effective Quantum Numbers for Isoelectronic Sequences[a]

Al $3s^2 3p \rightarrow 3s^2 n\ell$

			3d ^2D		4s ^2S		4p ^2P	
Atom	Q	n^*_0	n^*_{0d}	Δn^*_{0d}	n^*_{1s}	Δn^*_{1s}	n^*_{1p}	Δn^*_{1p}
Al	1	1.508	2.632	1.124	2.188	0.680	2.676	1.168
Si	2	1.825	2.892	1.067	2.573	0.748	2.946	1.121
P	3	2.015	2.795	0.780	2.806	0.791	3.114	1.099
S	4	2.145	2.767	0.622	2.962	0.817	3.234	1.089
Cl	5	2.240	2.756	0.516	3.072	0.832	--b	--
Ar	6	2.316	2.762	0.446	3.165	0.849	--	--
K	7	2.379	2.773	0.394	3.244	0.865	--	--
Ca	8	2.430	2.783	0.353	3.308	0.878	--	--
Sc	9	2.471	2.790	0.319	3.355	0.884	--	--
	•							
	•							
	•							
	c	3.000	3.000	0.000	4.000	1.000	4.000	1.000

a), b), c), See footnotes to Table 15A.

TABLE 15C

Effective Quantum Numbers for Isoelectronic Sequences[a]

Atom	Q	n_0^*	Atom	Q	n_0^*
Ne	1	0.794	Ar	1	0.927
Na	2	1.073	K	2	1.312
Mg	3	1.236	Ca	3	1.551
Al	4	1.347	Sc	4	1.721
Si	5	1.428	Ti	5	1.852
P	6	1.491	V	6	1.955
S	7	1.540	Cr	7	2.034
Cl	8	1.581	Mn	8	--b
Ar	9	1.615	Fe	9	2.165
K	10	1.644	Co	10	2.220
Ca	11	1.669	Ni	11	2.470
Sc	12	1.690			
Ti	13	1.709			
V	14	1.726			
Cr	15	1.740			
Mn	16	1.751			
Fe	17	1.762			
Co	18	1.773			
Ni	19	1.782			
Ca	20	1.790			
Zn	21	1.798			

a) Ionization potentials are from Ref. 21

b) Unreported.

and n^*_{1s} and n^*_{1p} also converge to their aufbau value, 3. The behavior of n^*_{1d} is particularly interesting: It begins at 3.003, then drops to 2.926 and, thereafter, gradually recovers to 2.956 at P XI. A similar situation exists in Table 15B for the Al sequence: The effective quantum number for the 3d ^{2}D term, n^*_{od}, starts at 2.632 and rises to 2.892, but subsequently drops to 2.756 before rising again to 2.790 at Sc IX. This kind of fluctuation does not occur in our approach: For the B sequence (Table 15A), Δn^*_{1d} changes smoothly from 1.723 to 1.103 and approaches the hydrogenic value of 1.000; and in Table 15B for the Al sequence, Δn^*_{od} various monotonically from 1.124 to 0.319 and converges to the hydrogenic value of 0.000. The values of Δn^*_{1s} and Δn^*_{1p} in Tables 15A and 15B also show smooth and monotonic changes. This observation strengthens our confidence in choosing the differences of effective quantum numbers as the measure of deviations from hydrogen-like behavior.

Therefore, this isoelectronic sequence study provides the foundation for the following: <u>First</u>, aufbau principal quantum numbers should be regarded as the only physically meaningful designations for inner-, valence- and extra-shell orbitals. <u>Second</u>, the quantity n^*_o for the valence orbital has a solid physical meaning, as evidenced by the Ne and Ar sequences in Table 15C as well as by Tables 15A and 15B for the B and Al sequences. <u>Third</u>, $\Delta n^*_{j\ell}$ values

provide consistently invaluable information about deviations from hydrogen-like behaviors. Fourth, the smooth change in $\Delta n^*_{j\ell}$ can be used to predict n^*_j's for unreported isoelectronic species.

V. LS TERMS AND THEIR FINE STRUCTURES

As mentioned earlier, the Rydberg equation works not only for terms but also for the fine structures which result from such terms. This is demonstrated for the inert gases in Table 16. The particular transition

$$n_o p^6 \rightarrow n_o p^5 \; n_j p \; [\tfrac{1}{2}] \; ; \; \text{core}(^2P^o_{1\frac{1}{2}}) \tag{40}$$

where the jℓ-coupling notation of Racah is used,[15] has two split levels: J=1 and 0. It is obvious from Table 16 that each of the levels

$$n_o p^5 \; n_j p \; [\tfrac{1}{2}] \; , \quad J = 1 \text{ or } 0 \tag{41}$$

possesses n^*_{jp} values that are typical of a Rydberg series: The decimal part is constant along the progression n_j , $j = 1,2,3,\ldots$ However, for the same designation, the corresponding n^*_{jp} for the inert gases exhibits a spread of ~0.30 whereas the spread of Δn^*_{jp} where

$$\Delta n^*_{jp} \equiv n^*_{jp} - n^*_{op} \tag{42}$$

is considerably smaller (see following data). We find the following average values for each level:

TABLE 16

Fine Structures for Inert Gases[a]

Transition: $n_0p^6 \rightarrow n_0p^5\, n_jp\, [\frac{1}{2}]$; core $(^2P^o_{3/2})$

	Ne		Ar		Kr		Xe	
J	1	0	1	0	1	0	1	0
n^*_{jp}								
j								
1	2.067	2.184	2.184	2.339	2.246	2.415	2.310	2.489
2	3.100	3.228	3.241	3.390	3.308	3.463	3.328	3.494
3	4.115	4.254	4.262	4.411	4.309	4.465	4.395	4.560
4	5.123	5.269	5.279	5.428	5.352	5.507	5.397	5.561
5	6.130	6.282	6.262	6.410	6.335	6.489	6.400	6.563
6	7.099	7.231	7.280	7.431	7.331	7.486	7.402	7.563
7	8.127	8.275	8.270	8.419		8.485	8.403	8.564

	Ne		Ar		Kr		Xe	
n^*_{op}	0.794		0.929		0.986		1.059	
J	1	0	1	0	1	0	1	0
Δn^*_{jp}								
j								
1	1.273	1.389	1.255	1.410	1.261	1.429	1.251	1.430
2	2.307	2.434	2.311	2.462	2.322	2.477	2.269	2.434
3	3.321	3.460	3.333	3.482	3.324	3.479	3.336	3.500
4	4.328	4.475	4.350	4.499	4.366	4.521	4.338	4.502
5	5.336	5.488	5.333	5.481	5.349	5.503	5.340	5.504
6	6.305	6.437	6.351	6.502	6.345	6.500	6.343	6.504
7	7.333	7.481	7.341	7.490		7.500	7.344	7.505

a) Data and notations are from Ref. 15 (see text).

	J=1	J=0
Δn^*_{op}	1.260±0.010	1.414±0.019
Δn^*_{2p}	2.302±0.023	2.452±0.021
Δn^*_{3p}	3.328±0.007	3.480±0.016

(43)

These values constitute n* differences for split levels of the $n_j p$ terms defined in Eq. (40).

The significance of Eq. (43) lies in the clue it provides that a similar processing is possible for the terms of other periodic groups. Indeed, Fano and Martin[22] surveyed the Z-dependence of spin-orbit coupling and found that the difference between the effective quantum numbers of two spin-orbit split terms can be expressed as:

$$\Delta n^*_j \text{ (S.O.)} \sim Z^{2.33} \tag{44}$$

where S.O. designates the spin-orbit splitting and Z is the atomic number. We feel that an investigation of the fine structures should produce similar results. Furthermore, we predict the possible existence of columnar averages as exemplified in Eq. (43) for inert gases.

Once this is realized, we can extend the building-up procedure into the domain of split terms rather than merely for configuration centers as epitomized in Tables 12, 13 and 14.

VI. RELATIONSHIP BETWEEN n_o^* AND ATOMIC RADII

Several studies of atomic properties as functions of the atomic number Z have revealed very interesting shell-structure dependencies.[11,13,23,24] Rau and Fano[11] employed the Herman-Skillman potential[14] to determine the behavior of the atomic potentials as a function of both Z and atomic radii, r. The maxima of this potential occurred at different ranges of r for the inert gases, Cu, Pd, and Au. Fano et al.[13] and Manson[24] found that the Z-dependence of the asymptotic quantum defect (i.e., the phase shift) was a monotonic increase for s- and p-waves and a multi-step function for d- and f-waves. Condo[23] discovered the correlation between the atomic radii of target metals and their K^- mesonic X-ray intensities.

The plots of $\bar{n}^*_{1s}$, $\bar{n}^*_{1p}$ and n_o^* as functions of Z in Figure 1 exhibited distinct shell structure. As suggested by Fano,[25] n_o^* should be correlated with atomic radii. Our plot in Figure 6, depicting atomic radii[26] as function of Z, shows indisputable support for Fano's suggestion. The clear resemblence between the atomic radii curve and those of n_o^*, $\bar{n}^*_{1s}$, and $\bar{n}^*_{1p}$ leaves no doubt about the relatedness between effective quantum numbers and atomic radii.

Questions concerning the inner-shell $n^*_{j\ell}$ functionalities remain. Since the most conspicuous shell effects occur near the surface of the atom, the valence-shell n_o^*

Figure 6. The radii of the outermost orbital of the elements from Ref. 26 are plotted against the atomic number, Z.

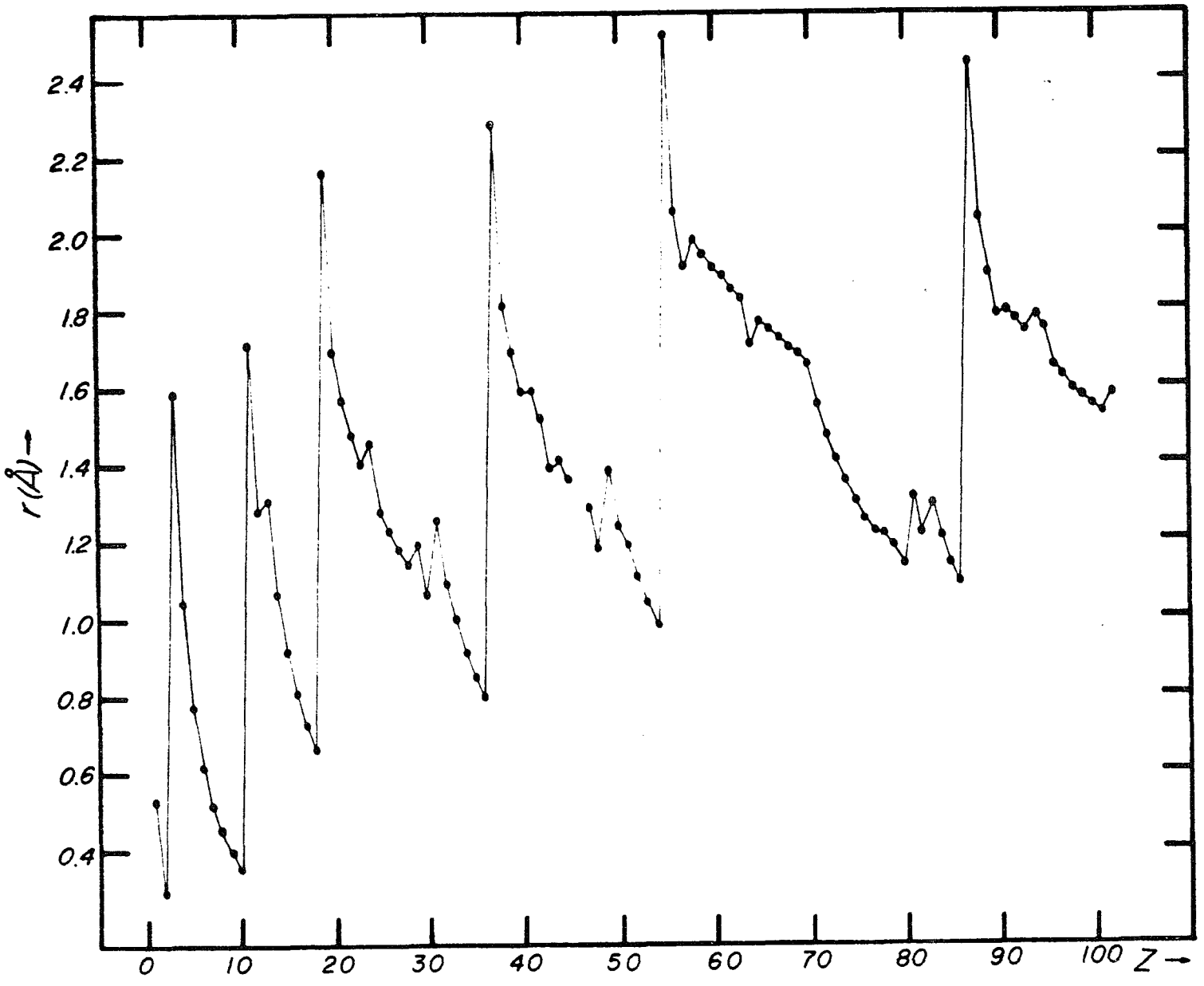
r(Å)→
2.4
2.2
2.0
1.8
1.6
1.4
1.2
1.0
0.8
0.6
0.4
0
10
20
30
40
50
60
70
80
90
100
Z→

plot exhibits a rich sub-shell structure similar to the curve of atomic radii. This presence of these sub-shell effects in the valence-shells is recapitulated by all outer shells. Thus, $\bar{n}^*_{1s}$ and $\bar{n}^*_{1p}$ possess the same appearances as n^*_o. However, for the inner-shells, the effects which are important at or near the "atomic surface" lose their influence. Therefore, inner-shell effective quantum numbers tend to be smoother functions of Z than do those of the valence- and extra-shells.

It is conceivable that the effective quantum number function is governed by the same factors that govern r. For the outermost orbitals of the valence-shell, n^*_o and r exhibit a one-to-one correspondence. A similar behavior is obvious for Rydberg orbitals. Consequently, for the case of inner-shell orbitals, we also ask whether the same one-to-one correspondence exists between effective quantum numbers and orbital sizes? If so, a close relationship should also exist between the n* differences and the corresponding orbital size differences and, hence, a measure of deviation from hydrogen-like behavior based on orbital sizes might be at hand.

In any event, good computations of inner-shell orbitals for the periodic system should easily answer the above question.

VII. THEORETICAL IMPLICATIONS

The effective quantum number is a dimensionless quantity. It is related to the binding energy in the following way

$$T_j = \frac{RQ^2}{(n_j^*)^2} \quad . \tag{45}$$

While energy is the main quantity provided by quantum mechanics, we feel that the effective quantum number holds the key to an understanding of the empirical correlations found in this work.

Equation (45) is usually imposed on the eigenvalue of the Schrodinger equation, rather than generated directly from theory.[8] The only theory that can reproduce the effective quantum numbers for Rydberg states is the "quantum defect theory",[4,9] which yields the phase shift δ_j and then converts it into quantum defect u_j via the relation

$$\delta_j = \pi u_j \quad . \tag{14}$$

We can get n_j^* from u_j by using

$$n_j^* = n_j - u_j \quad . \tag{10}$$

However, as we have shown, the quantum defect is not the

primary quantity defining the varieties of characteristic behaviors in which we are interested.

While we do not question the ability of conventional quantum mechanics and the quantum defect theory to provide theoretical and physical insight into the problems of atomic spectra, our "average atom" model and the inner-shell effective quantum numbers demand a new approach, one which focuses on effective quantum numbers instead of energies. In particular, it must be able to generate differences in effective quantum numbers: The average change of effective quantum numbers exists not only between different shells but also between split terms or levels within a configuration.

To start with, a rough model which can reproduce valence- and inner-shell effective quantum numbers will suffice. In order to achieve this, we must abandon some commonly accepted concepts about effective quantum numbers, or, specifically, quantum defects. As proven by a large number of empirical evidences, the differences of effective quantum numbers are better quantities for gauging deviations from hydrogen-like behavior. Besides, for valence- and inner-shell, it is hard to confer any meaning on the concept of a "quantum defect". The linkage of quantum defects with phase shifts is weakened by the

ambiguity expressed in Eq. (37) (namely, the inability to discriminate one u from others which differ from it by integers) and by the inability to devise a phase shift concept for inner shells.

The next step is to get the n* differences for configuration centers. Once this is achieved, the "average atom" is unequivocally defined. It is then possible to describe the whole periodic table in a unified way.

Finally, the LS term splitting and their fine structures should be studied. This will enable us to predict the electronic spectrum of an individual atom in detail.

The above speculations may be too unrealistic. A more practical proposal concerns the use of empirical regularities to devise model potentials which might provide both physical insight and computational advantage. Or, alternatively, one might use the n* differences to devise orbitals similar to Slater orbitals[8] which could enhance both the efficiency and accuracy of calculations.

In any event, the implications of this empirical study are largely unknown to us. It does possess an enormous empirical advantage -- and this, for the moment, is its most important content.

VIII. CONCLUDING REMARKS

Our quest of an average behavior in atomic spectra resulted in the following:

-----An "average atom" has been defined by using the differences between effective quantum numbers. Those n* differences also serve as measures of the deviation from hydrogen-like behavior.

-----The definition of effective quantum number has been extended into the domain of valence- and inner-shells. At the same time, the meaning of the term quantum defect in this domain has been called into question.

-----We have used isoelectronic sequence studies to support both the aufbau numbering of orbitals and our definition of n^*_o and $\Delta n^*_{j\ell}$ and their validity.

-----A characteristic behavior has been observed for fine structures, and the corresponding n* differences have been extracted from the experimental data.

-----A possible relationship between n* and orbital sizes has been elaborated.

-----Short remarks concerning doubly excited states and the (Z+1)-analogy have been made within the context of our correlative attitude.

-----Possible future studies have been discussed. The shortcomings of existing theories have been pointed out. Some practical uses of our empirical results have been suggested.

-----The close resemblence between n_o^*, $\bar{n}_{1s}^*$, $\bar{n}_{1p}^*$ and the atomic radii plots versus Z have been emphasized. They may offer more insight into the understanding of our findings than we comprehend now. Properties other than energy levels have been connected with atomic radii.[11,13,23] It is possible that these properties are controlled by some common factor which also determines atomic radii.

REFERENCES

1. J. J. Balmer, Ann. Phys. Chem. 25 (1885) 80.
2. J. R. Rydberg, Kgl. Svenska Akad. Handl. 23 (1889); Astrophys. J. 4 (1906) 91.
3. W. Ritz, Astrophys. J. 28 (1908) 237.
4. M. J. Seaton, Proc. Phys. Soc. (Lond.) 88 (1966) 801.
5. U. Fano, Phys. Rev. A 2 (1970) 353.
6. K. T. Lu, Phys. Rev. A 4 (1971) 579.
7. U. Fano, J. Opt. Soc. Am. 65 (1975) 979.
8. G. Simons, J. Chem. Phys. 60 (1974) 645.
9. a) F. S. Ham, "Solid State Physics", Vol. I, edited by F. Seitz and D. Turnbull, Academic Press, New York, 1955, p. 127.
   b) M. J. Seaton, C. R. Acad. Sci., Paris 240 (1955) 1317; Proc. Phys. Soc. 88 (1966) 801.
10. B. W. Shore and D. H. Menzel, "Principles of Atomic Spectra", John Wiley and Sons, Inc., New York, 1968, Chap. 2.
11. A. R. P. Rau and U. Fano, Phys. Rev. 167 (1968) 7.
12. W. H. Adams, J. Amer. Chem. Soc. 92 (1970) 2198.
13. U. Fano, C. E. Theodosiou and J. L. Dehmer, Rev. Mod. Phys., to be published.
14. F. Herman and S. Skillman, "Atomic Structure Calculations", Prentice-Hall Inc., Englewood Cliffs, New Jersey, 1963.
15. C.E. Moore, "Atomic Energy Levels", Natl. Bur. Std. (U.S.) Circular No. 467 (U.S. GPO, Washington, D.C., 1958).

16. K. Siegbahn, C. Nordling, A. Fahlman, R. Nordberg, K. Hamrin, J. Hedman, G. Johansson, T. Bergmark, S. Karlsson, I. Lindgren and B. Lindberg, "ESCA, Atomic, Molecular and Solid State Structure Studied by Means of Electron Spectroscopy", NOVA ACTA Regiae Societatis Scientairum Upsaliensis, Ser. IV, Vol. 20, Uppsala, 1967.

17. K. Siegbahn, C. Nordling, G. Johansson, J. Hedman, P. F. Heden, K. Hamrin, U. Gelius, T. Bergmark, L. O. Werme, R. Manne and Y. Baer, "ESCA Applied to Free Molecules", North-Holland Publishing Company, Amsterdam-London, 1969.

18. R. S. Mulliken, J. Amer. Chem. Soc. 86 (1964) 3183. For core orbitals, Mulliken used

$$T \equiv \frac{RQ^2}{(n^*)^2} \equiv \frac{RQ^2}{(n-\delta)^2}$$

and regarded n^* as having only a formal significance.

19. M. Nakamura, M. Sasanuma, S. Sato, M. Watanabe, H. Yamashita, Y. Iguchi, A. Ejiri, S. Nakai, S. Yamaguchi, T. Sagawa, Y. Nakai and T. Oshio, Phys. Rev. 178, (1969) 80.

20. W. H. E. Schwarz, Angew. Chem. Intern. Ed. 13 (1974) 454; Chem. Phys. 13 (1976) 153.

21. R. L. Kelly and D. H.Harrison, Jr., Atomic Data 3 (1971) 177.

22. U. Fano and W. C. Martin, "Topics in Modern Physics", edited by W. F. Britten and H. Odabasi, Colorado Associated U.P., Boulder, 1971, p. 147.

23. G. T. Condo, Phys. Rev. Lett. 33 (1974) 126.

24. S. T. Manson, Phys. Rev. 182 (1969) 97.

25. U. Fano, private communication.

26. The radii of the outermost orbitals of ground state neutral atoms are taken from: M. A. Morrison, T. L. Estle and N. F. Lane, "Quantum States of Atoms, Molecules, and Solids", Prentice-Hall Inc., Englewood Cliffs, New Jersey, 1976, p. 559.

CHAPTER TWO

MOLECULAR RYDBERG STATES

INTRODUCTION

The vast amount of experimental data for molecular Rydberg states has been documented by Duncan[1] and Robin.[2] However, except for some simple diatomic molecules, the assignments of most of these states remain speculative.

Several studies have been devoted to the systematics of assigning molecular Rydberg states: Lindholm[3] employed the quantum defect criterion; Robin[2] devised the "term value" rule; and Mulliken[4] discussed molecular Rydberg states in terms of MO's and their dependence on the internuclear distance(s), $\vec{D}$. The two former studies, though empirically helpful, have had no impact on theory. The last study, while furnishing some general understanding, was restricted to H_2 and He_2, and has had little impact on experiment.

For simple molecules, high-resolution studies can provide detailed information about the symmetry designations of electronic states. However, even the lowest-energy excited states of simple diatomics present a crucial problem: Are they to be characterized as valence or Rydberg states? One common approach to this question is the "united-atom concept". For example, H_2 and H_2O have "united atoms" He and Ne, respectively. Mulliken assigned the lowest-energy excited state of H_2 as the $2p\sigma$; $^1\Sigma_u$ Rydberg state,[4a]

and that of H_2O as the $3sa_1$; $^1B_1$ Rydberg state[4d] simply because they "looked like" the united-atom 2p and 3s orbitals of He and Ne, respectively. There are, however, empirical evidences which suggest that these assignments are incorrect.

For large molecules, the situation becomes very complicated. The number of excited states increases because of the large number of electrons and the lowering of symmetry; the orbital quantum number ℓ is no longer a constant of motion in the anistropic molecular potential; and the coupling of angular momenta with the axial electric field also complicates the situation considerably.

Therefore, in order to exploit the empirical information which is available for molecular Rydberg states, a reliable method of identification is needed. This work proposes to design a general scheme for the identification of molecular Rydberg states by utilizing the results obtained from the correlative study of atomic Rydberg states (Chapter One).

The atomic correlations, which were based on effective quantum numbers, must be modified when applied to molecular cases. The specific problems one encounters are the following:

1) The influence of chemical shifts on the inner-shell binding energies will certainly have some effects on the correlative attitude. Within the context of effective

quantum number ideology, one must first find a way to describe these shifts before attempting any correlations.

2) The valence-shell contains orbitals which exhibit different degrees of bonding. No concept of an "average bonding orbital" is available. Hence, the $\Delta n^*_{j\ell}$ quantities (Chapter One, Section II), which explicitly contain n^*_o, must be defined for each individual $n^*_{j\ell}$ and n^*_o. The dependence of $\Delta n^*_{j\ell}$ on the degree of bonding of the reference valence orbital may well be very important.

3) The character of an MO is a function of the internuclear distance(s), $\vec{D}$. It is known[4] that an MO which is Rydberg at the equilibrium internuclear distance, D_{eq}, may become a valence orbital at large $\vec{D}$. Consequently, in order to correlate the electronic states of different molecules, we must choose some fixed molecular conformation. Specifically, we must choose either D_{eq} or the internuclear distance which corresponds to the vertical Franck-Condon transition, D_v.

4) The presence of an anisotropic potential invalidates the characterization of electronic states ℓ. Consequently, we must inquire into the extent to which we can retain the atomic notations $n_j\ell$, with ℓ = s, p, d, f,..., for molecular orbitals.

5) The valence-shell counterpart of the inner-shell chemical shift is the "substituent effect". The former can be handled by regarding the substituents which surround

the chromophore as electronic charges which only exert electrostatic forces.[6] The latter is more complicated because chemical bonding effects are dominant in the valence-shell region. For Rydberg orbitals, the effects exerted by the substituents will undoubtedly be different from both the core and the valence MO subsets. The chemical shifts and substituent effects suffered by their "precursors" may well be merely recapitulated and the effects on the Rydberg orbitals themselves may well be small. In any event, the precursor concept for molecular Rydberg orbitals should be quite different from the atomic case and must be investigated.

We have now outlined the problems to be solved in this chapter. The first section is devoted to theoretical considerations of molecular potentials and their influences on Rydberg states. Following this, we will examine the influence of the chemical environment on inner-, valence-, and outer-shell orbitals. The precursor concept for molecules is developed in Section III. A discussion of geometry dependence of MO characterizations constitutes the bulk of Section IV. Section V examines the differences between inner-shell and valence shell excitation spectra. The development of $\Delta n^{*}_{j\ell}$ for various types of transition is contained in Section VI. Finally, multicenter chromophores are discussed in Section VII.

I. THE MOLECULAR POTENTIAL

Since we plan to generalize the correlations of atomic Rydberg states to the molecular situation, it seems appropriate to start with the Schrödinger equation for an atom

$$\left[\frac{d^2}{dr^2} - \frac{2}{r}\frac{d}{dr} - \frac{2m}{\hbar^2}\left(T_{j\ell} - \frac{\hbar^2}{2m}\frac{\ell(\ell+1)}{r^2} - V_a(r) + \frac{e^2}{r}\right)\right]\Psi_{j\ell}(r) = 0 \tag{1}$$

where

$$T_{j\ell} = \frac{R}{(n^*_{j\ell})^2} = \frac{R}{(n_{j\ell}-u_{j\ell})^2} \tag{2}$$

and $V_a(r)$ represents all potentials other than the Coulombic e^2/r . According to Fano and co-workers[9,10]

$$\Psi_{j\ell}(r) = \alpha_{j\ell}(r)\left\{f_{j\ell}(r)\cos[\delta_{j\ell}(r)] - g_{j\ell}(r)\sin[\delta_{j\ell}(r)]\right\} \tag{3}$$

where $\alpha_{j\ell}(r)$ is the amplitude, $f_{j\ell}(r)$ and $g_{j\ell}(r)$ are the regular and irregular solutions of Eq. (1) when $V_a(r) = 0$, and $\delta_{j\ell}(r)$ is the phase shift caused by $V_a(r)$. Substituting Eq. (3) into Eq. (1), one obtains[9]

$$\delta_{j\ell}(r) = N \int_0^r V_a(r') \{\psi_{j\ell}(r')\}^2 \, dr' \tag{4}$$

and

$$\pi u_{j\ell} \equiv \delta_{j\ell}(r_o) \tag{5}$$

where r_o is the radius of the atomic core. From Eqs. (4) and (5) we can see that $\delta_{j\ell}(r_o)$ (or $u_{j\ell}$) is a function of j,ℓ and $V_a(r)$. If $V_a(r)$ is a monotonically decreasing, non-negative function for $r \leq r_o$, $\delta_{j\ell}(r_o)$ (or $u_{j\ell}$) decreases with increasing j and finally converges to the asymptotic value at large j. From the relation

$$n^*_{j\ell} = n_{j\ell} - u_{j\ell} \tag{6}$$

it is clear that, when $u_{j\ell}$ decreases with increasing j, we will find

$$n^*_{j\ell} - n^*_{(j-1)\ell} > 0 \tag{7}$$

If $V_a(r)$ is a monotonically increasing, non-positive function for $r \leq r_o$, the opposite is true; i.e.,

$$n^*_{j\ell} - n^*_{(j-1)\ell} < 0 \tag{8}$$

The s and p Rydberg series of the inert gases shown in Figures 4 and 5 and Table 16 of Chapter One exhibit the trend of Eq. (7). We can conclude that, for inert gases, $V_a(r)$ is repulsive and probably exponentially decreasing.

For molecules, we add an extra term[5] to V(r), namely

$$V_m(\vec{r}) = V_a(r) + U_m(\vec{r}) \tag{9}$$

where $U_m(\vec{r})$ is the anisotropic molecular potential. The addition of the anisotropic $U_m(\vec{r})$ prevents the Schrödinger equation from being separated into radial and angular parts. It also prevents ℓ from being a good quantum number. However, at large r, it is known[7,8] that the factorization of the wave function into spherical harmonic and the radial parts is possible. Apparently, $V_m(\vec{r})$ is nearly centrosymmetric at large radial distance. Therefore, it is a good approximation to use ℓ as a constant of motion even for molecular Rydberg states.

The relationship between $V_m(\vec{r})$ and $V_a(r)$ in Eq. (9) can be conveniently described by providing apt definitions of the terms "chromophore" and "substituent". Thus, $U_m(\vec{r})$ constitutes a "substituent effect" exerted on the Rydberg electron and it becomes more important the more the molecule deviates from the atomic case.

Before proceeding further, it is appropriate to define some mode of comparison between molecules and atoms. It is

helpful to note that the presence of $U_m(\vec{r})$ not only makes ℓ unsuitable for valence orbital characterization, but that it also determines the trend of $n^*_{j\ell}-n^*_{(j-1)\ell}$ as a function of j for molecular Rydberg series. This topic will be elaborated in Chapter Three.

In the next section, the concept of the "chromophore" and its "substituent(s)" will be formulated. And, via empirical evidences, the rules for comparing a chromophore and its substituted offsprings will be obtained.

II. SUBSTITUENT EFFECTS AND CHEMICAL SHIFTS

There are a number of ways to connect the spectrum of a molecule with an atomic one. For example, CH_3OH can be regarded as a substituted oxygen atom. Or, it may be related to its united atom, Ar, with a one-to-one correspondence implied between each energy level of the two entities. Or, proceeding further, it can be viewed as the result of replacing a proton of H_2O by the CH_3 groups with H_2O itself being a derivative from Ne.

Any one of the above attitudes serves some purpose. For molecules containing a single atom from Group V, VI, or VII, we favor the last attitude; namely, we believe that these molecules should be compared with the inert gas in the same row of the periodic table. The reason for this choice are two-fold: First, the inert gases provide the most representative atomic behavior, as discussed in Chapter One. This is due to the strategic positions which the inert gases occupy in the periodic table and to the extensive data which are available for them. Second, empirical studies support such a choice, as evidenced in the following sections.

A. n_o^* for Molecules

Since the atomic correlation have been studied in the context of the effective quantum number, it seems mandatory

to use n^* of molecules for correlations with atoms and other molecules. While there is no difficulty in doing so for molecular Rydberg states, it is questionable if we can validly define n^* for the valence orbital of a molecule. For inner-shell orbitals, we feel that the situation is very similar in both atomic and molecular cases, except that the values for the latter are "chemically-shifted" from those of the former. However, within the valence-shell, chemical bonding dominates. With the exception of non-bonding orbitals, MO's in the valence region should deviate drastically from atomic orbital characteristics. Therefore, the definition of n_o^* for molecules is a major problem, especially when we recollect that the valence-shell was used as the reference for all other shells in the atomic correlations in Chapter One.

Our solution to this problem lies in empiricism. We divide the valence-shell orbitals into three categories: (i) Non-bonding and loosely bonding orbitals; (ii) bonding, especially σ bonding, orbitals; (iii) the anti-bonding orbitals. The third category, the anti-bonding orbitals, is exempted from n_o^* studies because these orbitals are usually unoccupied in molecular ground states. However, if we wish to obtain an average value of n_o^* for the n_o shell, they must be included. Furthermore, they may also mix with the lower Rydberg states and cause a lot of confusion in the identification of these states as

valence or Rydberg in nature.

For categories (i) and (ii), we proceed as follows: The prototype for our molecular n_o^* study is the hydrides of the Group IV, V, VI, and VIII elements and the methyl-substituted hydrides of the Group VI and VII elements. The valence-shell splitting of the ground states of these molecules is exemplified by Figure 1.[11] The valence-shell orbitals 2s and 2p of Ne are shifted to lower energies as protons are extracted from their nuclei. The 2s orbital remains unsplit but shows some broadening in the photoelectron spectra whereas the 2p orbital is subject to considerable splitting. For HF, we have a $^2\pi_{3/2,1/2}$ spin-orbit-split, non-bonding 2p and bonding σ MO's. In H_2O, the 2p (or π) orbital splits further into a non-bonding b_1 and a slightly-bonding a_1, while b_2 is the σ-bonding orbital. Ammonia, NH_3, has a slightly bonding a_1 and a σ-bonding e orbital. Finally, for CH_4, there is only the σ-bonding t_2 orbital. Similar hydrides for elements in succeeding rows of the periodic table are identical except that the aufbau quantum number corresponding to n_o changes from 2 to 3, 4, 5, etc. For Groups VI and VII, methyl substitution amounts merely to a change in the σ-bonding and the slightly-bonding orbitals.

It seems that non-bonding orbitals can be related to the inert gas atomic orbitals. The slightly-bonding and σ-bonding orbitals exhibit distinct Franck-Condon envelopes

Figure 1. Photoelectron spectra of Ne, HF, H_2O, NH_3 and CH_4, taken from Ref. 11, exhibit the chemical shifts of the 2s orbital and the splitting of the 2p orbital.

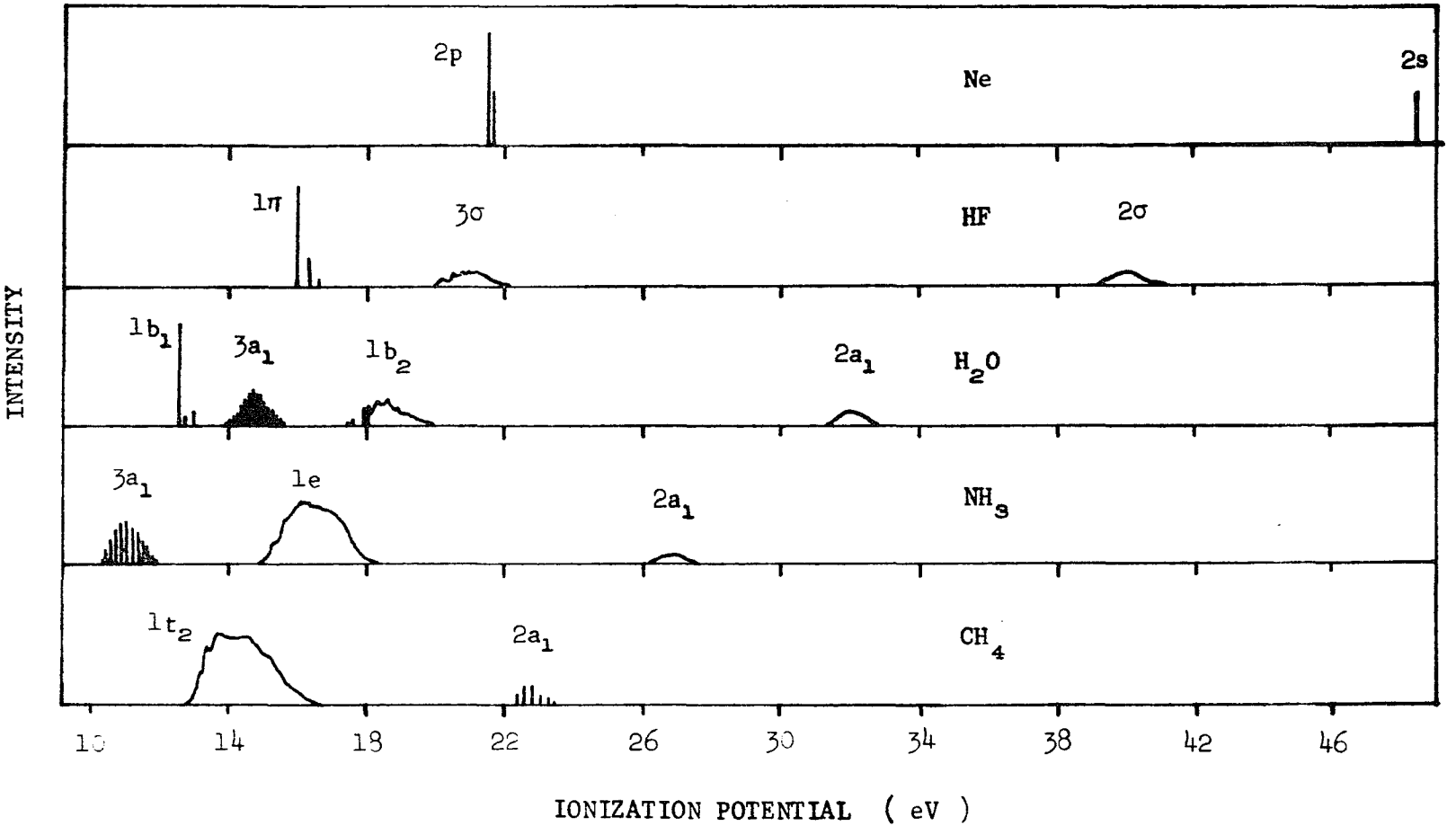
2p
Ne
2s
1π
3σ
HF
2σ
1b1
3a1
1b2
2a1
H2O
3a1
1e
2a1
NH3
1t2
2a1
CH4
INTENSITY
10
14
18
22
26
30
34
38
42
46
IONIZATION POTENTIAL (eV)

which imply chemical bonding. We treat these three types of orbitals separately on the basis of their different degrees of bonding.

Figure 2 shows a plot of n_o^* for non-bonding valence electrons against n_o^* for the atomic case. The ionization potentials for the inert gases and the halides were taken to be an average of the spin-orbit split doublets. There are several interesting features in this plot: First is the linearity exhibited by all HX, CH_3X, H_2Y, and $(CH_3)_2Y$ groups, where X represents Group VII elements F, Cl, Br, and I, while Y represents Group VI elements O, S, Se, and Te. Second, the deviations of HX from the inert gases (IG) is effectively one half of those for H_2Y and an identical relationship exists for deviations of CH_3X and $(CH_3)_2Y$. Furthermore, the deviations of CH_3YH is the sum of the deviations of HX and CH_3X. The numerical data are given in Table 1, where we use the definition

$$\delta n^*_{on}(\text{molecule}) \equiv n^*_{on}(\text{molecule}) - n^*_o(\text{IG}) \qquad (10)$$

and where the subscript n denotes a non-bonding orbital.

From Figure 2 and Table 1, we conclude that we have a useful definition of n^*_{on} and that the substituent effect is dramatically evinced in terms of n^*. A close inspection of Figure 1 reveals a parallelism between the shifts of the sub-shell 2s orbital and the 2p non-bonding orbital. Upon

Figure 2. n^*_{on}'s of HX, CH_3X, H_2Y, CH_3YH and $(CH_3)_2Y$, where $X \in \{F, Cl, Br, I\}$ and $Y \in \{0, S, Se, Te\}$, are plotted against n^*_{op}'s of Ne, Ar, Kr and Xe.

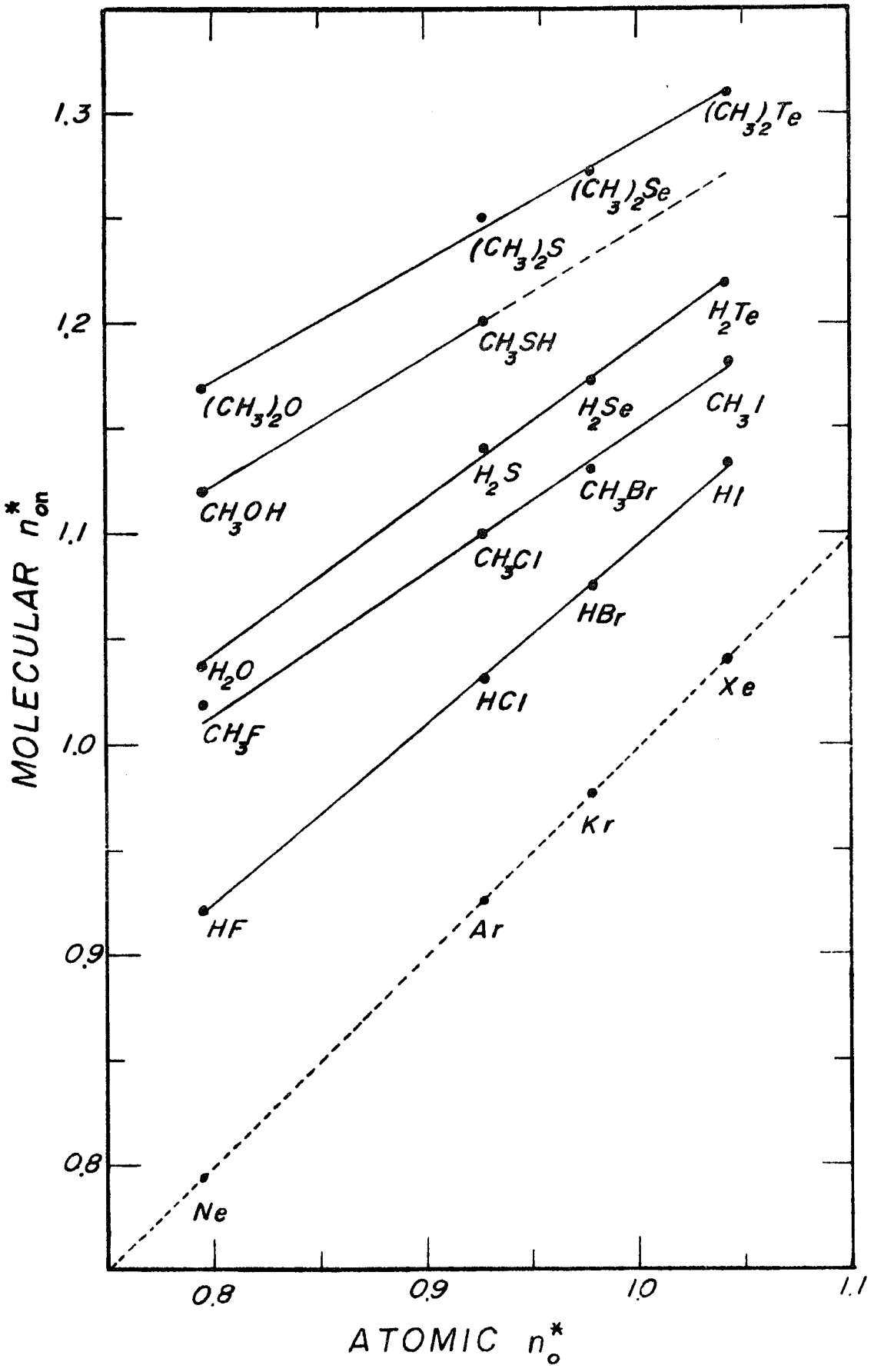
MOLECULAR n^*_{on}
ATOMIC n^*_o
1.3
1.2
1.1
1.0
0.9
0.8
0.8
0.9
1.0
1.1
$(CH_3)_2Te$
$(CH_3)_2Se$
$(CH_3)_2S$
CH_3SH
$(CH_3)_2O$
H_2Te
H_2Se
CH_3I
H_2S
CH_3Br
CH_3OH
HI
CH_3Cl
HBr
H_2O
HCl
Xe
CH_3F
Kr
HF
Ar
Ne

TABLE 1

SUBSTITUENT EFFECTS FOR GROUP VI AND VII MOLECULES

X	$\delta n^{*}_{on}(HX)$	$\delta n^{*}_{on}(CH_3X)$
F	0.128[a]	0.225[d]
Cl	0.105[b]	0.172[e]
Br	0.097[c]	0.150[e]
I	0.092[c]	0.141[e]

Y	$\delta n^{*}_{on}(H_2Y)$	$\delta n^{*}_{on}(CH_3YH)$	$\delta n^{*}_{on}(CH_3YCH_3)$
O	0.245[f]	0.326[g]	0.376[h]
S	0.212[g]	0.273[g]	0.323[i]
Se	0.195[g]		0.295[i]
Te	0.180[g]		0.270[i]

a) Ref. 12.

b) Ref. 13.

c) Ref. 14.

d) Ref. 15.

e) Ref. 16.

f) Ref. 17.

g) Ref. 18.

h) Ref. 2a.

i) Ref. 19.

converting the ionization potentials of the 2s orbitals[11] of HF, H_2O, NH_3, and CH_4 into n^*_{os}, we obtain the following numbers

	Ne	HF	H_2O	NH_3	CH_4	
IP(eV)	48.47	39.0	32.2	27.0	22.91	
n^*_{os}	0.530	0.591	0.650	0.710	0.771	
δn^*_{os}	-----	0.061	0.120	0.180	0.241	(11)

The difference between successive substitutions is almost exactly 0.060. This incremental behavior suggests a relatedness among n_{os} for these molecules and Ne.

For the σ-bonding orbitals, the effective quantum numbers, $n^*_{o\sigma}$, are related to each other rather than to Ne. Using $n^*_{o\sigma}(HX)$[12,13,14] as a standard and comparing them with those of the other groups via the definition

$$\delta n^*_{o\sigma}(\text{molecule}) \equiv n^*_{o\sigma}(\text{molecule}) - n^*_{o\sigma}(HX) \qquad (12)$$

we obtain Figure 3. With the exception of NH_3, we again find linearity and near-parallelism for each group of molecules.

It is evident that, by defining an n^*_o for valence-shell orbitals, we have attained an effective mode of comparison.

Figure 3. $n^*_{o\sigma}$'s of the σ-bonding orbitals of the hydrides of Group IV, V and VI elements are plotted against $n^*_{o\sigma}$'s of HX, X∈{F, Cl, Br, I}. (Data for HF, HCl and H_2O are from References 12, 13 and 17, respectively. Those for HBr and HI are from Ref. 14. For H_2S, H_2Se and H_2Te, they are from Ref. 18. And, for Group IV and Group V hydrides, they are from References 11 and 20, respectively.)

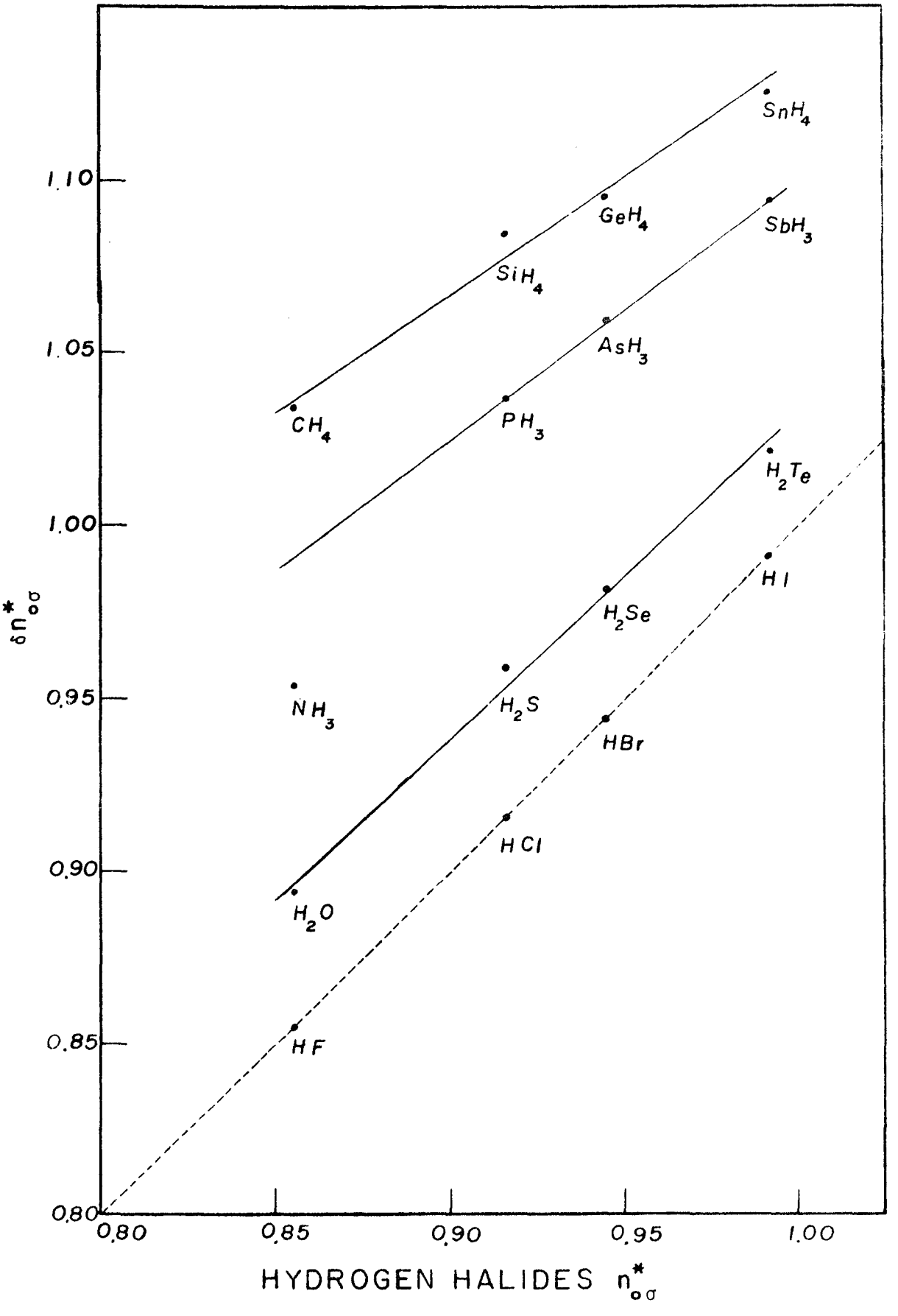
1.10
1.05
1.00
0.95
0.90
0.85
0.80
$\delta n^*_{o\sigma}$
SnH_4
GeH_4
SbH_3
SiH_4
AsH_3
CH_4
PH_3
H_2Te
HI
H_2Se
NH_3
H_2S
HBr
HCl
H_2O
HF
0.80
0.85
0.90
0.95
1.00
HYDROGEN HALIDES $n^*_{o\sigma}$

B. n^*_{-1} for Molecules

It is known[6] that the inner-shell binding energies of an atom in a molecule undergo changes which depend on the way in which the other atoms in the same molecule are attached to it. We expect these chemical shifts to follow the pattern of the non-bonding valence-shell substituent effects. Both types of deviation can be attributed to the effects on an essentially atomic orbital produced by the surrounding substituents (which act primarily as electrostatic charges). The only available data refer to H_2O and H_2S[6]. If we define

$$\delta n^*_{-1s}(H_2Y) \equiv n^*_{-1s}(H_2Y) - n^*_{-1s}(IG) \ , \tag{13}$$

we obtain the following numbers

	Ne	Ar	H_2O	H_2S	
n^*_{-1s}	0.125	0.204	0.159	0.241	
$\delta n^*_{-1s}(H_2Y)$	-----	-----	0.034	0.037	(14)

Although the evidence is sparce, it nevertheless shows the group behavior we are anticipating.

C. $n^*_{j\ell}$ for Molecular Rydberg States

The substituents influence Rydberg orbitals in a different manner than they do the valence- or inner-shell

orbitals. In the latter two cases, the orbital is encompassed by the substituents. For a Rydberg orbital, the substituents are a part of the total charge distribution of the core which influences the Rydberg orbital, primarily through the anisotropic potential $V_m(\vec{r})$. Depending on the anisotropy and the range of this potential, $n^*_{j\ell}$ can be shifted one way or the other. Hence, substituent effects for Rydberg states should be studied by observing the trend of the changes in $n^*_{j\ell}-n^*_{(j-1)\ell}$ $(j>0)$ from the chromophore to the substituted molecule. This will be discussed in Chapter Three. Meanwhile, we will investigate the topic of molecular precursors in the next section.

III. PRECURSORS FOR MOLECULES

We studied the relationship between n^*'s of atoms and molecules in the preceeding section. Such relations, being restricted to the same $n_{j\ell}$ sub-shell, were adequate to the task of unmasking substituent effects and chemical shifts. The vertical correlation between different $n_{j\ell}$'s represents another kind of comparison between atomic and molecular cases. Namely, we now link the effects of atomic precursors and molecular precursors together for comparison.

Unlike atomic instances, a precursor to a molecular orbital is hard to define. Especially for valence-shell orbitals, the extensive splitting makes the task of obtaining $\Delta n^*_{j\ell}$ very difficult. The loss of ℓ as a characterization index for the valence orbital further impedes study.

For Rydberg states, obtained via the excitation of an electron from a bonding orbital to a Rydberg orbital it is probably correct to regard the former orbital as the only real precursor. The bonding orbital, after all, has no identificable inner-shell analogue. Thus, for Rydberg states of this nature, we can only rely on the corresponding $n^*_{o\ell}$ and $n^*_{j\ell}$ values in correlating them. Any comparison with atoms appears to be infeasible, but comparison with similar molecules might be helpful. For a non-bonding orbital, we may still retain the ℓ quantum number and regard all other orbitals of all $n_{j\ell}$ subshells with $j<0$ as

its precursors. Rydberg states attained by exciting a non-bonding electron into the corresponding Rydberg orbitals share the same real precursors as the non-bonding orbital plus the non-bonding orbital itself as a real precursor if it is still occupied.

The building-up scheme for molecular $n^*_{j\ell}$ values from K- or L-shell values can not be developed as completely as the atomic case in Chapter One. This unfortunate situation is caused primarily by the lack of adequate data. The required data can be summarized as follows: First, the inner-shell binding energies of a large number of related molecules; second, a compilation of chemical shifts as functions of substituents; and, third, reliable Rydberg states assignments. The two former types of data can be obtained by ESCA.[6] The third task proves to be the most difficult problem.

The available data for the hydrides of the Group IV, V, VI, and VII elements are presented in Table 2. These two tables, 2A and 2B, are shown for the purpose of illustrating the precursor concept for molecules. The symbol n^*_{ob} refers to the effective quantum number of the slightly bonding orbitals of H_2Y and ZH_3 with $Z \in \{N, P, As, and Sb\}$ (see Figure 1).

From Table 2B, we can see that the general agreements for specific n* differences are very good. Especially, we would like to point out the following: The Δn^*_{-1s} values

TABLE 2A

EFFECTIVE QUANTUM NUMBERS FOR MOLECULES[a,b]

	n^*_{-1s}	n^*_{-1p}	n^*_{os}	n^*_{o}	n^*_{ob}	n^*_{on}	n^*_{1s}
Ref.	6	21	14	11	11	11	22
HF			0.591	0.844[c]		0.921[c]	
HCl		0.256	0.728	0.915[d]		1.032[d]	2.001
HBr			0.747	0.944[e]		1.075[e]	2.008
HI			0.792	0.991[e]		1.133[e]	2.000
H_2O	0.159		0.650	0.894[f]	0.994[f]	1.038[f]	1.963[g]
H_2S	0.241	0.282	0.783	0.959	1.032	1.140	
H_2Se			0.805	0.982	1.048	1.174	
H_2Te			0.855	1.022	1.082	1.220	
NH_3	0.183		0.710	0.953	1.158		
PH_3		0.314	0.846	1.038	1.167		
SnH_3			0.846	1.060	1.173		
SbH_3			0.887	1.093	1.196		
CH_4	0.216		0.780	1.038[h]			
SiH_4		0.356	0.871	1.083[h]			
GeH_4			0.864	1.095[h]			
SnH_4			0.903	1.125[h]			

a) For nomenclature, see text and Chapter 1
b) Except for n_op shell, all values are for configuration centers.
c) Ref. 12.
d) Ref. 13.
e) Ref. 14.
f) Ref. 17.
g) This work, Chapter 4.
h) Ref. 20.

TABLE 2B

DIFFERENCES IN n* FOR MOLECULES[a]

	Δn^*_{-ls}	$n^*_{os}-n^*_{-lp}$	$n^*_{o}-n^*_{os}$	$n^*_{ob}-n^*_{os}$	$n^*_{on}-n^*_{os}$	Δn^*_{ls}
HF			0.258		0.330	
HCl		0.472	0.187		0.304	1.273
HBr			0.197		0.328	1.261
HI			0.199		0.341	1.208
H_2O	0.491		0.244	0.344	0.376	1.301
H_2S	0.542	0.501	0.176	0.249	0.357	
H_2Se			0.177	0.243	0.369	
H_2Te			0.167	0.227	0.365	
NH_3	0.527		0.243	0.448		
PH_3		0.532	0.192	0.321		
AsH_3			0.214	0.327		
SbH_3			0.206	0.309		
CH_4	0.564		0.256			
SiH_4		0.515	0.212			
GeH_4			0.231			
SnH_4			0.222			

a) Δn^*_{-ls} and Δn^*_{ls} were defined in Chapter One.

have an average of 0.531 ± 0.031, which is very similar to the inert gas value of 0.470 ± 0.045 (Chapter One). For Δn^*_{1s}, the molecular value is 1.261 ± 0.039 and the corresponding atomic value is 1.130 ± 0.005. The deviation is ~0.13. The smaller deviation of Δn^*_{-1s} indicates that the chemical shift of $n_{-1}s$ and the substituent effect on $n_o s$ are of the same sign and similar magnitude. The column of $n^*_{os}-n^*_{-1p}$ also illustrates this parallelism between inner-shell and valence-shell shifts. The larger deviation of Δn^*_{1s} indicates that the $n_1 s$ orbital sees the substituents differently. The accumulated shifts of $n_o s$ and $n_1 s$ are contained in the following difference

$$n^*_{1s} - n^*_{-1s} = 0.531+1.261 = 1.792 \qquad (15)$$

Providing n^*_{-1s} is available for a molecule, we can predict its n^*_{1s} from Eq. (15). From Table 2A, we have $n^*_{-1s} = 0.159$ for H_2O. The estimated n^*_{1s} is 1.951 in good agreement with the experimental value of 1.963.

The columns of Table 2B which involve different orbitals from the n_o shell demonstrate the influence of chemical bonding. For example, the column of $n^*_{o\sigma}-n^*_{os}$ shows different values for different groups of molecules, although the values within any one group do remain fairly constant. Nonetheless, this column is quite different from the other two. The second row molecules, HF, H_2O, NH_3, and

CH_4 have larger values between n^*_{os} and the split n^*_{op}'s (see columns 4, 5 and 6). This can be rationalized as follows: The n_op orbital for those molecules is ~2p and has no precursor in the inner-shell. Molecules in the third, fourth and fifth rows already have n_jp ($j<0$) precursor(s); hence, their values tend to stabilize.

Tables 2A and 2B demonstrate the plausibility of correlating the inner-shell, valence, and Rydberg orbitals of molecules by using concepts of precursor, chromophore, substituent, and chemical bonding which are framed in an effective quantum number context.

The binding energies used in constructing Table 2 correspond to different molecular conformations. For inner-shells, the vertical (or ground state fixed geometry, D_v) values are used. For valence and Rydberg states, the adiabatic (or equilibrium geometry, D_{eq}) values are used. D_v for inner-shell states is identical to D_{eq} of non-bonding valence states and Rydberg states excited from non-bonding orbitals. For bonding valence states and corresponding Rydberg states, it is quite different. Next section will discuss this in detail.

IV. GEOMETRY DEPENDENCE OF MO's

As mentioned in the Introduction, a molecular orbital changes its character with change of molecular geometry. This effect is completely absent in the inner-shells since the geometry change influences the magnitude of the chemical shift and not the orbital character. In the valence- and outer-shell, geometry changes may produce major changes. In order to correlate states of various $n_j\ell$ within the same molecule, with other molecules, or with atoms, it is imperative to investigate this question further.

The question of how to correlate a molecular state with an atomic state centers around the choice of a certain conformation for the molecule. The Rydberg formula (Chapter One)

$$\nu_{j\ell} = IP - \frac{RQ^2}{(n^*_{j\ell})^2} \tag{16}$$

dictates an alignment of all states relative to the ground state. Thus, the ground state conformation appears to be the natural choice. Furthermore, almost all theoretical calculations use the ground state geometry as a standard and express all transitions in a fixed ground state geometric frame. Unfortunately, this choice proves to be inappropriate.

A molecular Rydberg state can be envisioned as the combination of a core with charge Q and an electron in a bound state. This electron, being in a Rydberg orbital, exerts little influence on the geometric arrangement of the core. So, the core has a geometry essentially identical to the corresponding ion with charge Q. Experimentally, this means that the Franck-Condon pattern of the Rydberg transition in the absorption spectrum is very similar to the photoelectron spectrum (PES). The n_o^* corresponding to the ionization event in PES is related to the energy difference between the ground state and the ionic state. Depending on the value of $\vec{D}$ we choose for the ionic state, the energy difference and, hence, the value of n_o^* will be different. For Rydberg states, the same $\vec{D}$ chosen for the ionization limit must be used to obtain the value of n*. Otherwise, we would correlate effective quantum numbers corresponding to different geometries.

We can regard the combination of a Rydberg electron and the core as a scattering problem, with the latter as the target. The electron can be viewed as moving in the field of a core which possesses an ionic state geometry. The resulting binding energy determines which Rydberg state the system is in. Since the core remains in the same geometric framework regardless of the movement of the electron, it is logical to treat the core as if it exhibited a fixed D_{eq} which is characteristic of the ionic state.

Thus, we can refer the binding energies of the electron in various Rydberg orbitals to a fixed D_{eq} of the core. The choice of D_v seems to be unreasonable for this situation.

If the Franck-Condon patterns for Rydberg states and the ionic state are identical, the binding energy expressed with reference to either D_{eq} or D_v will be the same. However, the Franck-Condon pattern is a sensitive function of the geometry change which occurs during an electronic transition. A small difference in the geometries of a Rydberg state and the ionic state is capable of causing the corresponding Franck-Condon patterns to have their maxima at very different vibrational levels. Depending on the magnitude of the vibrational frequency, the resulting energies could be large enough to produce discrepancies in the correlation of n*. Furthermore, if more than one vibrational mode is excited, we may not have a single maximum in the Franck-Condon envelope. This undoubtedly will further impede any correlative effort.

According to the above discussion, D_{eq} is the better choice of geometric framework for determining n* for both Rydberg and ionic states. For inner-shell or non-bonding valence-shell orbitals, vertical and adiabatic energies are coincident. Hence, no difficulty occurs. For bonding or slightly bonding orbitals, even though it may be troublesome to obtain the real origin. One way to avoid this trouble is to measure the inner-shell excitations.

The resulting spectrum consists of vertical Franck-Condon envelopes only. This topic is pursued in the following section.

V. INNER- AND VALENCE-SHELL EXCITATIONS

The advantages of using inner-shell excitation spectra instead of the conventional valence-shell spectrum is manifold. The removal of an inner-shell electron has very little effect on the molecular geometry. The result is a simple clear spectrum with vertical Franck-Condon transition envelopes. There is no difficulty in correlating different states within the same molecule, or similar states of different molecules, since the geometry dependence of the MO constituents can be eliminated by comparison in a fixed geometric frame. Furthermore, excitation from an essentially atomic inner-shell orbital produces a spectrum consisting of much fewer electronic bands than does the valence-shell excitation (which is complicated by the split of the valence orbitals and the variety of possible transitions resulting from them).

The disadvantage of inner-shell excitations are twofold. First, the energy region corresponding to this kind of experiment lies deep in the far vacuum-ultraviolet or even soft X-ray range. Suitable light or electron sources and adequate resolution are the major limitations. In addition, auto-ionization, photoionization and photodissociation processes can complicate these spectra considerably.

For valence-shell excitations, experimental facilities with very high resolution are commonplace. The competition

between discrete transitions and other processes is relatively minor. The only drawback is the complexity of the spectrum. Transitions originating from different valence orbitals interfere with one another in the form of overlapped bands, and perturbations due to configuration mixing are common. Non-vertical Franck-Condon envelopes are more the rule than the exception and this makes the interpretation very difficult indeed.

The best way appears to consist of a combination of inner-shell and valence-shell excitation spectra. However, one must be cautious in doing so. The excitation from an inner-shell orbital corresponds to the average of excitations from all split valence-orbitals. For example, H_2O has three split 2p orbitals: $2b_2$, $3a_1$, and $1b_1$ (see Figure 1). They are, respectively, σ-bonding, slightly bonding and non-bonding. We can excite one electron to the $3sa_1$ orbital in five different ways. The elctron can be from the oxygen 1s and 2s orbital, or, it can be from one of the three split 2p orbitals. We get the following results (four cases only)

Transitions	n^*_{1s}	n^*_{op}	n^*_{1s}
a) $1sa_1$; $\tilde{X}^1A_1 \rightarrow 3sa_1$; $^1A_1$	0.159		1.89
b) $1b_1$; $\tilde{X}^1A_1 \rightarrow 3sa_1$; $^1B_1$		1.038	1.963
c) $3a_1$; $\tilde{X}^1A_1 \rightarrow 3sa_1$; $^1A_1$		0.994	1.621
d) $1b_2$; $\tilde{X}^1A_1 \rightarrow 3sa_1$; $^1B_2$		0.894	unknown

where n^*_{-1s} and n^*_{op} are from Table 2, the rest are from Chapter Four. Note that the 3s effective quantum numbers are different for the various types of excitation. The value 1.89 from transition (a) of Eq. (17) should correspond to the average center of the values from the three valence transitions. In other words, if we can properly average the $1b_2$, $3a_1$, and $1b_1$ orbitals and excite an electron from this averaged orbital, the resulting 3s should have $n^*_{1s} = 1.89$. From Table 2, we have $\Delta n^*_{1s} = 1.24$. A similar experimental datum for H_2S is also available.[21] The excitation to n_1s orbital was originated from the n_{-1p} shell. The resultant n^*_{1s} is 2.05 and Δn^*_{1s} is 1.27, which compares very favorably with the H_2O value. The n^*_{1s} value of H_2O listed in Table 2 is 1.963 instead of the average value because such inner-shell excitation results are very scarce for other molecules.

The above results for H_2O and H_2S are very interesting. It is thought that these two molecules have no intravalence transitions and their first excited state is an n_1s Rydberg state.[2a] Although the corresponding transitions in the VUV are very broad and show no resemblence to the PES Franck-Condon envelope, it is generally agreed that they are excitations to the n_1s state.[2a] However, the respective n^*_{1s} values for H_2O and H_2S are 1.62 and 1.78, and are very abnormal compared with $n^*_{2s} = 2.94$ and 2.97, respectively. So, it is possible that the "real" n_1s

states are perturbed to such an extent that transitions to them carry very little intensities (see Chapter Four). Thus, we believe that the existing assignments are wrong. In any event, inner-shell excitation spectra unequivocally prove the existence of normal n_1s states for H_2O and H_2S.

We have demonstrated the advantage of comparing inner- and valence-shell excitation spectra. It is believed that as experimental facilities improve and the inner-shell excitation spectra of molecules become more abundant, many of the problems of molecular Rydberg states will be solved. However, it is possible that the inner-shell spectrum of a molecule will turn out to be more complicated than the valence-shell version. Competing processes such as those mentioned earlier, together with various relaxation mechanisms, can distort the spectrum and render any comparison impossible. When this occurs, the only simple means of studying Rydberg states will be valence-shell spectroscopy.

As indicated earlier, there is no reliable rule for obtaining the average center of split molecular orbitals. Nor are inner-shell values for n* always available. Hence, we propose to study the valence-shell spectrum by utilizing the values of $n^*_{o\ell}$ for the split valence MO subset. If regularity of $\Delta n^*_{j\ell}$ exists for values of $n^*_{o\ell}$ derived by this means, we can forego any examination of precursor, substituent, or chemical shift effects.

In order to do this, we must carefully divide the valence orbitals into groups depending on the type and the degree of bonding which they exhibit. Then, for each group, we must develop $\Delta n^*_{j\ell}$ differences which are characteristic for the whole group.

VI. $\Delta n^*_{j\ell}$ FOR MOLECULAR RYDBERG STATES

As evidenced in Figures 2 and 3, orbitals with different bonding characteristics can be correlated with each other. Non-bonding orbitals can be connected with atomic orbitals and bonding orbitals can be linked with each other. In ordinary molecules, we can categorize bonding orbitals as "slightly-bonding", "π-bonding" and "σ-bonding". In this section, we will discuss the "slightly bonding", the σ-bonding, and the "non-bonding" MO's. The "π-bonding orbitals" will be investigated in Section VII.

A. σ-Bonding Orbitals

The σ-bond is the most common bond. Almost every ordinary molecule possesses one. It possesses the highest binding energy of all chemical bonds. As a result, excitations involving σ-bonding orbitals lie at quite high energy. If a molecule contains other types of valence orbital, the σ-orbital excitations may well mix with those of the other valence orbitals. Since removing a σ electron is traumatic, the resulting Franck-Condon envelopes will be non-vertical and very broad. Consequently, they are not easy to analyze.

All these factors produce a scarcity of reliable data for σ excitations. We present only those for H_2, HCl,

HBr, and CH_4.

1) H_2 is the simplest prototypical molecule. Experimental studies of H_2 are plentiful. Highly-detailed analyses of its spectra[23] provide a great deal of understanding. We will focus our attention only on the lowest-energy excited states.

The united atom of H_2 is He. The ground state MO of H_2 is

$$\Psi \sim 1s_1 + 1s_2 \tag{18}$$

It seems that the first excited state MO should be

$$\Psi' \sim 1s_1 - 1s_2 \tag{19}$$

which is an antibonding orbital. The next MO, according to comparison with He, should be 2s (or n_1s). Thereafter, we should find $n_1p\pi$, $n_1p\sigma$, $n_1d\sigma$,... . Contrary to this, Mulliken[4] suggested that the lowest excited state was $n_1p\sigma$, $^1\Sigma_u^+$, rather than of the antibonding state Ψ' [see Eq. (19)]. He observed that the calculated MO of lowest energy looked like $2p\sigma$ at D_{eq} and tended towards $1p\sigma$(?) as $D \to 0$. Only when D was large, did this orbital resemble the antibonding Ψ' of Eq. (19).

This analysis raises several unsettling questions: First, the experimentally observed first excited state has

a vibrational frequency of ~1320 cm^{-1}. Compared with ~2200 cm^{-1} for higher npσ states and for the cationic $^2\Sigma_g^+$ state, it is obvious that the state in question has a very different geometry from the rest of the np Rydberg series. The much smaller vibrational frequency indicates less bonding strength. Its triplet counterpart $^3\Sigma_u$ is also known[23d] to be highly repulsive. All these facts suggest antibonding characteristics. Second, while 2pπ[23a] lies very close to 2sσ[23e], the "alleged" 2pσ is lower than 2sσ by ~1.11 eV, which is a bit too much. The average center of 2pσ and 2pσ is, in fact, lower than 2sσ, which is contradictory to the case of He.

We propose to use the n* correlation to investigate the plausibility of Mulliken's assignment for the lowest excited state. Δn^*_{1s} and $n^*_{1p}-n^*_{os}$ of H_2 are compared with He and Be in the following:

	Δn^*_{1s}	$n^*_{1p}-n^*_{os}$
He	0.982	1.211
Be	1.002	1.161
H_2	1.033[23]	1.194[23]
H_2 (Ref. 4a)	--	1.043[23]

(20)

By assuming that the lowest excited state is the antibonding valence state and that the assigned "3pσ" is the real 2pσ, we find an average center for 2pσ; $^{3,1}\Sigma$ and 2pσ; $^{3,1}\Pi$, which gives $n^*_{1p}-n^*_{os}$ = 1.194. If we use the existing

assignment, the difference is 1.043. By inspection of Eq. (20), we see that the $2s\sigma$ state gives $\Delta n^*_{1s} = 1.033$ which is very similar to the values for He and Be. The $n^*_{1p}-n^*_{os}$ value for H_2 , 1.194, is in good agreement with 1.211 of He and 1.161 of Be. The old assignment gives a center with $n^*_{1p}-n^*_{os} = 1.043$, which is quite deviant from the atomic values. Since H_2 has only a real precursor of s type, as do He and Be, there is no reason for $n^*_{1p}-n^*_{os}$ to deviate much from the average value. Therefore, based on this n* correlation, we favor the assignment of the lowest excited state of H_2 as the intra-valence antibonding state.

2) HCl and HBr

The σ bond for HX is a mixture of 1s(H) and np(X). There is no equivalent atomic case. Consequently, we merely present the data and demonstrate the constancy of $n^*_{2s}-n^*_{o\sigma}$ and $n^*_{1p}-n^*_{o\sigma}$. Terwillinger and Smith[24] reported autoionization Rydberg states corresponding to excitation of σ electrons for HCl and HBr.[24] We converted their data as follows:

	$n^*_{o\sigma}$	n^*_{2s}	n^*_{1p}	$n^*_{2s}-n^*_{o\sigma}$	$n^*_{1p}-n^*_{o\sigma}$
HCl	0.916	2.795	2.322	1.879	1.406
HBr	0.944	2.748	2.349	1.804	1.405

(21)

Note that they only observed the n_2s states. If we assume constant quantum defects, we find $n^*_{1s}-n^*_{o\sigma} = 0.88$ and 0.80 for HCl and HBr, respectively.

The constancy of $n^*_{1p}-n^*_{o\sigma}$ suggests that σ-orbital excitation follows n* correlation attitudes.

3) CH_4 Molecule

The observed spectrum for methane gives $n^*_{o\sigma} = 1.038$[20] and $n^*_{1s} = 1.868$.[2a] Thus, we have $n^*_{1s}-n^*_{o\sigma} = 0.830$, which agrees with the extra-polated values for HCl and HBr.

From the results for HCl, HBr and CH_4, we can see that their σ-orbital excitations behave similarly to each other as far as n* differences are concerned. Furthermore, these differences are similar to the non-bonding values (see Section VI-C).

B. Slightly Bonding Orbitals

We can discuss only two groups of molecules: The H_2Y and the ZH_3 groups. For the former, n^*_{ob} of Table 2 refers to the value for the $3a_1$ or $4a_1$ orbital of H_2O or H_2S, respectively. For ZH_3, the orbital in question is the highest occupied orbital in the ground state. Excitations from this type of orbital cause the molecule to open up its bonding angle. Therefore, the corresponding Franck-Condon patterns show long progressions of bands (see Figure 1). An examination of $n^*_{1s}-n^*_{ob}$ reveals a striking regularity which is characteristic for this type of orbital. The

following data clearly show the effectiveness of the n* difference criterion:

	n^*_{ob}	$n^*_{1s}-n^*_{ob}$	
H_2O	0.994	0.626	
H_2S	1.032	0.621	
NH_3	1.158	0.594	
PH_3	1.167	0.593	
AsH_3	1.173	0.602	(22)

C. Non-Bonding Orbitals

In Table 2, we have already shown some results for HX and H_2O. Here, we also present results for CH_3X and compare them with inert gases. The data for HX are from Ref. 22. Those for the atoms are from Chapter One. Values are for configuration centers, except for H_2O and H_2S and n_1p for the halides.

	n^*_{on}	$n^*_{1s}-n^*_{on}$	Δn^*_{1p}
Ne	0.794	0.873	1.345
Ar	0.927	0.880	1.339
Kr	0.978	0.867	1.341
Xe	1.041	0.849	1.343

(continued)

	n^*_{on}	$n^*_{ls}-n^*_{on}$	n^*_{lp}	
H_2O	1.038	0.925	1.281	
H_2S	1.140	---	1.297	
HCl	1.032	0.969	1.248	
HBr	1.075	0.933	1.231	
HI	1.133	0.867	1.217	
CH_3Cl	1.100	0.834	1.278	
CH_3Br	1.130	0.810	1.264	
CH_3I	1.181	0.814	1.268	(23)

The Δn^*_{lp} column shows apparent constancy for all molecules, but the values of the $n^*_{ls}-n^*_{on}$ column tend to separate into two distinct groups. For HX and H_2Y , they are ~0.93 and for CH_3X, ~0.82, whereas the inert gas value of ~0.86 lies inbetween. We will provide explanations for this observation in Chapter Three.

VII. MULTICENTER CHROMOPHORES

As exemplified in earlier sections, molecules with a single-center chromophore can be correlated with their cognate atoms. Except for the valence orbitals, which are involved in chemical bonding, the comparison with atomic behavior is straightforward.

Although the bonding orbitals of single-center molecules can be regarded as multicenter orbitals, they can be bypassed in studying Rydberg states when inner-shell excitation spectra are available. However, for molecules with multicenter chromophores, like $CH_2{=}CH_2$, H_2CO, $CH{\equiv}CH$, etc. and their derivatives, there is no clearly related atom with which to make comparison. The inner-shell precursors are simply too difficult to decipher. Our correlative approach, as a consequence, relies mainly on valence orbitals and the effect of substitution on them. Rydberg states may be treated as having only one precursor; i.e. the valence orbital they originate from.

We will concentrate on two types of multicenter chromophores. One is the ethylene group and conjugated polyenes, the other is the monocarbonyls. The former has characteristic delocalized π-orbitals, the latter has non-bonding orbitals centered on the oxygen atom, but affected by the adjacent carbon in such a way as to behave differently from ordinary oxo-compounds.

A. Substituent Effects on n_o^*'s

Meeks et al.[25] observed substituent additivity in the ionization potentials (IPs) of monocarbonyls. We will try to establish similar additivity for values of n_{on}^* for the non-bonding orbitals. Of course, if additivity exists in one case, it need not hold in the other. For the purpose of collation, we include both types of substituent effects in our data.

Since there is no suitable atom to compare with, we choose formaldehyde, H_2CO, as the fundamental chromophore. Table 3 shows the substituent effects of CH_3 and C_2H_5 groups. Included in Table 3 are also the IPs in eV. The following data serve to clarify the difference in using n_{on}^* and IPs:

	Difference in n_{on}^*	Dev.	Difference in IP (eV)	Dev.
$H \rightarrow CH_3$	0.032 ± 0.003	9%	0.552 ± 0.089	16%
$H \rightarrow C_2H_5$	0.044 ± 0.003	7%	0.757 ± 0.086	11%

(24)

It is obvious that n_{on}^* is the superior quantity for expressing substituent effects on monocarbonyls.

For alkylethylenes, we present similar data depicting substituent effects in both n_{on}^* and IPs in Tables 4A and

TABLE 3

SUBSTITUENT EFFECTS ON MONOCARBONYLS[a,b]

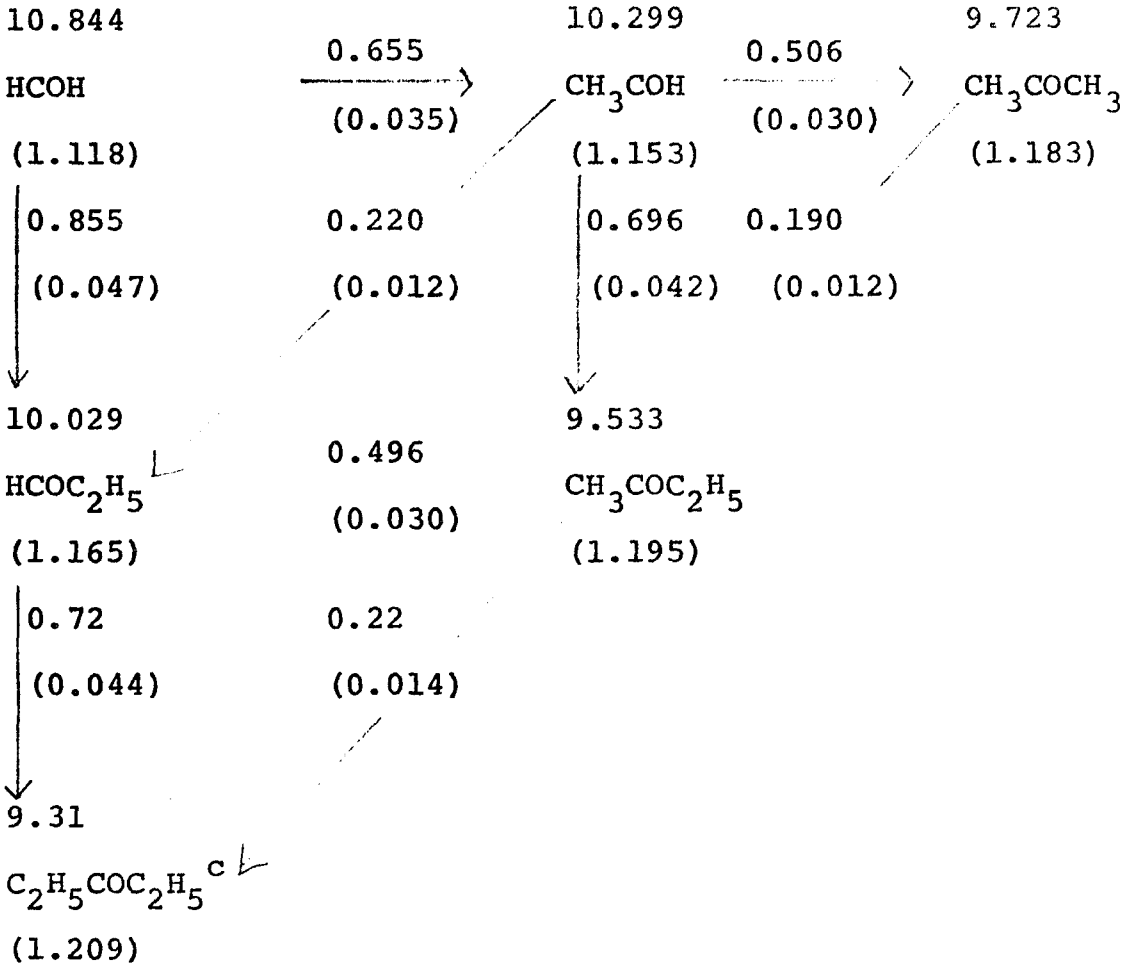

a) Data are from Ref. 2b.

b) Numbers in parentheses are n^*_{on}'s and their differences. Others are ionization potentials and difference between them (eV).

TABLE 4A

SUBSTITUENT EFFECTS OF ALKYLETHYLENES[a,b]

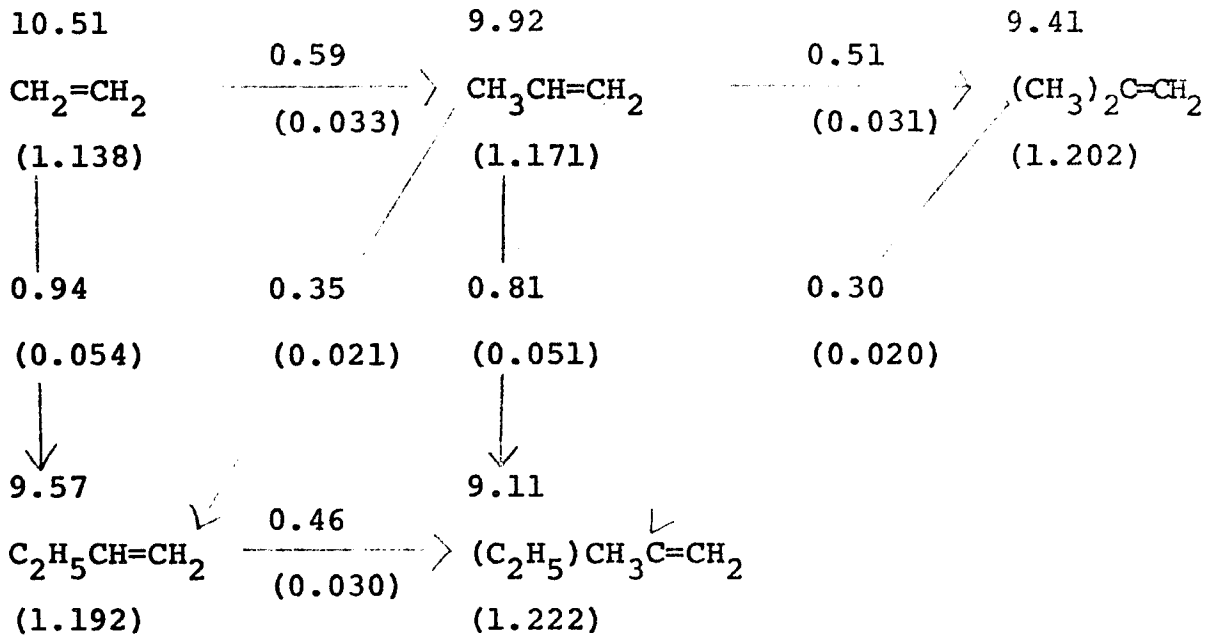

a) Data are from Ref. 2b.

b) Numbers in parentheses are $n^*_{o\pi}$'s and their differences dn^*_{on}. Others are ionization potentials and differences between them (eV).

and 4B. In Table 4A, the equivalent values for mono-carbonyls are exhibited. Table 4B shows a different type of substitution in which ethylene is substituted on both ends by alkyl groups. We combine results in Table 4A and 4B to get the following averages:

	Difference in $n^*_{o\pi}$	Dev.	Difference in IP(eV)	Dev.
$H \rightarrow CH_3$	0.033 ± 0.004	12%	0.52 ± 0.08	16%
$H \rightarrow C_2H_5$	0.052 ± 0.002	3%	0.88 ± 0.07	7%

(25)

The values for methyl substitution of carbonyls and ethylenes are about the same, whereas ethyl substitution effects for ethylenes are larger than for carbonyls. This is of interest because the orbitals involved for these two types of molecules are quite different. For carbonyls, it is the non-bonding orbital localized on the oxygen atom which is of interest here. For ethylenes, it is the delocalized π-orbital which is of interest. The similarity of methyl substitution effects may indicate that the methyl group acts primarily as a point charge and exerts only an electrostatic force on the chromophore. The difference of ethyl substitution effects may imply that the ethyl group is too large to be regarded as a point charge and that, as a result, its influence on the delocalized π-orbital is

TABLE 4B

SUBSTITUENT EFFECTS ON ALKYLETHYLENES[a,b,c]

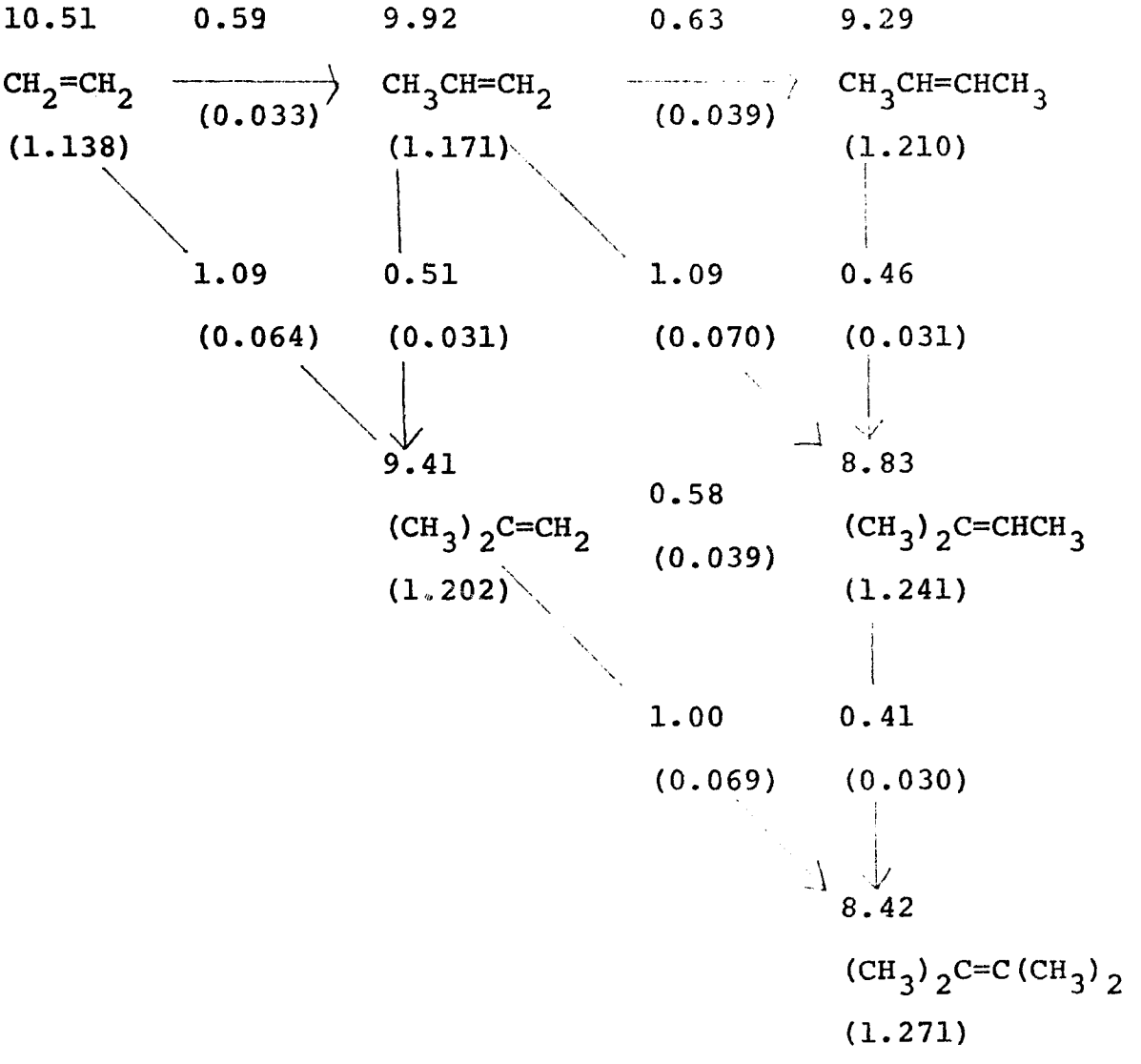

a) Data are from Ref. 2b.

b) Numbers in parentheses are $n^*_{o\pi}$'s and their differences. Others are ionization potentials and difference between them (eV).

c) Values for $CH_3CH=CHCH_3$, are for the cis-conformation.

larger than on the non-bonding localized orbital of the oxygen atom.

Note also that, in Table 4B, the substitution of a methyl group to the second end of the already substituted π-bond creates a change of 0.039 in $n^*_{o\pi}$, which is a much larger change than for all other methyl substitutions. This suggests the relative vulnerability of the delocalized π-orbital to substitution effects.

B. Rydberg States of the Monocarbonyls

Since the carbonyl group possesses a non-bonding orbital, we should expect its n_1s Rydberg state to behave much as for the atomic case. From Eq. (23), we have the following inert gas average:

$$n^*_{1s}-n^*_{op} = 0.867\pm0.013 \qquad (26)$$

The data for monocarbonyls are given in Table 5. The overall value of $n^*_{1s}-n^*_{on}$ is very similar to that for the inert gas. The substitution of CH_3 or C_2H_5 increases the n* difference, with the latter giving larger increments. The di-C_2H_5-substituted molecule has the largest difference.

C. Rydberg States of Alkylethylenes

The highest occupied MO in the ground state of the alkylethylenes is the π-orbital. The delocalization of the

TABLE 5

RYDBERG STATES OF MONOCARBONYLS[a]

Molecule	n^*_{on}	$n^*_{1s}-n^*_{on}$
H_2CO	1.118	0.780
CH_3CHO	1.153	0.844
$(CH_3)_2CO$	1.183	0.830
C_2H_5CHO	1.165	0.882
$CH_3COC_2H_5$	1.195	0.856
$C_2H_5COC_2H_5$[b]	1.201	0.905
Inert Gases[c]		0.867

a) Data are converted from energies in Ref. 2b.

b) Data for $C_2H_5COC_2H_5$ in Table 3 are adiabatic values. In this table, we use vertical values because the n_1s transition energy listed in Ref. 2b is also a vertical value.

c) See Eq. (26).

2p electrons makes comparison with atoms implausible. However, since these molecules exhibited similar substituent effects to the carbonyls, we may speculate that the $n^*_{1s}-n^*_{o\pi}$ difference is similar to the carbonyls and, thus, to the inert gas value also.

The available data are collected in Table 6. The differences in n* are indeed very close to the inert gas value. The slightly larger values belong to the ethyl-substituted or the both-ends-substituted molecules. As mentioned earlier, the $n^*_{o\pi}$ values for these molecules also yield abnormal substituent effects. We can argue that the π-systems in these molecules are distorted by the substituents and therefore, that their Rydberg states also deviate *from* the norm. Recall that the di-C_2H_5-substituted carbonyl also gave an abnormally high $n^*_{1s}-n^*_{on}$.

D. Conjugated Polyenes

We would like to investigate two important polyenes. The two molecules are trans-butadiene and benzene. Both of them possess conjugated π-systems.

For trans-butadiene, the ionization potential is 73115 cm^{-1}[27], or, equivalently, $n^*_{o\pi} = 1.225$. The lowest-energy assigned[2b] Rydberg state gives $n^*_1 = 2.374$ and $n^*_1-n^*_{o\pi} = 1.149$, which is far from the n_1s value of ethylene. If we assign the band at ~48000 cm^{-1} as the n_1s Rydberg state (instead of the commonly accepted valence state

TABLE 6

RYDBERG STATES OF ALKYLETHYLENES[a]

Molecule	n_o^*	$n_{1s}^*-n_o^*$
$CH_2=CH_2$	1.138	0.863
$CH_3CH=CH_2$	1.171	0.849
$(CH_2)_2C=CH_2$	1.202	0.848
$(CH_3)_2C=CHCH_3$	1.241	0.965
$(CH_3)_2C=C(CH_3)_2$	1.271	0.960
$C_2H_5CH=CH_2$	1.192	0.951

a) Data are converted from energies in Ref. 2b.

characterization), we get $n^*_{1s} \cong 2.090$ and $n^*_{1s}-n^*_{o\pi} \cong 0.865$, which is in excellent agreement with ethylene. Based on this, we suggest that the n_1s state for trans-butadiene lies at ~48000 cm^{-1}.

For benzene, the IP is 74587 cm^{-1}[28]. The corresponding $n^*_{o\pi}$ is 1.213. The accepted[2b] lowest-energy Rydberg state for excitation from a π-orbital is at 55881 cm^{-1} which gives $n^*_1 = 2.422$ and $n^*_1-n^*_{o\pi} = 1.209$. This is easily recognized as the n_1p Rydberg state [see Eq. (23)]. If we now reassign the band at 49920 cm^{-1}[29] as n_1s, we have $n^*_{1s} = 2.109$ and $n^*_{1s}-n^*_{o\pi} = 0.896$. According to this, we suggest that the band in question is n_1s state and not the valence $^1B_{1u}$ as usually assigned.[2b]

VIII. CONCLUDING REMARKS

We have extended the atomic correlation developed in Chapter One into the molecular realm. The criterion of n* differences, with some modifications, has been successfully applied to molecules. Specifically, we conclude the following:

-----The definition of chromophore and substituent simplified the molecular correlations. Substituent effects and chemical shifts were discussed on the same footing by assuming that the substituents were acting like electrostatic charges.

-----Molecular precursors were categorized into inner-shell and valence-shell types. The split of the valence orbitals forced the correlation to adopt a criterion involved with the degree of bonding. Anti-bonding orbitals were excluded from the correlative effort on the grounds that they are rarely occupied in the ground state. However, their tendency to interfere with Rydberg states was mentioned and we emphasize that further work is needed in order to characterize them.

-----Considerations of the geometry dependence of MO's resulted in the choice of adiabatic transition energies as the data correlating molecular Rydberg states. We also indicated the utility of inner-shell excitation spectra in solving problems of molecular Rydberg state assignments.

-----The n* difference rule based on valence-shell orbitals proved to be very useful. We applied this criterion to a number of molecules with single-center or multi-center chromophoric groups. We found many group characteristics as well as some discrepancies. For the latter, we have suggested alternative assignments.

-----Finally, we would like to link our attitude with the "quantum defect"[3] and the "term value"[2] criteria. Robin[2] asserts that the term value [Eq. (2)] of n_1s of a molecule lies between 22000 cm^{-1} and 34000 cm^{-1}, regardless of the type of orbital in which the excitation originates. The spread of the term value is 12000 cm^{-1} or $\sim$1.5 eV which covers quite a large spectral range. Consequently, the predictability is rather limited. The quantum defect criterion[3] states that $n^*_{1s} \tilde{=} 2$, which is essentially another way of stating what Robin proposes[2]: The term value limits correspond to $n^*_{1s} \tilde{=} 2.23$ and 1.80.

-----Our rule of $n^*_{1s} - n^*_{op} \tilde{=} 0.86$ combined with the limits of n^*_{1s} cited above gives us $n^*_{op} \tilde{=} 1.37$ and 0.94 which correspond to ionization potentials of 7.25 eV and 15.4 eV, respectively. It happens that the lowest IP's of the majority of molecules lie in this region. Thus, it is now obvious why the "quantum defect" or the "term value" criterion are often useful.

It is believed that our n* difference study will eventually solve the problem of identifying molecular

Rydberg states. The study on anti-bonding n_o^* values mentioned earlier should provide more support to our correlative work.

REFERENCES

1. A. B. F. Duncan, "Rydberg Series in Atoms and Molecules", Academic Press, New York, 1971.
2. a) M. B. Robin, "Higher Excited States of Polyatomic Molecules", Vol. 1, Academic Press, New York, 1974.
   b) M. B. Robin, "Higher Excited States of Polyatomic Molecules", Vol. 2, Academic Press, New York, 1975.
3. E. Lindholm, Arkiv Fysik 40 (1969) 97.
4. a) R. S. Mulliken, J. Amer. Chem. Soc. 86 (1964) 3183. b) 88 (1966), 1849. c) 91 (1969) 4615. d) J. Chem. Phys. 3 (1935) 506.
5. U. Fano, Comments At. Mol. Phys. 1 (1969) 140.
6. K. Siegbahn, C. Nordling, G. Johansson, J. Hedman, P. F. Heden, K. Hamrin, U. Gelius, T. Bergmark, L. O. Werme, R. Manne and Y. Baer, "ESCA Applied to Free Molecules", North-Holland Publishing Company, Amsterdam, 1969.
7. A. Temkin and K. V. Vasavada, Phys. Rev. 160 (1967) 109.
8. J. Tully and R. S. Berry, J. Chem. Phys. 51 (1969) 2056.
9. U. Fano, C. E. Theodosiou and J. L. Dehmer, Rev. Mod. Phys., to be published.

10. J. L. Dehmer and U. Fano, Phys. Rev. A 2 (1970) 304.

11. A. W. Potts and W. C. Price, Proc. Roy. Soc. Lond. A 326 (1972) 181.

12. J. Berkowitz, Chem. Phys. Lett. 11 (1971) 21.

13. M. J. Weiss, G. M. Lawrence and R. A. Young, J. Chem. Phys. 52 (1970) 2867.

14. H. J. Lempka, T. R. Passmore and W. C. Price, Proc. Roy. Soc. A 304 (1968) 53.

15. C. R. Brundle, M. B. Robin and H. Basch, J. Chem. Phys. 53 (1970) 2196. These authors assigned the PES band of CH_3F at ~13 eV as the ionization of the 2e orbital centered on the CH_3 group. However, there is a break in the vibrational progression in this band system at 13.1 eV. We take this 13.1 eV band as the possible origin of the ionization of a non-bonding electron localized on the F atom.

16. W. C. Price, J. Chem. Phys. 4 (1936) 539.

17. L. Karlsson, L. Mattsson, R. G. Albridge, S. Pinchas, T. Bergmark and K. Siegbahn, J. Chem. Phys. 62 (1975) 4745.

18. W. C. Price, J. P. Teegan and A. D. Walsh, Proc. Roy. Soc. Lond. A 201 (1950) 600.

19. J. D. Scott, G. C. Causley and B. R. Russell, J. Chem. Phys. 59 (1974) 6577.

20. A. W. Potts and W. C. Price, Proc. Roy. Soc. Lond. A 326 (1972) 165.

21. W. Hayes and F. C. Brown, Phys. Rev. A 6 (1972) 21.

22. a) S. G. Tilford, M. L. Ginter and J. T. Vanderslice, J. Mol. Spect. 33 (1970) 505.

b) M. L. Ginter and S. G. Tilford, J. Mol. Spect. 34 (1970) 206.

c) S. G. Tilford, M. L. Ginter and A. M. Bass, J. Mol. Spect. 34 (1970) 327.

23. a) A. Monfils, J. Mol. Spect. 25 (1968) 513.

b) S. Takezawa, J. Chem. Phys. 52 (1970) 2575.

c) G. Herzberg and Ch. Jungen, J. Mol. Spect. 41 (1972) 425.

d) T. A. Miller and R. S. Freund, J. Chem. Phys. 61 (1974) 2160.

e) H. M. Crosswhite, "The Hydrogen Molecule Wavelength Tables of Gerhard Heinrich Dieke", Wiley-Interscience, New York, 1972.

24. a) D. T. Terwillinger and A. L. Smith, J. Mol. Spect. 45 (1973) 366.

b) D. T. Terwillinger and A. L. Smith, J. Mol. Spect. 50 (1974) 30.

25. J. L. Meeks, H. J. Maria, P. Brint and S. P. McGlynn, Chem. Rev. 75 (1975) 603.

26. B. J. Cocksey, J. H. D. Eland and C. J. Danby, J. Chem. Soc. (B) (1971) 790.

27. W. C. Price and A. D. Walsh, Proc. Roy. Soc. 174 (1940) 220.

28. P. G. Wilkinson, Can. J. Phys. 34 (1956) 596.

29. E. E. Koch and A. Otto, Chem. Phys. Lett. 12 (1972) 476.

CHAPTER THREE

PROGRESSIONS OF ATOMIC AND MOLECULAR RYDBERG SERIES

INTRODUCTION

The energy dependence of $u_{j\ell}$ has not been considered for the development of atomic and molecular Rydberg correlations. States higher than $n_1\ell$ follow the Rydberg formula, and $n^*_{j\ell}-n^*_{(j-1)\ell}$ with $j\geq 2$ is always ~ 1. However, as indicated in Chapter Two, Section VI-C the values of $n^*_{1s}-n^*_{op}$ for different groups of molecules exhibit certain characteristic deviations from the atomic averages. If these deviations from the atomic value are attributed to the anisotropic $U_m(\vec{r})$ [Chapter Two, Eq. (9)], we can rationalize them by comparing $V_m(\vec{r})$ and $V_a(r)$.

The influence of the centrifugal barrier (Chapter One, Section I) on molecular electrons with high ℓ is also of interest: The competition between the centrifugal force and the molecular potential $V_m(\vec{r})$ should determine the pattern of the absorption and photoionization spectra which involve electrons with $\ell\geq 2$.[1]

We propose to study these effects in HI, CH_3I, $(CH_3)_2CO$ and $CH_2{=}CH_2$. These choices are dictated by the availability of reliable data and the relatedness between the inert gases and these molecules as established in Chapter Two.

First, we present assignments for CH_3I and HI which are based on the relatedness of these entities to Xe. The results are then analyzed in the context of the n* differences and of the nature of $V_m(\vec{r})$. $(CH_3)_2CO$ and $CH_2{=}CH_2$ will also be used to illustrate this study.

I. THE ANALOGY BETWEEN Xe AND IODIDES

The close relationship between HI, CH_3I and Xe has been demonstrated in the studies of substituent effects (Chapter Two, Fig. 2) and n* differences (Chapter Two, Section VI-C). For Xe, the transitions of interest are

$$n_o p^6;\ ^1S_o \rightarrow n_o p^5 n_j \ell;\ \Gamma\ , \qquad j \geq 1 \tag{1}$$

where $n_o = 5$ and Γ designates the symmetry. For HI and CH_3I, the related transitions originate from non-bonding valence orbitals.

Figure 1 shows the autoionization spectra of Xe measured by Huffman et al.[2] Two series are present. One is $n_j d'$, and the other is $n_j s'$. Both converge to the second spin-orbit split level $^2P_{1/2}$. Figure 2 shows the spectra of CH_3I in the region between the two spin-orbit split $^2E_{3/2,1/2}$ cationic states. The close resemblance of Figures 2 and 1 leaves no doubt about the assignments of the CH_3I bands. Besides the $n_j d'$ and $n_j s'$ series, the extra bands which are observed correspond to transitions to $n_j p'$ which are forbidden in Xe. In addition, we observe a d series ($v'_2=1$) which converges on the first excited vibrational level of the $^2E_{1/2}$ cationic state. Figure 3 contains the equivalent region for HI. Again, we can assign s', p', and d' series without any difficulty.

Figure 1. The autoionization spectrum of Xenon between the spin-orbit split $^2P_{3/2}$ and $^2P_{1/2}$ levels. Measured by Huffman et al. (Ref. 2). The prime in the nd' and ns' designation serves to distinguish them from series converging to the lower cationic level, $^2P_{3/2}$.

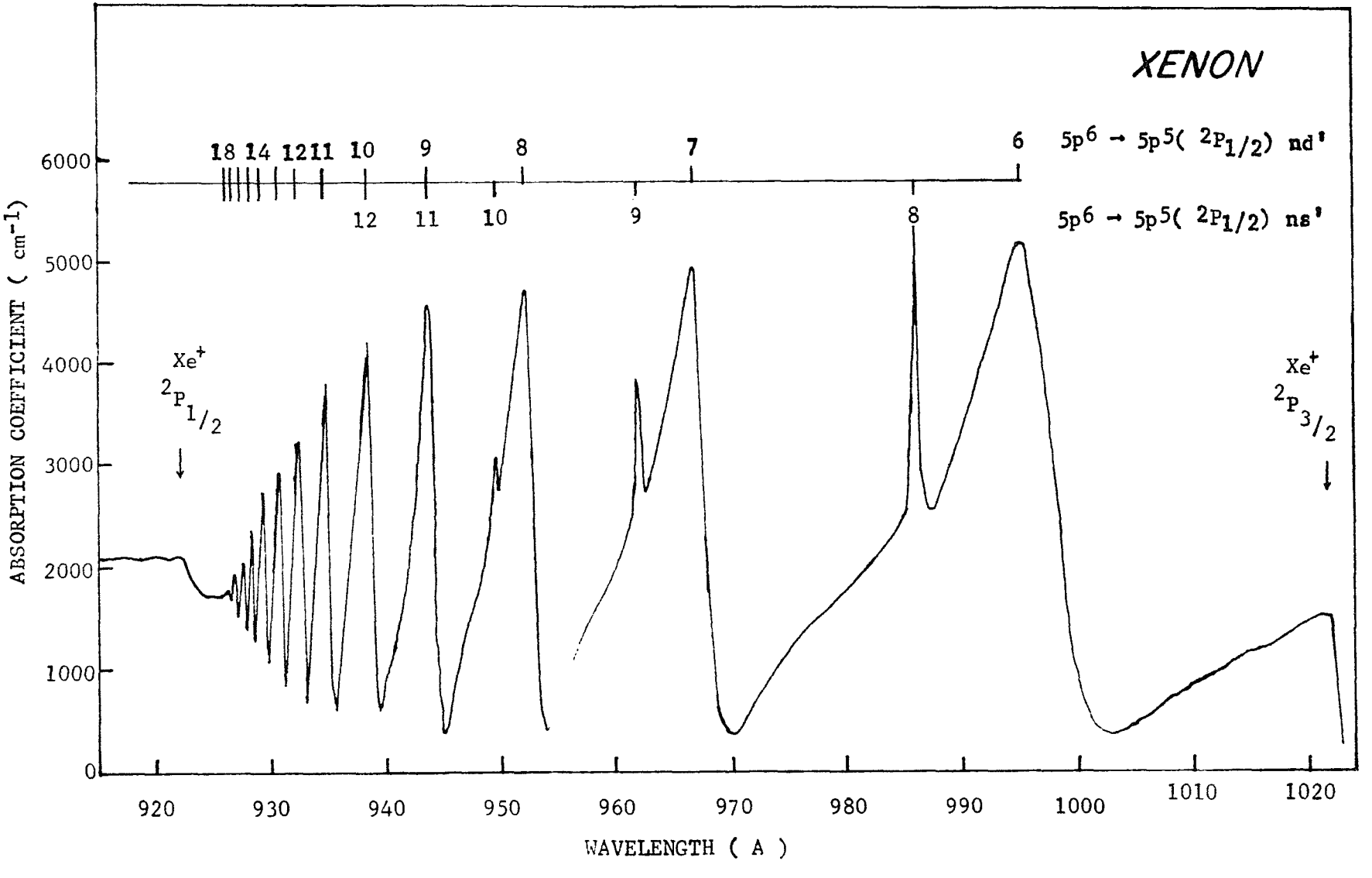
XENON
$5p^6 \rightarrow 5p^5(\ ^2P_{1/2})\ nd'$
$5p^6 \rightarrow 5p^5(\ ^2P_{1/2})\ ns'$
18 14 12 11 10 9 8 7 6
12 11 10 9 8
Xe^+ $^2P_{1/2}$
Xe^+ $^2P_{3/2}$
ABSORPTION COEFFICIENT (cm^{-1})
0 1000 2000 3000 4000 5000 6000
920 930 940 950 960 970 980 990 1000 1010 1020
WAVELENGTH (A)

Figure 2. Absorption spectrum of CH_3I between the $^2E_{3/2}$ and $^2E_{1/2}$ cationic states. The prime in the designations of ns', np' and nd' serves to distinguish them from the series converging to $^2E_{3/2}$ cationic state.

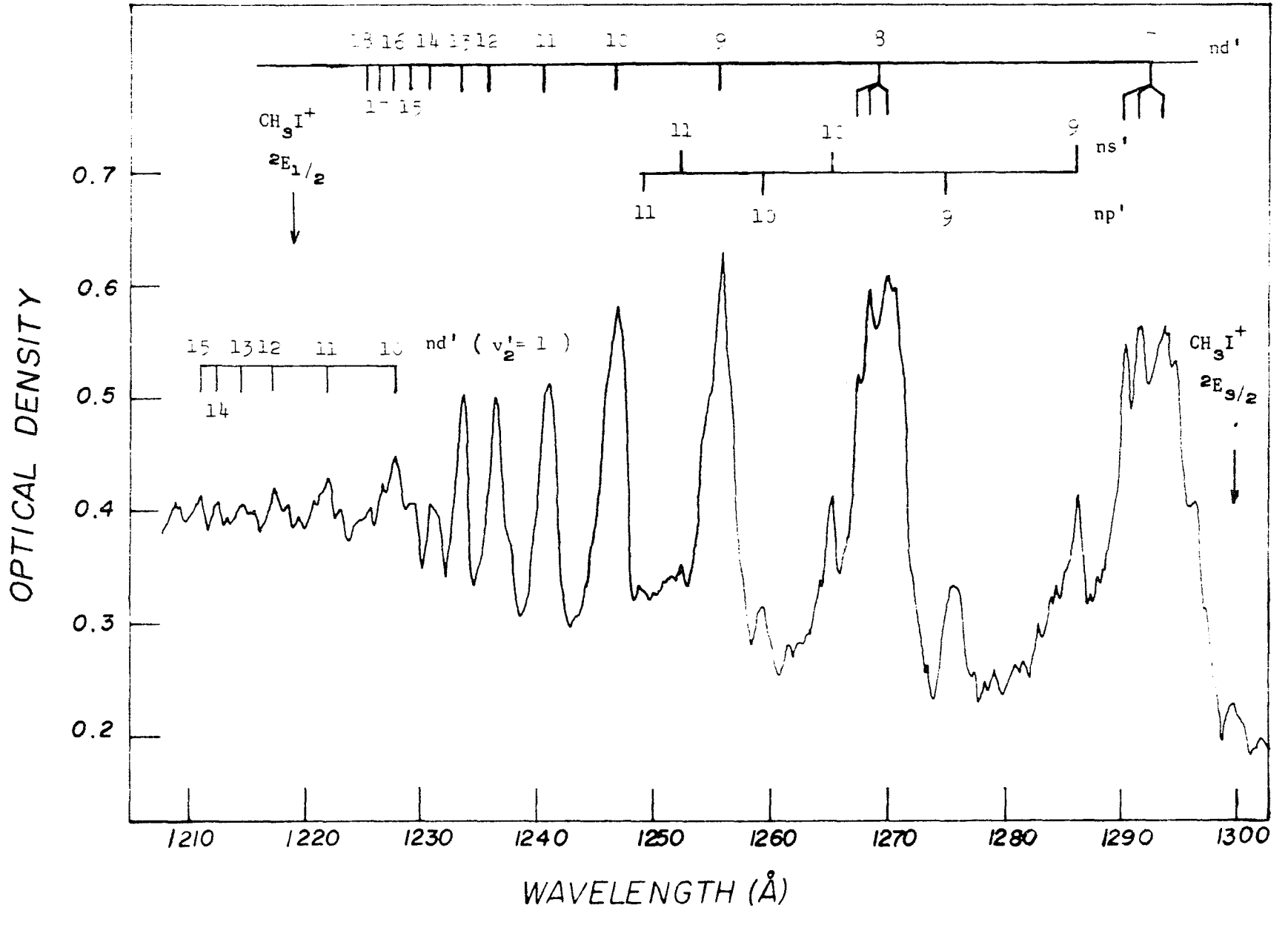
nd'
ns'
np'
CH_3I^+
$^2E_{1/2}$
nd' (v_2'= 1)
CH_3I^+
$^2E_{3/2}$
OPTICAL DENSITY
0.7
0.6
0.5
0.4
0.3
0.2
1210
1220
1230
1240
1250
1260
1270
1280
1290
1300
WAVELENGTH (Å)

Figure 3. Absorption spectrum of HI in the region between the $^2\Pi_{3/2}$ and $^2\Pi_{1/2}$ cationic states. The prime in the ns', np' and nd' designations serves to distinguish them from the series converging to the $^2\Pi_{3/2}$ cationic state.

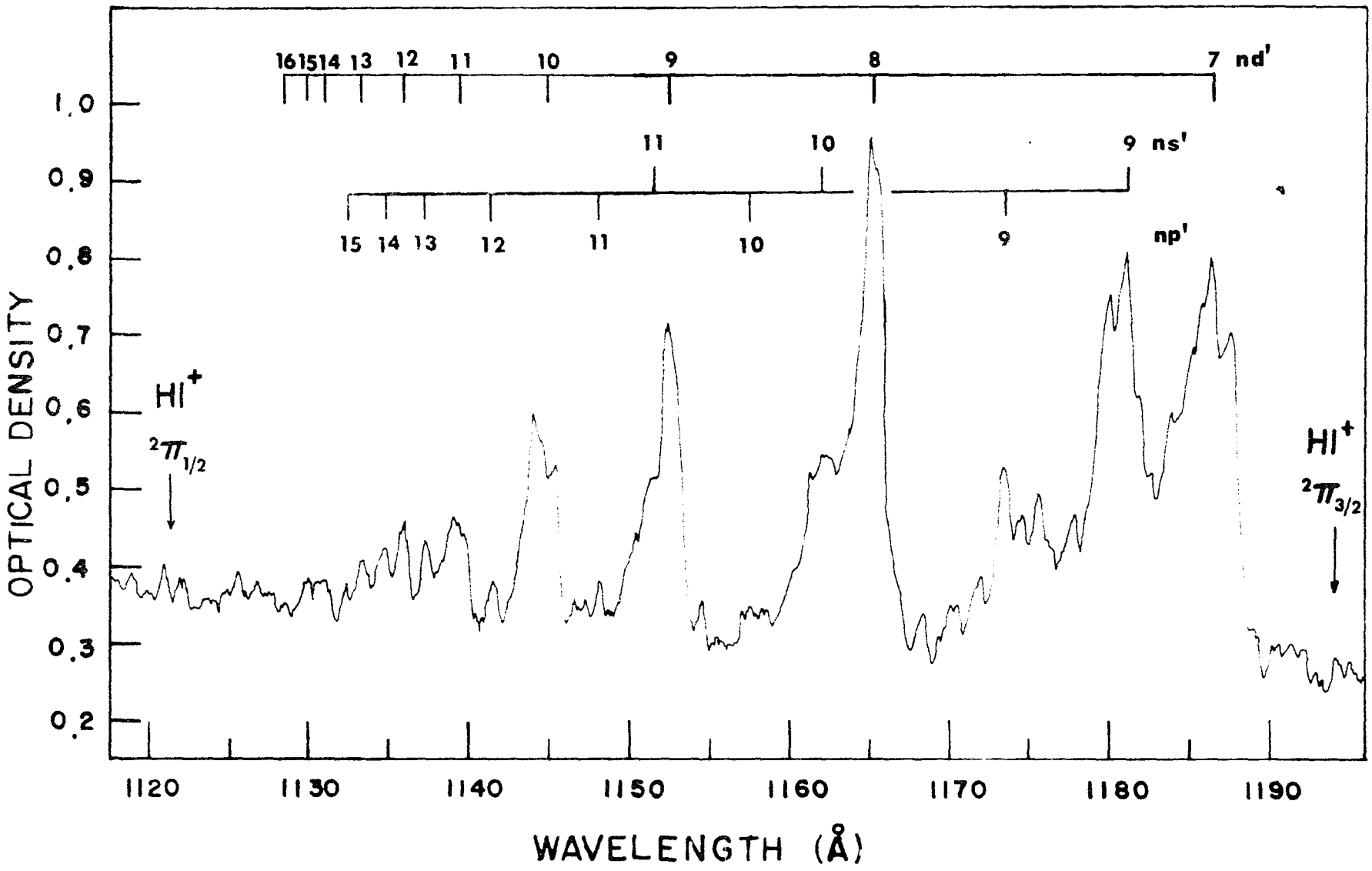
16 15 14 13 12 11 10 9 8 7 nd'
11 10 9 ns'
15 14 13 12 11 10 9 np'
HI+
2π1/2
HI+
2π3/2
OPTICAL DENSITY
1.0
0.9
0.8
0.7
0.6
0.5
0.4
0.3
0.2
1120
1130
1140
1150
1160
1170
1180
1190
WAVELENGTH (Å)

Figure 4. Absorption spectrum of CH_3I in the region below the $^2E_{3/2}$ cationic state. The primed Rydberg states 7p', 6d', 8s' and 8p' are converging to the $^2E_{1/2}$ cationic state.

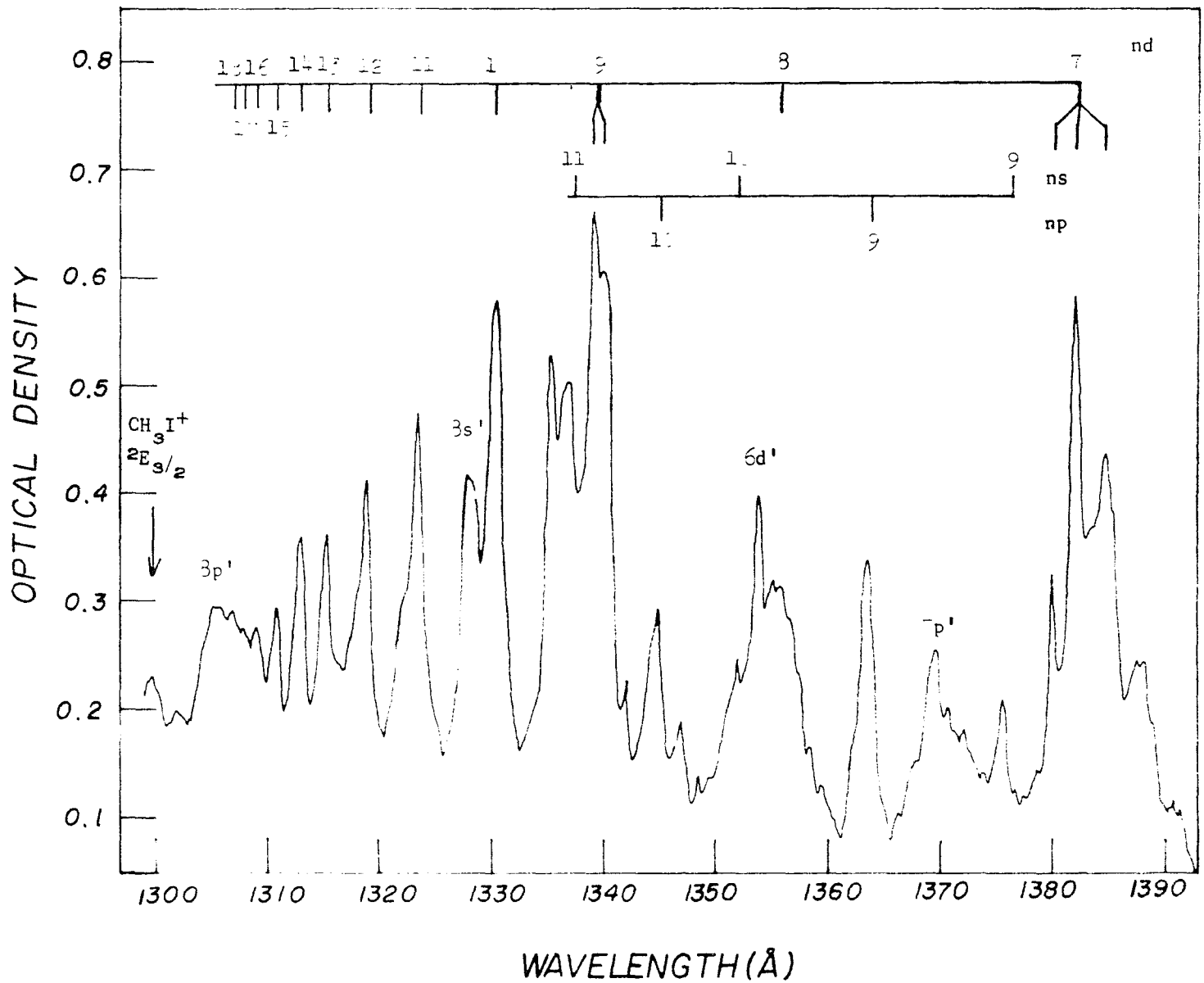
OPTICAL DENSITY
0.8
0.7
0.6
0.5
0.4
0.3
0.2
0.1
1300
1310
1320
1330
1340
1350
1360
1370
1380
1390
WAVELENGTH (Å)
nd
ns
np
8
7
9
CH3I+
2E3/2
3p'
3s'
6d'
p'

Once the higher members of a series are assigned, it is easy to recognize the lower ones by an extrapolation using constant $u_{j\ell}$. Furthermore, the identical series which converge on the lower cationic state of the spin-orbit split doublet can also be discerned. Figure 4 illustrates this clearly.

The results for CH_3I and HI, obtained in this way, are collected in Table 1. The corresponding data for Xe are presented for comparison in Table 2. It is interesting to note that the values of n^*_{jd} for the d series which converges to the higher spin-orbit split limit of Xe, HI and CH_3I are almost identical. The same similarity also exists between the values of n^*_{jd} for Xe and CH_3I, for the d series which converges to the lower ionization limit. The s series are different in the sense that the values of n^*_{js} for CH_3I are slightly higher than those for Xe, while the opposite is true for HI (except for n^*_{1s}).

These similarities provide a rather unique example of the manner in which molecular interpretations can be extracted from atomic spectroscopic data.

TABLE 1

RYDBERG SERIES FOR CH_3I AND HI

	CH_3I				HI	
n_o^*	1.194	1.157	1.194	1.157	1.110	1.110
j	n_{js}^*		n_{jd}^*		n_{js}^*	n_{jd}^*
1	2.008	2.004	2.814	2.702	2.023	2.720
2	2.995	3.001	3.660	3.671	2.919	3.699
3	4.051	4.043	4.810	4.817	3.916	4.733
4	5.072	5.064	5.900	5.787	4.931	5.722
5	6.055	6.063	6.845	6.762	5.920	6.710
6	7.113	7.108	7.821	7.752	6.926	7.772
7			8.844	8.754		8.725
8			9.811	9.786		9.743
9			10.851	10.714		10.723
10			11.801	11.775		11.780
11			12.788	12.769		12.764
12			13.851	13.756		13.760
13			14.859	14.809		
14			15.828	15.792		
core	$^2E_{3/2}$	$^2E_{1/2}$	$^2E_{3/2}$	$^2E_{1/2}$	$^2\Pi_{1/2}$	$^2\Pi_{1/2}$

TABLE 2

RYDBERG SERIES FOR Xe[a]

	$n_j s(3/2)^0$; J=1	$n_j s(1/2)^0$; J=1	$n_j d(3/2)^0$; J=1	$n_j d(3/2)^0$; J=1
j				
1	1.919	1.876	2.805	2.727
2	2.976	2.955	3.750	3.715
3	3.988	3.975	4.630	4.707
4	4.987	4.984	5.904	5.717
5	6.002	5.982	6.855	6.720
6	6.995	6.984	7.834	7.717
7	8.008	7.985	8.822	8.724
8	9.005	8.986	9.815	9.719
9	10.004	9.987	10.809	10.715
10			11.806	11.717
11			12.802	12.718
12			13.800	13.717
13			14.798	14.718
14			15.790	15.716
CORE	$^2P_{3/2}$	$^2P_{1/2}$	$^2P_{3/2}$	$^2P_{1/2}$

a) Data are from Moore[3] and Yoshino.[4]

II. MOLECULAR POTENTIALS OF CH_3I AND HI

As discussed in Chapter Two, Section I, the potential for a Rydberg electron of Xe can be expressed as

$$\frac{\hbar^2}{2m}\frac{\ell(\ell+1)}{r^2} + V_{Xe}(r) - \frac{e^2}{r} \qquad (2)$$

where $V_{Xe}(r)$ is exponentially decreasing and repulsive. Rau and Fano,[5] using the Herman-Skillman potential,[6] showed that, for $\ell \geq 2$, the potential of an atom can exhibit a barrier which inhibits intrusion of extra-core electrons into the core. This barrier, being caused primarily by centrifugal forces, is called the "centrifugal barrier". It can prevent electrons with $\ell \geq 2$ from penetrating into the inner part of the core (Chapter One, Section I).

For HI and CH_3I, the potential can be written as

$$\frac{\hbar^2}{2m}\frac{\ell(\ell+1)}{r^2} + V_{Xe}(r) + U_m(r) - \frac{e^2}{r} \qquad (3)$$

The sign of $U_m(\vec{r})$ depends on whether it is attractive or repulsive. Since the values of n^*_{jd} for CH_3I and HI are essentially the same as for Xe, we can argue that, for $\ell=2$, the centrifugal barrier is about the same for all three species. This implies that the combined results of all terms in Eq. (3) remain almost identical as we proceed outwards from the barrier. The "valley" inside the barrier

remains anisotropic for molecules, but spherical symmetry is attained outside of it.

If the barrier is adequately high, u_{jd} will be nearly an integer. The fact that it is ~0.2 lower than the integer value suggests a low barrier and, consequently, some tunneling. The shape of the inside well causes Xe to differ from the molecules because of the $U_m(\vec{r})$ term. Since tunneling is operative, the differences of the interior well will influence the energy eigenvalues. Yet, there is very little difference in the values of n^*_{jd} for Xe, HI and CH_3I. Thus, we conclude that $V_{Xe}(r)$ is the dominating term for the interior valley and $U_m(\vec{r})$ has very little influence there.

When $\ell=0$, there is no barrier to confine the effects of the anisotropic $U_m(\vec{r})$ term. The Rydberg electron is exposed to both $V_{Xe}(r)$ and $U_m(\vec{r})$. However, due to the dominance of $V_{Xe}(r)$, the energy levels of HI and CH_3I are not very different from those of Xe. The slight differences in values of n^*_{js} can then be attributed to $U_m(\vec{r})$ which, presumably, must be smaller than $V_{Xe}(r)$.

The n^*_{js}-n^*_{op} values for the s series of CH_3I, HI and Xe are listed in Table 3. The trend exhibited in going from lower j to higher j is interesting. Figure 5 shows the ns $[\frac{3}{2}]^o$, j=1 series for Ne, Ar, Kr, and Xe. The upward trend depicts a repulsive $V_a(r)$ for these inert gases. For CH_3I and HI, the pattern is a little different.

TABLE 3

s RYDBERG SERIES FOR CH_3I, HI AND Xe

	CH_3I		HI	Xe	
j	$n^*_{js}-n^*_{on}$		$n^*_{js}-n^*_{on}$	$n^*_{js}-n^*_{op}$	
1	0.814	0.847	0.913	0.860	0.870
2	1.801	1.844	1.810	1.917	1.949
3	2.857	2.886	2.806	2.929	2.969
4	3.878	3.907	3.821	3.928	3.978
5	4.861	4.906	4.810	4.942	4.976
6	5.919	5.951	5.850	5.936	5.978
Core	$^2E_{3/2}$	$^2E_{1/2}$	$^2\Pi_{1/2}$	$^2P_{3/2}$	$^2P_{1/2}$

Figure 5. Plot of $n^*_{js}-n^*_{op}$ for the $n_op^6;{}^1S_0 \rightarrow n_op^5n_js[3/2]^0$; J=1 series of Ne, Ar, Kr and Xe with the $^2P_{3/2}$ core. The index m is defined in Chapter One, Figure 5.

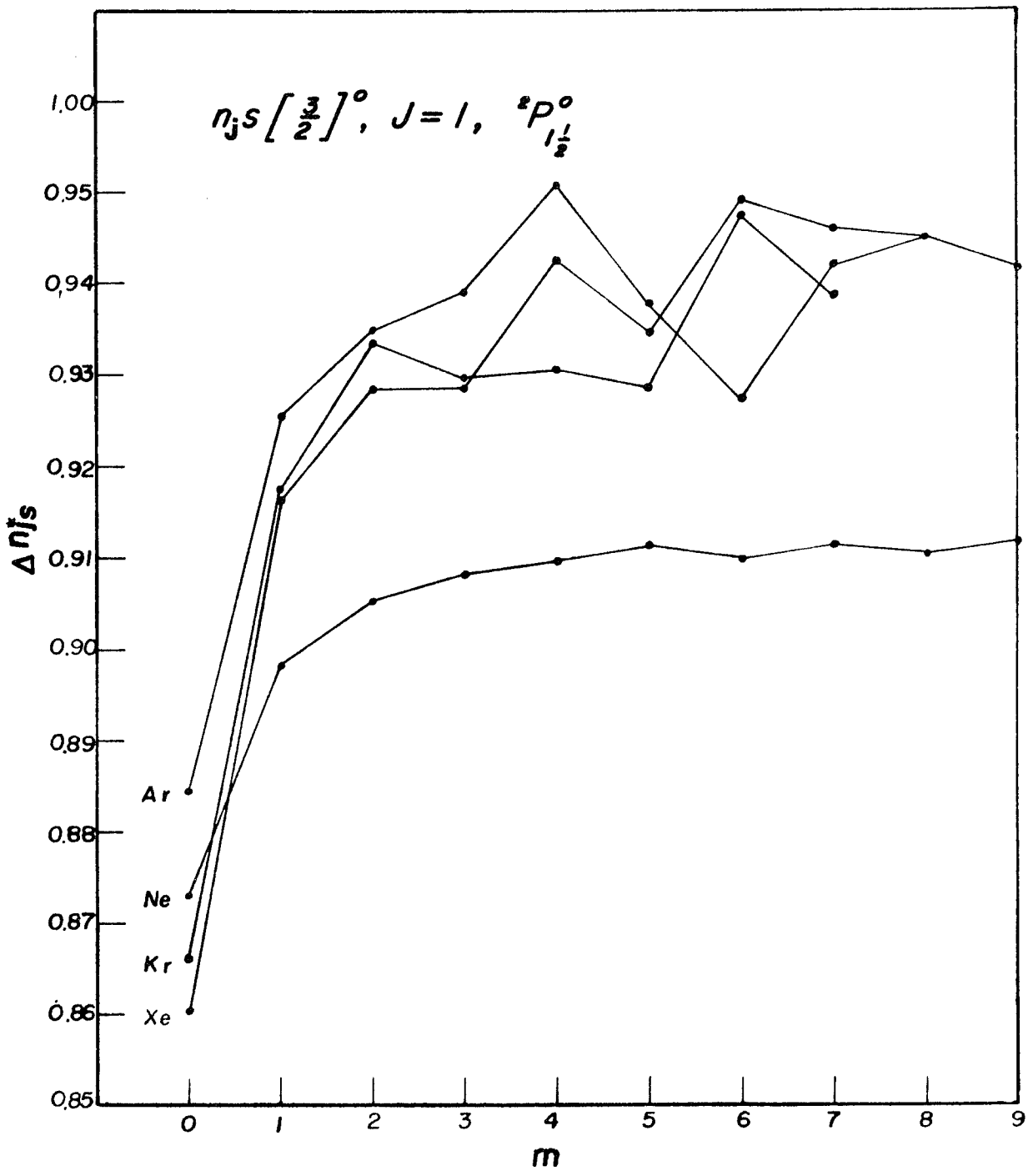
$n_j s\left[\frac{3}{2}\right]^o$, $J=1$, $^2P^o_{1\frac{1}{2}}$
1.00
0.95
0.94
0.93
0.92
0.91
0.90
0.89
0.88
0.87
0.86
0.85
Δn_{js}^*
Ar
Ne
Kr
Xe
0
1
2
3
4
5
6
7
8
9
m

There is a drop from n_1s to n_2s or n_3s and, thereafter, a continuous increase which resembles the inert gases. From Eqs. (4) and (5) of Chapter Two, we can rationalize the irregular behavior of the lower molecular s states by introducing an attractive potential $U_m(\vec{r})$ which prevails at small r. At large r, although still present, it is dominated by $V_a(r)$. The much larger n_1s to n_2s drop for HI indicates that $U_m(\vec{r})$ is more attractive for HI and, since the drop continues to n_3s, that is also of longer range.

III. ACETONE AND ETHYLENE

The non-bonding orbital in acetone and the π-orbital in ethylene have been discussed in Chapter Two, Section VII. Their corresponding $n_j s$ Rydberg series are described in Table 4. The same trend in $n_j s^*$'s as found for CH_3I and HI is evident. The initial drop is larger for ethylene. In this instance, we can not specify the nature of $V_a(r)$ since no obvious related atom exists. Nevertheless, it is safe to assume that an attractive potential is coupled with a repulsive one.

The initial steeper drop of HI and $CH_2{=}CH_2$ seems to suggest that methyl substitution neutralizes the attractive potential at small r.

TABLE 4

s RYDBERG SERIES OF ACETONE AND ETHYLENE[a]

	Acetone		Ethylene	
j	n^*_{js}	$n^*_{js}-n^*_{on}$	n^*_{js}	$n^*_{js}-n^*_{o\pi}$
1	2.014	0.830	2.001	0.863
2	2.901	1.718	2.910	1.722
3	3.956	2.772	3.918	2.780
4	4.977	3.794	4.919	3.781
5	5.993	4.810	5.926	4.788
6	6.988	5.805		
7	8.008	6.825		
8	8.973	7.789		
9	9.983	8.800		
10	10.98	9.80		

a) Data for ethylene are from Ref. 7. Those for acetone are from Ref. 8.

IV. CONCLUDING REMARKS

By studying the trend of $n^*_{j\ell}$ along Rydberg series, one can get information which is not obtainable from a study of the lowest-energy series members. Unfortunately, long Rydberg progressions are usually unobservable for large molecules and, even when observed, their assignment may well be questionable.

The molecular data cited in this chapter serves as a qualitative example of the kinds of information that may be extracted from well-assigned Rydberg series. Of particular interest are the suggestions with respect to the centrifugal barrier in molecules. Evidence such as this can be used in investigations of other phenomena.[1]

REFERENCES

1. U. Fano, Comments At. Mol. Phys. 1 (1969) 140.
2. R. G. Huffman, Y. Tanaka and J. C. Larrabee, J. Chem. Phys. 39 (1963) 902.
3. L. E. Moore, "Atomic Energy Levels", Natl. Bur. Std. (U. S.) Circular No. 467 (U.S. GPO, Washington, D. C., 1958).
4. K. Yoshino, to be published.
5. A. R. P. Rau and U. Fano, Phys. Rev. 167 (1968) 7.
6. F. Herman and S. Skillman, "Atomic Structure Calculations", Prentice-Hall, Inc., Englewood Cliffs, N. J. (1963).
7. W. C. Price and W. T. Tutte, Proc. Roy. Soc. 174 (1940) 207.
8. P. Brint, K. Wittel, W. S. Felps and S. P. McGlynn, to be published.

CHAPTER FOUR

THE ELECTRONIC STRUCTURE OF THE WATER MOLECULE

INTRODUCTION

The electronic structure of the water molecule has been extensively studied, both experimentally and theoretically. Since the early 1930's, photoabsorption, photoionization,[12] photodissociation,[13] and, recently, photoelectron[17-21] and electron impact[22-30] spectra have been investigated numerous times. Detailed, high-quality calculations have also become available in the last few years.[31-35]

Despite this effort, many problems remain unsolved. The inelastic broad feature observed at 4.0 eV - 6.0 eV in electron-impact spectra has been variously attributed to water dimer,[32] water aggregates, dissociation products,[36] negative ions,[30] contaminations,[37] non-Franck-Condon transitions[33] and the neutral water molecule. This band has no clearly defined maximum and is usually referred to as the "4.5 eV band". While the experimental results support the supposition that this band is the lowest triplet state of the neutral water molecule,[26,28,29] all recent quantum chemical calculations indicate[32-35] that the lowest triplet state can not have energy lower than ~6.5 eV.

All recent calculations are unanimous in assigning the 7.4 eV absorption band as a transition to a 3s Rydberg

level ($1b_1 \rightarrow 3sa_1$ in MO terms) or to a mixed Rydberg/intravalence level, $3sa_1/4a_1$, in which the Rydberg character is dominant. In contrast to this band, the higher ns members of the same Rydberg progression have quantum defects which are quite normal and very different from that of the 7.4 eV band. In view of this, we note that if the 7.4 eV band is dominantly intravalence (i.e., $1b_1 \rightarrow 4a_1/3sa_1$), it follows that the $1b_1 \rightarrow 3sa_1/4a_1$ Rydberg excitation should appear elsewhere in the spectrum, it should exhibit a somewhat normal quantum defect, and its location should be predictable with some accuracy.

In addition to these lower-energy states, many of the higher energy states, which are undoubtedly of Rydberg nature, either are uninvestigated or lack any unanimity of assignment.

This investigation attempts to provide a unified interpretation of the lower-energy transitions of water. It also proposes to induce some consistency into the assignments of the higher-energy states. Prior to so doing, however, it appears necessary to provide some background material. This latter is the purpose of the next section.

I. STATUS AND BACKGROUND

The MO's of H_2O are shown in Figure 1. The ground state electronic configuration is $(1a_1)^2(2a_1)^2(1b_2)^2(3a_1)^2(1b_1)^2$; $\tilde{X}\ ^1A_1$. The energies of the higher-energy filled MO's are known and are given in Table 1. The geometries of the various cationic states with respect to ∢HOH are also given in Table 1. The binding energy of the $1b_2$ MO is much larger than those of $3a_1$ and $1b_1$. Consequently, the only excitations of interest in this work are those involving promotions of electrons from the $3a_1$ and $1b_1$ MO's.

The only vacant valence MO's are $2b_2$ and $4a_1$ ($2\sigma_u$ and $3\sigma_g$ in $D_{\infty h}$). Excitations to these orbitals are of quite high energies and it is probable that they may be dissociative. The lowest-energy Rydberg orbitals may occur in the same energy region as $2b_2$ and $4a_1$, and it is possible that the entirety of the VUV spectrum of H_2O consists only of Rydberg transitions.

The Rydberg orbitals of interest in this work are:

ns : a_1 (σ_g)

np : b_2 (σ_u) ; a_1, b_1 (π_u)

nd : a_1 (σ_g) ; a_1, b_1 (π_g) ; a_2, b_2 (δ_g)

Figure 1. Molecular orbital diagram for the water molecule (schematic). MO's below the dashed line are filled in the ground state electronic configuration.

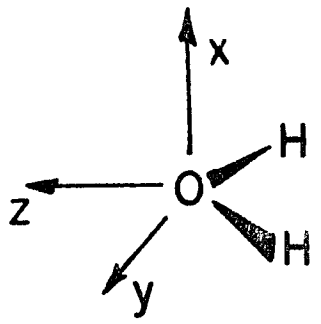

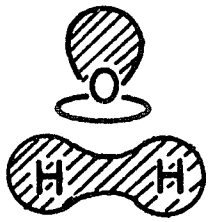

$4a_1$ $3\sigma_g$

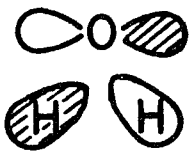

$2b_2$ $2\sigma_u$

ENERGY

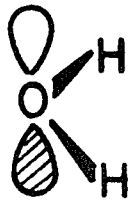

$1b_1$

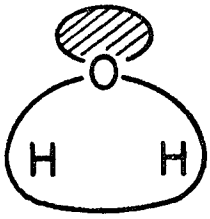

$3a_1$

$1\pi_u$

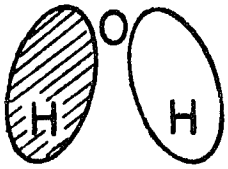

$1b_2$ $1\sigma_u$

MO $\Gamma(C_{2v})$ $\Gamma(D_{\infty h})$

TABLE 1

IONIZATION POTENTIALS[a,b] (eV)

Ionization Event	H_2O	D_2O	MO	Geometry
$\tilde{X}\ ^1A_1 \rightarrow\ ^2B_1(0,0,0)$	12.615±0.001	12.633±0.001	$1b_1$	bent
$^2A_1(0,1,0)$	13.839±0.007	13.847±0.008	$3a_1$	linear
$^2B_2(0,0,0)$	17.189±0.004	17.272±0.005	$1b_2$	bent

a) Data are taken from Ref. 20. The MO designation is based on Koopman's theorem: $IE_u = -\varepsilon_u^{SCF}$.

b) The notation for the cationic state is $^2\Gamma(v_1', v_2', v_3')$ where v_i' is the number of quanta of vibrational mode i excited in the $^2\Gamma$ cationic state.

where n = 3,4,5... and the notations in parentheses correspond to $D_{\infty h}$.

Mulliken[38] suggested that the lowest-energy absorption band, $\lambda_{max} \cong 1670$ Å (7.4 eV), was the $1b_1 ; \tilde{X}\ ^1A_1 \rightarrow 3sa_1, ^1B_1$ transition. Others[39,40] argued that the upper state of this transition was mixed valence and Rydberg: $3sa_1/4a_1; ^1B_1$ or $4a_1/3sa_1 ; ^1B_1$, where the numerator denotes the dominant component. Jones[6] assigned the second major absorption band, $\lambda_{max} \cong 1280$ Å, as $3a_1$, $\tilde{X}\ ^1A_1 \rightarrow 3sa_1; ^1A_1$. Walsh[40] pointed out that the upper state of this transition was also a mixture: $3sa_1/4a_1 ; ^1A_1$ or $4a_1/3sa_1 ; ^1A_1$.

Price[3] found four VUV Rydberg series, which he designated A, B, C and D. Of these, A and B consisted of three members whereas C and D consisted of long series that merged at higher members. The first member of the A series, 1A (1240 Å), and the first member of the B series, 1B (1219 Å), exhibit considerable fine structure, both rotational and vibrational. They have been studied by Johns[6] and Bell[8] and, as a result, can be assigned with some certitude as $1b_1 ; \tilde{X}\ ^1A_1 \rightarrow 3pa_1; ^1B_1$ and $1b_1; \tilde{X}\ ^1A_1 \rightarrow 3pb_1; ^1A_1$, respectively. The 1C and 1D members occur at 1128 Å and 1115 Å, respectively; they were considered[3] to be the $1b_1; \tilde{X}\ ^1A_1 \rightarrow 4sa_1; ^1B_1$ and $1b_1; \tilde{X}\ ^1A_1 \rightarrow 3d$ transitions. Finally, the extensive study by Katayama et al.[11] has extended the number of C and D series members from 6 to 9.

Some rather extensive quantum mechanical computations exist.[31-35] They are in good agreement with the experimental results cited above, except for the $1b_1$; $\tilde{X}\,{}^1A_1 \rightarrow ns\,a_1$; ${}^1B_1$ series. They are also unable to account for any excited state of H_2O with energy less than ~6.5 eV. Most of the recent electron impact studies[22-30] of triplet states and of ${}^1A_2$ states, while rich in terms of the data they provide, have remained interpretively subservient to the computational results. As a result, they have not helped to unravel the controversies involving the lower-energy excited states of water.

The study of photochemistry has provided some relevant insights to the spectroscopic problems. The primary process which follows photo-excitation in the 1670 Å band is[13]

$$H_2O(^1B_1) \rightarrow OH(\tilde{X}^2\Pi) + H(^2S)$$

with the OH species possessing a room-temperature equilibrated rotational and vibrational population. It was deduced[13,31] that the ${}^1B_1$ state dissociated along the antisymmetric stretching coordinate, Q_3. At energies higher than 1280 Å, an electronically-excited OH fragment is produced via the process[31]

$$H_2O + h\nu(\lambda<1280\ \text{Å}) \rightarrow OH(\tilde{A}^2\Sigma^+) + H(^2S) \ .$$

Two distinct rotational populations of the OH ($\tilde{A}^2\Sigma^+$) state were observed[14]: One is a normal room-temperature population; the other is dominant and possesses a distribution which is skewed toward higher rotational levels. It would appear that the 1280 Å excitation generates two different excited states of H_2O. One of these dissociates via the antisymmetric stretching mode, in the same way as does the 1670 Å state. The other, the one which yields the abnormal rotational distribution, dissociates via the symmetric bending coordinate, Q_2, and momentum is transferred from the opening motion of the HOH to the OH ($A^2\Sigma^+$) radical.

There has been some dispute concerning the appearance of the normal room-temperature population in the $\lambda < 1280$ Å photolysis. Tanaka, Carrington and Broida[14] first reported the existence of such a population distribution. However, Carrington,[15] in a follow-up report, did not find any signs of it. This prompted Flouguet and Horsley[41] to argue that, since the normal room-temperature population was always observed in electron-impact dissociation,[42] the normal population distribution must be due to an excited triplet state of H_2O. However, Byer and Welge[16] observed two fluorescence peaks of photodississociatively produced OH in the range 1400 - 1000 Å. In a recent review, Tsurubuchi[43] explained this by assuming that the $3sa_1$; $^1A_1$ state which is

responsible for the abnormal population, predissociates the $3pa_1$; $^1B_1$ state lying at slightly higher energy.

To complement these last photochemical experiments, Chamberlain and Simons[44] performed polarized photoexcitation experiments on water. They concluded that the observed reaction

$$H_2O + h\nu(\sim 1300\ \mathring{A}) \rightarrow OH(\tilde{A}^2\Sigma^+) + H(^2S)$$

proceeded from a $^1B_1$ state of H_2O. This conclusion contradicts the usual belief that only the $3a_1$; $\tilde{X}\ ^1A_1 \rightarrow 3sa_1$: $^1A_1$ transition occurs in this region. The new state is either a pure electronic $^1B_1$ state or, as the authors suggested,[44] a pure $^1A_2$ state to which one quantum of the antisymmetric vibrational mode is coupled.

Mohlmann et al.[45] used mono-energetic electron (0 - 1000 eV) to dissociate H_2O. They observed the normal population even at very high energy and thus ruled out the triplet state assumption by Flouquet and Horsley.[41]

The existing information on vibrational frequencies of H_2O and D_2O is synopsized in Table 2.

TABLE 2

VIBRATIONAL FREQUENCIES (cm^{-1})

Electronic State	Γ	H_2O ν_1	ν_2	ν_3	D_2O ν_1	ν_2	ν_3
Ground	$\tilde{X}\ ^1A_1$	3657[a]	1595[a]	3756[a]	2670[b]	1178[b]	2782[b]
$3pa_1$ Rydberg[c]	$^1B_1$	3179	1407	(3238)[d]	2338	1038	(2427)
$3pb_1$ Rydberg[c]	$^1A_1$	3268	1636	(3335)	2381	1223	(2483)
cationic[b]	$^2B_1$	3242	1428	(3299)	2363	1064	(2444)
cationic[b]	$^2A_1$		913[e]			677	
cationic[b]	$^2B_2$	2928	1524		2242	1129	

a) Ref. 46.

b) Ref. 20.

c) Ref. 8.

d) ν_3 is estimated.

e) ν_2 is averaged over the whole progression.

II. EXPERIMENTAL

Pure samples of H_2O and D_2O were degassed prior to use by a repetitive freeze-evacuate-thaw cycle. The ultra pure grade H_2O sample was supplied by Hartman-Leddon Co. The D_2O sample was of 99.8% minimum isotopic purity and was supplied by Diaprep, Inc.

Spectra were obtained on a McPherson 225 1m VUV spectrometer. The grating was blazed at 1200 Å and contained 1200 lines/mm. The reciprocal linear dispersion was 8.3 Å/mm. Monochromator slits varied from 40 to 120 μm, corresponding to a band pass of 0.3 to 1.0 Å. The light source was a Hinteregger hydrogen discharge lamp. The lamp was equipped with a cam-operated sliding plunger which permitted windowless operation.

The spectra are of room temperature samples and were obtained using a 100 mm long stainless steel sample cell equipped with 2 mm thick LiF windows. A specially designed stainless steel sample cell was also used to obtain the spectra of H_2O and D_2O in pathlengths of 4 and 0.127 mm. To obtain an absorbance of unity for each band system using a 0.127 mm pathlength, cell temperatures of 75°C to 105°C were necessary to produce the required sample pressures of 300 to 900 mm. An examination of the spectra obtained using the three different pathlength cells revealed a normal

Beer-Lambert law behavior for both H_2O and D_2O to well within the limits of experimental error. Except for the normal high temperature broadening of the sharp high-energy bands, the spectra obtained in 100 mm and 0.127 mm path-lengths were indistinguishable.

The measurements of band maxima for H_2O and D_2O were found to agree within the limits of experimental error with those of certain other authors.[5,8]

III. RESULTS AND DISCUSSION

A. The 1670 Å Absorption Band

This broad feature extends from 1860 Å to 1450 Å. It appears to consist of one major component with maximum at 1670 Å. A weak shoulder occurs at ~1530 Å. This band is shown in Figure 2. Little or no information concerning the weak shoulder can be extracted from the spectrum and speculation concerning its nature will be deferred until the end of this section.

The band at 1670 Å is diffuse and exhibits a poorly defined progression in the symmetric-bending vibration ν_2. The vibrational progression is shown in Figure 2 and is analyzed in Table 3. The frequency ν_2' is ~20% larger in the excited state corresponding to this transition than it is in $\tilde{X}\ ^1A_1$. Hydrogen sulfide possesses a very similar band, except that ν_2' is slightly smaller than it is in the ground state of H_2S.[47]

The diffuse nature of this band suggests that it may be dissociative with respect to some normal coordinate other than Q_2. In accord with this, photodissociation studies[13] indicate that a "break-up" into $OH(\tilde{X}^2\Pi)$ and $H(^2S)$ fragments occurs along the antisymmetric stretching coordinate Q_3.

The increase in ν_2' relative to ν_2 in $\tilde{X}\ ^1A_1$ or the known cationic states indicates that the excited state is

Figure 2. The absorption spectrum of H_2O (~1.0 mm pressure) and D_2O (~1.2 mm pressure) in the 1670 Å region. The baseline is presented for H_2O. The baseline for D_2O was approximately zero throughout the spectral region shown.

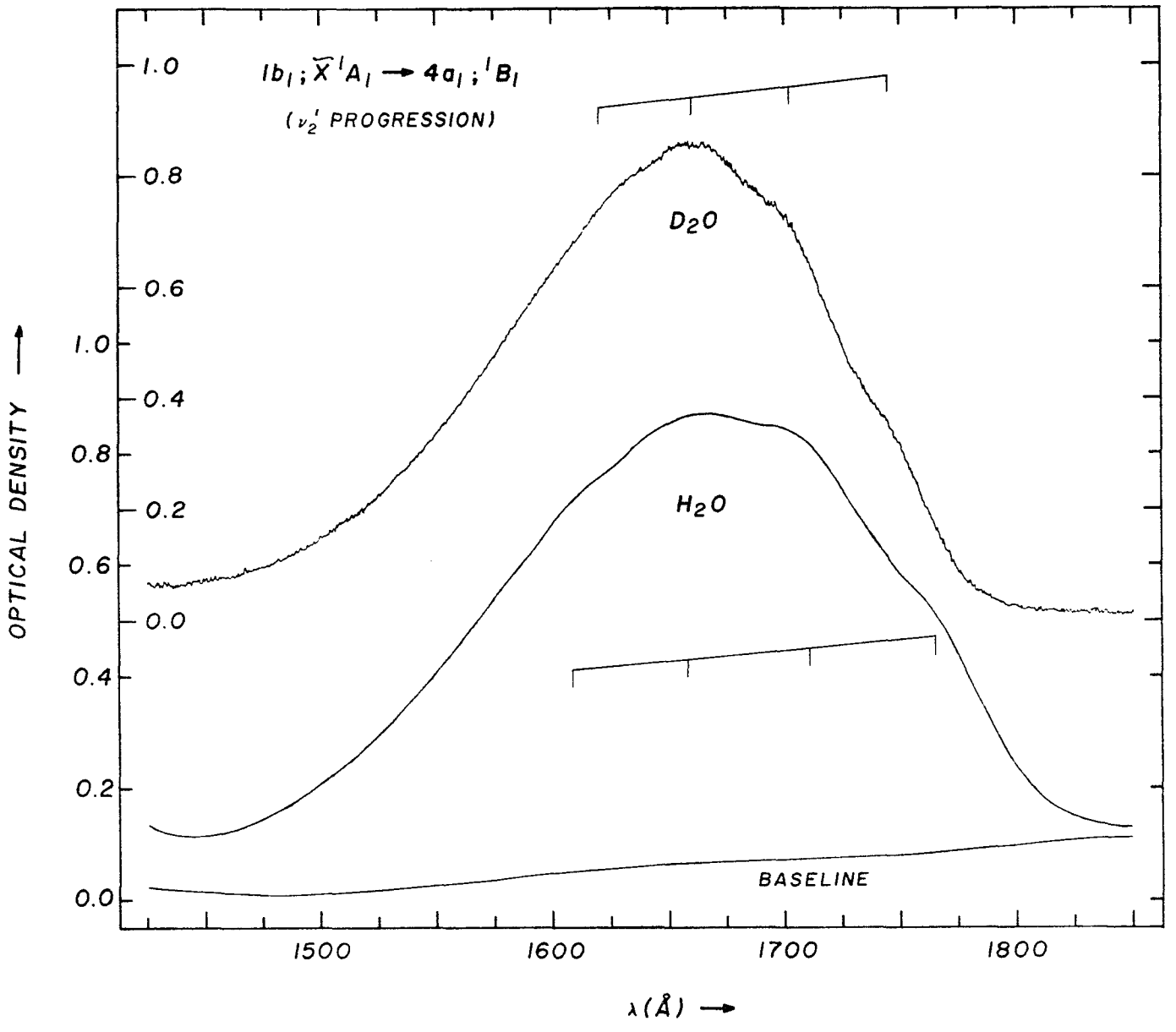
$1b_1; \tilde{X}\,^1A_1 \rightarrow 4a_1; {}^1B_1$
(ν_2' PROGRESSION)
D_2O
H_2O
BASELINE
OPTICAL DENSITY
1.0
0.8
0.6
0.4
0.2
0.0
1.0
0.8
0.6
0.4
0.2
0.0
1500
1600
1700
1800
λ(Å)

TABLE 3

THE 1670 Å BAND (1860 - 1450 Å)

$\tilde{X}\ ^1A_1 \rightarrow 4a_1/3sa_1; ^1B_1$ TRANSITION

H_2O			D_2O		
Band Maxima		ν_2'	Band Maxima		ν_2'
λ (Å)	ν (cm^{-1})	(cm^{-1})	λ (Å)	ν (cm^{-1})	(cm^{-1})
1766	56630	1850	1745	57310	1440
1710	58480	1870	1702	58750	1490
1657	60350	1840	1660	60240	1490
1608	62190		1620	61730	
Average 1850			Average 1470		

somewhat more H-H bonding than normal. In MO terms, since the initial $1b_1$ MO is H-H non-bonding, it is implied that the terminal, excited orbital is slightly H-H bonding. This, in turn, leads to the firm conclusion that the terminal orbital is of species a_1. In fact, a study of any MO set relative to this one fact leads to the conclusion that the transition in question must be $1b_1$; $\tilde{X}\ ^1A_1 \rightarrow a_1$; $^1B_1$.

The assignment $1b_1$; $\tilde{X}\ ^1A_1 \rightarrow a_1$; $^1B_1$ agrees with that which is commonly accepted, that is, $1b_1$; $\tilde{X}\ ^1A_1 \rightarrow 3sa_1$; $^1B_1$. However, our results do not speak directly to the nature of the terminal a_1 MO (i.e., whether Rydberg $3sa_1$, intravalence $4a_1$, or mixed $3sa_1/4a_1$). All recent quantum chemical computations of high quality are unanimous in their predictions of a highly Rydberg 3s character.[31-35] We find it difficult to argue with this conclusion, particularly because of the unanimity. Nonetheless, there are certain features of the experimental spectrum of water which suggest that this question be kept open. We will now discuss some of these.

Given that the 1670 Å band is, in an MO sense, described by $1b_1 \rightarrow 3sa_1$ (i.e., $2p \rightarrow 3s$ on oxygen), the corresponding exchange energy $2K = 2\langle 2p(1)3s(2)|\frac{1}{r_{12}}|2p(2)3s(1)\rangle$ is readily evaluated and is ~0.5 eV. Thus, the related $^3B_1$ state should be observable at ~6.9 eV. Such a band has been observed at 7.0 eV in electron scattering[28]

and has been assigned[28,29] accordingly. However, another, and very much lower-energy band has been observed in electron scattering at 4.0 eV - 6.0 eV. Once the $^3B_1$ assignment at 7.0 eV is accepted as unalterable, no assignment of the "4.5 eV band" to a stationary state of H_2O is possible. It is for this reason that this band has been variously attributed to water dimer, dissociation products, transient H_2O^{-} species, contamination, a non-Franck-Condon state, etc. Nonetheless, the experimentalists seem to prefer the attribution to a stationary state of monomeric H_2O. Given this preference, it is of interest to inquire into the location of a $^3B_1$ counterpart of the $^1B_1$ state when the $^1B_1$ state is described, in the MO sense, as $2p \rightarrow 4a_1$ (i.e., as intravalence). The exchange splitting in this case is $2K = 2\langle 2P_x(1)4a_1(2)|\frac{1}{r_{12}}|2P_x(2)4a_1(1)\rangle$. This integral is readily evaluated[48] and yields $2K \tilde{=} 1.8$ eV. Hence, the $3B_1$ state is expected to occur at 5.6 eV, which is in the region of the low-energy electron scattering band. Thus, a determination of the nature of the 4.0 - 6.0 eV electron scattering band (i.e., whether it does or does not refer to a stationary state of the neutral H_2O monomer) is crucial to the determination of the MO excitation nature of the $^1B_1$ state.

The united atom which correlates with the $\tilde{X}\ ^1A_1$ state of H_2O is $Ne(^1S_0)$. Since this is a closed-shell atom, all of its excited states are, by definition,

Rydberg states. It has been usual to suppose, therefore, that the lower-energy excited states of H_2O must also be Rydberg.[38,46] Such arguments are fallacious. Firstly, if this argument pertains to H_2Y, $Y \in \{O,S,Se,Te\}$, it must also apply to HX, $X \in \{F,Cl,Br,Cl\}$. However, it is well established[49] that the low-energy excited states of the hydrogen halides are intravalence (i.e., non-Rydberg). Secondly, the extension of united-atom considerations into the molecular realm invokes the non-crossing rule as the sole exemplar of configuration interaction (which is otherwise neglected) and, as a result, united-atom/molecule correlations may well be erroneous. Thus, united-atom configurations do not preclude a $1b_1$, $X\ ^1A_1 \rightarrow 4a_1$, $^1B_1$ intravalence assignment for the 1670 Å band.

The $4sa_1$, $^1B_1$ and $5sa_1$, $^1B_1$ states of H_2O have been assigned (vide infra). Their effective quantum numbers are $n^* = 2.945$ and 3.960, respectively. By extrapolation, the $3sa_1$, $^1B_1$ state should possess $n^* \tilde{=} 1.95$. Hence, the $1b_1$, $\tilde{X}\ ^1A_1 \rightarrow 3sa_1$, $^1B_1$ absorption should occur at ~1370 Å. This location is considerably far removed from 1670 Å! In addition, we will later demonstrate the presence in both H_2O and D_2O of an absorption band at ~1370 Å which can be assigned as $1b_1$, $\tilde{X}\ ^1A_1 \rightarrow 3sa_1$, $^1B_1$ transition, thus removing any need to assign the 1670 Å band as such.

Neither the shape of this band nor any of its details exhibit any resemblance to the $^2B_1$ PES band[17-21] which is

associated with the removal of a $1b_1$ electron. One must conclude, as a result, that the upper state of the 1670 Å transition is vastly different from the $^2B_1$ cationic state. In turn, this implies that the occupied virtual orbital of the upper state is most probably of intravalence nature.

The electron-impact band at 7.0 eV, instead of being assigned as $1b_1$; $\tilde{X}\ ^1A_1 \rightarrow 3sa_1$; $^3B_1$, could be interpreted as either $1b_1$; $\tilde{X}\ ^1A_1 \rightarrow 2b_2$; $^3A_2$, or $3a_1$; $\tilde{X}\ ^1A_1 \rightarrow 2b_2$; $^3B_2$. The weak shoulder at 1530 Å (8.1 eV) could be the $3a_1$; $\tilde{X}\ A_1 \rightarrow 2b_2$; $^1B_2$ intravalence transition, although we have no evidence to suppose so. The possibility that the 7.0 eV band is the triplet counterpart of the 8.1 eV transition will be elaborated later.

B. The 1280 Å Absorption Band

A low-resolution spectrum of this absorption band is shown in Figure 3. Some of the vibrational maxima for H_2O have been given by Watanabe and Zelikoff[5] and some of those for D_2O by Bell.[8] No vibrational analysis has been attempted previously. Our effort is given in Table 4.

The 1280 Å band is similar to the $\tilde{X}\ ^1A_1 \rightarrow ^2A_1$ PES band in all but a few regards. Both consist of long progressions in v_2'; v_2' is $\sim v_2''/2$ in both instances; the Franck-Condon maximum occurs at large values of v_2' (i.e., $v_2' \tilde{=} 9$ for H_2O and 12 for D_2O, see Table 4) in both cases; and the vibrational-substructure of the VUV and PES bands

Figure 3(a) The absorption spectrum of H_2O in the 1300 Å region at various pressures: (a) ~750 μm, pressures for (b), (c), (d), (e) and (f) are uncertain. The lower O. D. scale is for spectrum (a) and the baseline. The upper O. D. scale is for spectra (b)-(e).

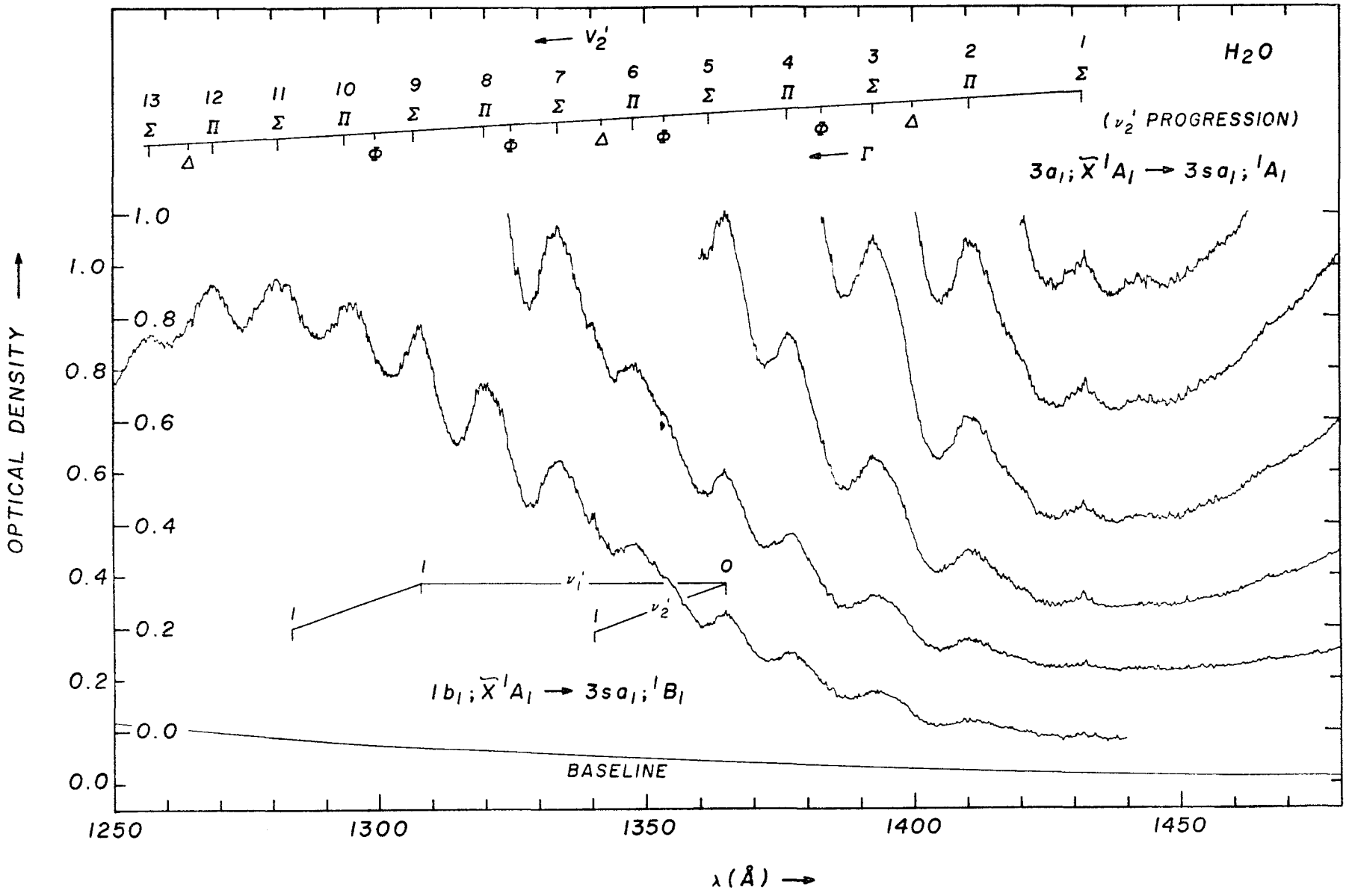
H2O
ν_2'
13 12 11 10 9 8 7 6 5 4 3 2 1
Σ Π Σ Π Σ Π Σ Π Σ Π Σ Π Σ
Δ Φ Φ Δ Φ Φ Δ Γ
(ν_2' PROGRESSION)
$3a_1; \tilde{X}\,^1A_1 \rightarrow 3sa_1; {}^1A_1$
$1b_1; \tilde{X}\,^1A_1 \rightarrow 3sa_1; {}^1B_1$
ν_1'
ν_2'
BASELINE
OPTICAL DENSITY
λ (Å)
1250
1300
1350
1400
1450
0.0
0.2
0.4
0.6
0.8
1.0

Figure 3(b) The absorption spectrum of D_2O in the 1300 Å region at various pressures: (a) ~800 μm; pressures for (b), (c), (d), (e) and (f) are uncertain. The lower O. D. scale is for spectrum (a) and the baseline. The upper O. D. scale is for spectra (b)-(e).

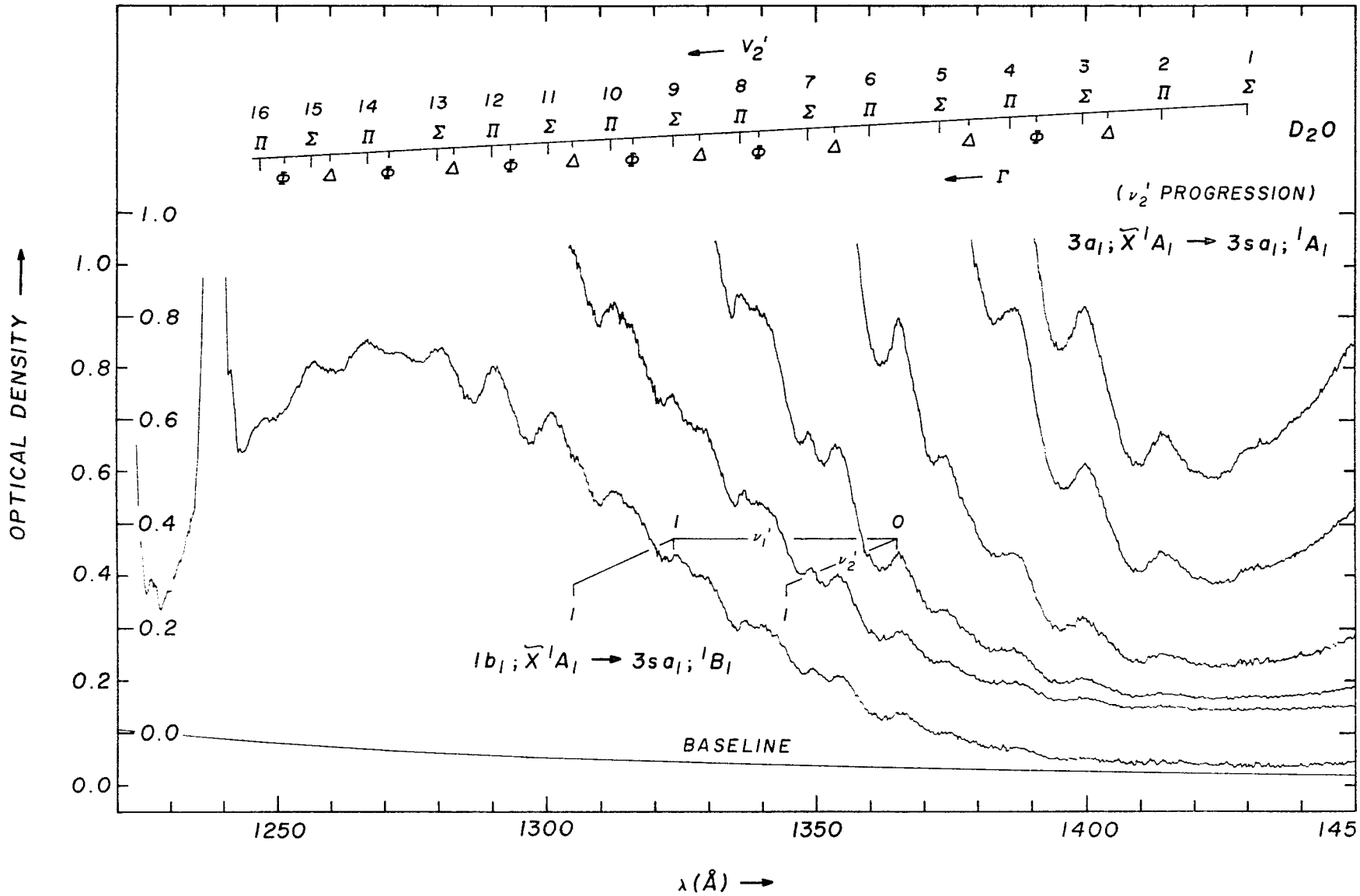
V_2'
16 15 14 13 12 11 10 9 8 7 6 5 4 3 2 1
Π Σ Π Σ Π Σ Π Σ Π Σ Π Σ Π Σ Π Σ
Φ Δ Φ Δ Φ Δ Φ Δ Φ Δ Φ Δ
Γ
D_2O
(ν_2' PROGRESSION)
$3a_1; \tilde{X}\,^1A_1 \rightarrow 3sa_1; {}^1A_1$
$1b_1; \tilde{X}\,^1A_1 \rightarrow 3sa_1; {}^1B_1$
1
ν_1'
0
ν_2'
1
1
BASELINE
OPTICAL DENSITY →
1.0
0.8
0.6
0.4
0.2
0.0
1250
1300
1350
1400
1450
λ(Å) →

TABLE 4A

THE 1280 Å ABSORPTION BAND OF H_2O

BAND MAXIMA (Å)		Sub-band	STATE					
			$3sa_1, {}^1A_1$		$3sa_1, {}^1B_1$			
This Work	Watanabe[a] & Zelikoff	Γ[b]	v_2'	$\nu_2'(cm^{-1})$	v_1'	$\nu_1'(cm^{-1})$	v_2'	$\nu_2'(cm^{-1})$
1438.0[c]								
1432.0		Σ	1					
1410.8	1411	Π	2	1050				
1400.0		Δ						
1392.7	1393	Σ	3	921				
1383.0		Φ						
1376.6	1378	Π	4	840				
1364.8	1364				0		0	
1362.0		Σ	5	778				
1353.5		Φ						
1347.8	1348	Π	6	774				
1341.0		Δ						
1340.2					0		1	1345
1333.7	1335	Σ	7	784				
1325.0		Φ						
1320.0	1321	Π	8	779				
1307.8	1308				1	3193	0	
1306.7[d]		Σ	9	771				
1299.5		Φ						
1293.8	1295	Π	10	763				
1283.5					1		1	1448
1281.3[e]	1281	Σ	11	754				
1269.0	1269	Π	12	756				
1264.3		Δ						
1257.0	1256	Σ	13	752				

a) Ref. 5.

b) For Σ and Π, maxima of sub-bands are given. For Δ and Φ, extra maxima at lower energy than that of Σ and Π are given.

c) The overall absorbance minimum.

d) The most intense vibronic sub-band after subtracting the underlying continuum.

e) The overall absorbance maximum.

TABLE 4B

THE 1280 Å ABSORPTION BAND OF D_2O

BAND MAXIMA (Å)		Sub-band b	STATE					
			$3sa_1; {}^1A_1$		$3sa_1; {}^1B_1$			
This Work	Bell[a]		v_2'	$\nu_2'(cm^{-1})$	v_1'	$\nu_1'(cm^{-1})$	v_2'	$\nu_2'(cm^{-1})$
1430.0		Σ	1					
1425.0[c]								
1414.0		Π	2	790				
1404.0		Δ						
1399.5		Σ	3	735				
1391.0		Φ						
1386.0		Π	4	695				
1378.5		Δ						
1373.0		Σ	5	685				
1365.0	1265.2				0		0	
1360.0		Π	6	695				
1353.5	1354.2	Δ						
1348.5	1348.9	Σ	7	625				
1345.5					0		1	1060
1339.5		Φ						
1336.0	1336.0	Π	8	695				
1328.5	1328.4	Δ						
1323.5	1323.2	Σ	9	705	1	2295	0	
1316.0		Φ						
1312.0	1311.2	Π	10	665				
1305.0		Δ			1		1	1075
1300.5	1302	Σ	11	675				
1293.5		Φ						
1290.0[d]	1290	Π	12	625				
1283.0		Δ						

Table 4B (cont'd)

BAND MAXIMA (Å)		Sub-band	STATE			
			$3sa_1; {}^1A_1$		$3sa_1; {}^1B_1$	
This Work	Bell[a]	Γ[b]	v_2'	$\nu_2'(cm^{-1})$	v_1' $\nu'(cm^{-1})$	v_2' $\nu_2'(cm^{-1})$
1280.0	1280	Σ	13	605		
1275.0[e]						
1271.0		Φ				
1267.0[f]	1266	Π	14	800		
1260.0		Δ				
1256.5	1256	Σ	15	660		
1251.5		Φ				
1247.0		Π	16	605		

a) Ref. 5.

b) For Σ and Π, maxima of sub-bands are given. For Δ and Φ, extra maxima at lower energy than that of Σ and Π are given.

c) The overall absorbance minimum.

d) The most intense vibronic sub-band after subtracting the underlying continuum.

e) Unaccounted perturbation

f) Overall absorbance maximum.

are more or less the same. These topics will be discussed in detail later. For now, we note that the primary difference between the 1280 Å VUV band and the 13.84 eV PES band is one of shape: The VUV band appears to be superposed on an underlying absorption continuum which possesses little or no vibronic structure. Apart from this, the great similarity of the VUV and PES systems is adequate proof that the VUV absorption event and the PES ionization event both initiate in the same $3a_1$ MO.

The $3a_1$ MO is strongly H-H bonding. Removal of a $3a_1$ electron, whether by electronic excitation or by ionization, should increase ∢HOH and decrease ν_2'. Indeed, ∢HOH increases considerably because it is well established that the $^2A_1$ state of H_2^+O is essentially linear[20,21] and is more properly described as a Renner-Teller component of a $^2\Pi_n$ cationic state.[20,21] We will now investigate ∢HOH for the excited 1280 Å state of water.

By using the valence-force approximation,[50] the isotope shift $[E(\nu_2', H_2O) - E(\nu_2', D_2O)]/E(\nu_2', H_2O)$, or $\Delta E(\nu_2')/E(\nu_2')$ can be obtained for different ∢HOH. Some calculated values, as a function of ∢HOH, are listed in Table 5. The stretching and bending force constants of the ground state were used in generating Table 5. In Table 6, the isotope shift data for the 1280 Å absorption band are presented along with those for the 968 Å absorption band (data being taken from Katayama et al.[11])

TABLE 5

CALCULATED ISOTOPE SHIFTS FOR H_2O AND D_2O[a]

∢HOH	$\frac{\Delta E(v_2')}{E(v_2')}$
180°	0.276
150°	0.251
120°	0.201
90°	0.158

a) Taken from J. W. Rabalais, "Principles of Ultraviolet Photoelectron Spectroscopy", Wiley-Interscience, a division of John Wiley and Sons, Inc., to be published.

TABLE 6

ISOTOPE SHIFTS (eV) FOR H_2O and D_2O

$[\Delta E(v_2') = E(v_2', H_2O) - E(v_2'; D_2O)]$

	1280 Å Band[a]			968 Å Band[b]			$^2A_1$ Cationic State[c]		
v_2'	H_2O	D_2O	$\Delta E(v_2')$	H_2O	D_2O	$\Delta E(v_2')$	H_2O	D_2O	$\Delta E(v_2')$
1	8.658	8.669	-0.011	12.803[d]	12.845	-0.042	13.839	13.847	-0.008
2	8.788	8.767	0.021	12.918	12.940	-0.022	13.931	13.926	0.005
3	8.902	8.858	0.044	13.036	13.023	0.013	14.048	14.005	0.043
4	9.007	8.944	0.063	13.154	13.123	0.031	14.157	14.082	0.075
5	9.103	9.029	0.074	13.277	13.209	0.068	14.268	14.164	0.104
6	9.199	9.115	0.084	13.387	13.300	0.087	14.384	14.246	0.138
7	9.296	9.193	0.103	13.526	13.389	0.137	14.503	14.332	0.171
8	9.393	9.279	0.114	13.640	13.481	0.159	14.620	14.419	0.201
9	9.488	9.367	0.121	13.771	13.573	0.198	14.745	14.507	0.238
10	9.583	9.449	0.134	13.884	13.666	0.218	14.870	14.596	0.274
11	9.677	9.532	0.145	13.997	13.754	0.243	14.995	14.683	0.312
12	9.770	9.610	0.160	14.106	13.850	0.256	15.124	14.774	0.350
13	9.864	9.685	0.179	14.212	13.943	0.269	15.252	14.864	0.388
14				14.334	14.032	0.302	15.376	14.957	0.419
15				14.459	14.121	0.338	15.507	15.048	0.459

a) This work.
b) Ref. 11.
c) Ref. 20.
d) Though Katayama et al.[11] listed 12.687 eV as the lowest member of the vibrational progression, we determine from isotope shift data, that 12.803 eV is the origin.

and the $3a_1$ PES ionization band (data being taken from Karlsson et al.[20]). The plots of $\Delta E(v_2')/E(v_2')$ for these three states are given in Figure 4. By comparing the slopes of the plotted lines with the calculated ones, we can conclude that the $^2A_1$ state is essentially linear; that the 968 Å state has $150^\circ \leq \measuredangle HOH \leq 180^\circ$ and, in view of the approximations involved, is either linear or close to linear; and that the 1280 Å state is linear or close to linear for $v_2' \leq 4$. For $v_2' \geq 5$, a perturbation occurs in the 1280 Å state. This perturbation reduces the initial slope from 0.250 to a final value of 0.125 and renders geometric considerations based on isotope effects invalid. In any event, whatever the nature of the perturbation, the 1280 Å state must remain linear, or nearly so, for all values of v_2'.

We now know that the 1280 Å absorption band involves excitation of a $3a_1$ electron and that the excited state so achieved is linear or nearly so. We now wish to determine the nature of the terminal orbital. For this purpose, we use empirical quantum defect considerations. The criterion which is commonly used to characterize the lowest-energy s-type Rydberg states of molecules, namely that their effective quantum numbers n^* should be an integer or nearly so,[51] is not valid when the electron which is excited is a bonding electron. The origin of the 1280 Å band yields $n^* = 1.621$, which is quite different

Figure 4. The isotope shift $\Delta E(\nu_2')=E(\nu_2',H_2O)-E(\nu_2',D_2O)$ plotted against the transition energies $E(\nu_2',H_2O)$ of H_2O. The upper line represents $\tilde{X}$; $^1B_1 \rightarrow {}^2A_1$ PES band. The middle line represents the 968 $\mathring{A}$, $3a_1$; $\tilde{X}^1A_1 \rightarrow 5sa_1$; $^1A_1$, band. The lower line represents the 1280 $\mathring{A}$, $3a_1$; $\tilde{X}^1A_1 \rightarrow 3sa_1$; $^1A_1$, band. The coordinates are arranged according to the relative positions of the lines they describe.

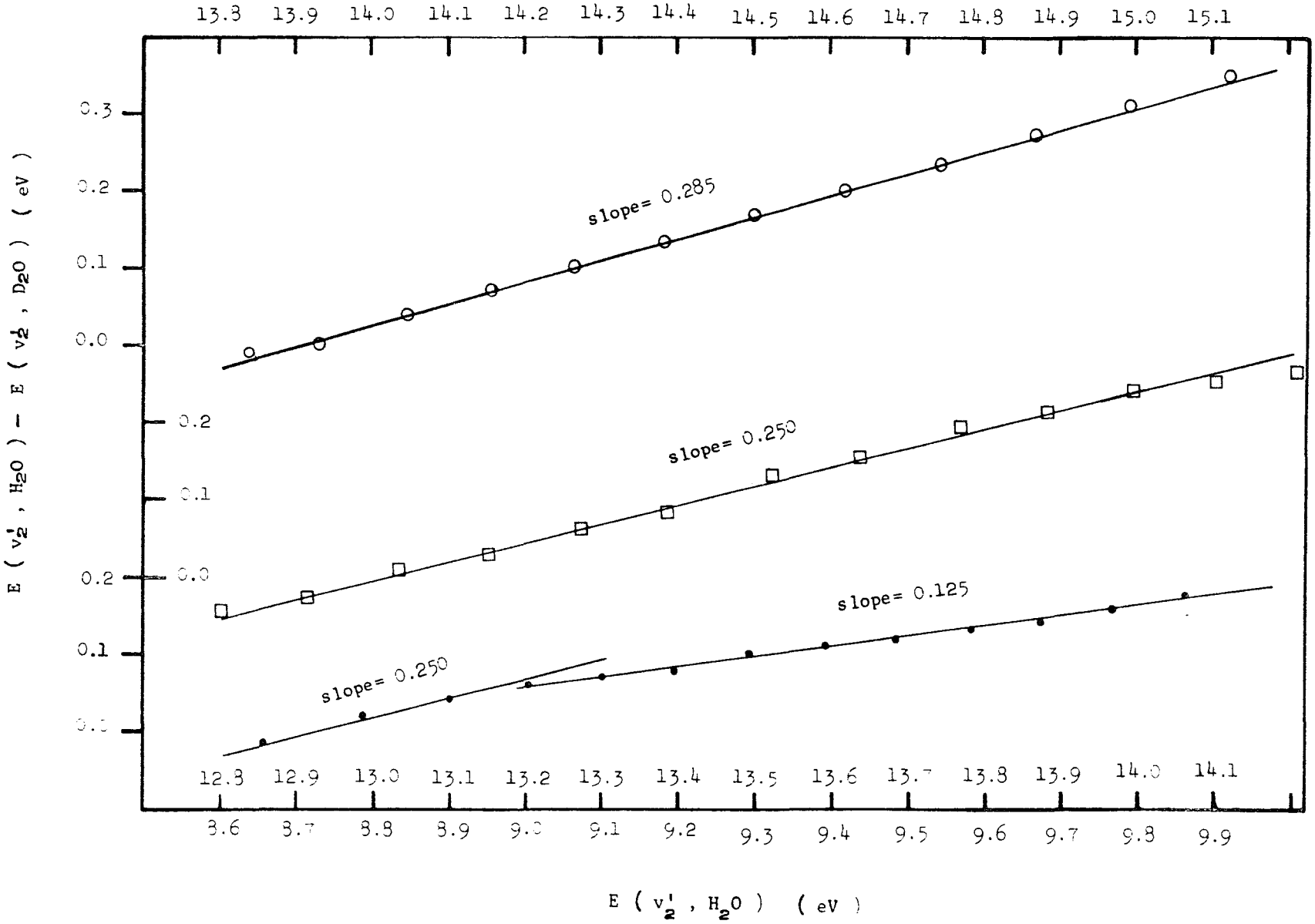
13.8 13.9 14.0 14.1 14.2 14.3 14.4 14.5 14.6 14.7 14.8 14.9 15.0 15.1
0.3
0.2
0.1
0.0
slope= 0.285
0.2
0.1
0.0
slope= 0.250
0.2
0.1
slope= 0.250
slope= 0.125
12.8 12.9 13.0 13.1 13.2 13.3 13.4 13.5 13.6 13.7 13.8 13.9 14.0 14.1
8.6 8.7 8.8 8.9 9.0 9.1 9.2 9.3 9.4 9.5 9.6 9.7 9.8 9.9
E (v'2 , H2O) − E (v'2 , D2O) (eV)
E (v'2 , H2O) (eV)

from the value of ~2.0 expected for a 3s terminal orbital. Now, the topmost filled MO of ZH_3 species, $Z \in \{N,P,As\}$, is very similar to the $3a_1$ MO of H_2O and, like the $3a_1$ MO, it is largely responsible for the pyramidal non-planar configuration of ZH_3 entities. The lowest s Rydberg states of ZH_3 entities are treated from a quantum defect viewpoint in Table 7 where they are compared with the 1280 Å band of H_2O. There can be little doubt, on the basis of Δn^* comparisons, that the terminal orbital of the 1280 Å excitation is a 3s MO. Thus, the 1280 Å state is best described as $3a_1(^1\pi_u) \rightarrow 3sa_1(\sigma_g^+)$; $^1A_1(^1\Pi_u)$ where the bracketed notation refers to the $D_{\infty h}$ point group.

The $^1\Pi_u$ Rydberg state should exhibit a Renner-Teller splitting into two components, either one or both of which may be bent.[52] Since it has been established that the 1280 Å component is linear, the Renner-Teller effects should lead to characteristic splittings of the vibronic bands. These effects have been discussed for the $^2A_1$ PES band of H_2O and D_2O by Dixon et al.[21] and Karlsson et al.[20] and will not be elaborated here. The effects to be expected are: (i) The vibrational bands should be alternately broad and sharp -- sharp for odd v_2' and broad for even v_2'. This effect is clearly discernible in the majority of the bands of Figure 3. Compare, for example, bands 1, 2, 3 and 4 of H_2O or bands 2, 3 and 4 of D_2O. (ii) All vibronic bands should have their sharp edges on

TABLE 7

EFFECTIVE PRINCIPAL QUANTUM NUMBERS[a] FOR THE LOWEST-ENERGY RYDBERG STATES OF ZH_3, $Z \in \{N,P,As\}$ AND THE 1280 Å BAND OF H_2O

	NH_3[b]	PH_3[b]	AsH_3[b]	H_2O[b,c]
n^*	1.752	1.762	1.775	1.621
n_o^*	1.158	1.169	1.173	0.992
Δn^*	0.594	0.593	0.602	0.629

a) n^* is defined as

$$n^* \equiv \sqrt{\frac{R}{T}}$$

where

$$T \equiv IP-\nu$$

and ν is the Rydberg transition energy, IP is the ionization limit and R is the Rydberg constant.

n_o^* is defined as

$$n_o^* \equiv \sqrt{\frac{R}{IP}}$$

and

$$\Delta n^* \equiv n^*-n_o^*$$

b) Adiabatic energies used throughout.

c) Since the 1280 Å band corresponds to a linear state split from $^1\Pi_u$ by the Renner-Teller effect, the origin of this band has v'=1 instead of v'=0. The same situation applies to the $^2A_1$ ionization limit (see Ref. 20)

the higher-energy side. This sort of effect is not particularly prominent in Figure 3 because of the diffuse nature of the spectrum. Nonetheless, it is evident in bands 2, 3 and 10 of D_2O and bands 2, 3, 6, 7 and 8 of H_2O. (iii) Except for the vibronic sub-bands of Σ type, all others (i.e., Π, Δ, Φ, ...) should be subject to erratic energy shifts and resonances. The sub-band structures are marked on Figure 3 and are clearly discernible. Their spacings relative to the Σ sub-bands are erratic, as expected. Indeed, the only meaningful analysis for ν_2' intervals is based on the high-energy Σ sub-band components, and, to some extent, on the Π components. This analysis is given in Table 4. (iv) If there be a low-energy potential barrier at the linear configuration, vibrational levels below this barrier should exhibit positive anharmonicity whereas those above it should exhibit negative anharmonicity. This is characteristic of the $^2A_1$ cationic state but not of either the 968 $\mathring{A}$ or the 1280 $\mathring{A}$ excited electronic states (see Table 8). In fact, the 1280 $\mathring{A}$ state exhibits a striking positive anharmonicity throughout all the observed v_2' progression. From this, we may conclude that the bottom of the potential well for the 1280 $\mathring{A}$ state has a curvature which is less than that of a harmonic well. (v) After subtraction of the underlying "continuum" of the 1280 $\mathring{A}$ band, the most intense sub-bands occur at $v_2' = 9$ (H_2O) and 12 (D_2O). The corresponding

TABLE 8

ν_2' FOR THREE LINEAR STATES

	1280 Å State		968 Å State[a]		$^2A_1$ Cationic State[b]	
	ν_2' (cm^{-1})		ν_2' (cm^{-1})		ν_2' (cm^{-1})	
v_2'	H_2O	D_2O	H_2O	D_2O	H_2O	D_2O
1-2	1050	790	930	770	742	637
2-3	921	735	950	670	943	637
3-4	840	695	950	800	879	621
4-5	778	685	999	700	895	581
5-6	774	695	881	730	935	661
6-7	784	625	1120	720	960	694
7-8	779	695	920	740	943	702
8-9	771	705	1060	740	1008	710
9-10	763	605	910	750	1008	718
10-11	754	675	910	710	1008	708
11-12	756	625	880	780	1040	734
12-13	752	605	860	750	1032	726
13-14		800	980	710	1000	750
14-15		660	1010	720	1057	734
15-16		605		754	1016	766
16-17				709	1032	742
17-18				725	1057	758
18-19					1040	758
19-20					1005	758
Average	810	684	954	735	979	705

a) Ref. 11.

b) Ref. 20.

maxima in the $\tilde{X}\ ^1A_1 \rightarrow ^2A_1$ band occur at $v_2' = 9$ (H_2O) and 13 (D_2O).

There is little doubt that the v_2' progression in this region is associated with a $3a_1$; $\tilde{X}\ ^1A_1 \rightarrow 3sa_1$; $^1A_1$ pure or nearly pure, Rydberg excitation. The small differences relative to the structure of the $^2A_1$ PES band are due to the intrusion of another electronic state (or states). This intrusion leads to irregularities which initiate at ~1365 Å in H_2O. These irregularities will be discussed in the next section.

C. The 1365 Å Absorption Irregularity

The majority of the bands in the 1280 Å band follow the even/odd//broad/sharp categorization discussed above. The primary exceptions are the $v_2' = 5$, 7, 9 and 11 bands of H_2O which exhibit quite irregular behavior. The most deviant behavior is shown by the $v_2' = 5$, 1362 Å Σ sub-band. Instead of being sharp and intense, this Σ band, which should not be perturbed by Renner-Teller effects, appears to be submerged under a more intense band at 1364.8 Å. This 1364.8 Å band, then, must be supposed to be a new state. If this state be assigned as $3sa_1$; $^1B_1$ (0,0,0), the effective quantum number is $n^* = 1.963$ which is in excellent accord with values of n^* for the excitation of a non-bonding electron to a 3s Rydberg orbital

and with values of n* for two higher energy bands of H_2O which are assigned as $4sa_1$; $^1B_1$ (for which n* = 2.945) and $5sa_1$; $^1B_1$ (for which n* = 3.960). In addition, the irregularities of bands v_2' = 7, 9 and 11 of H_2O are readily explicable as the result of perturbations by the $3sa_1$; $^1B_1$ (0,1,0), (1,0,0) and (1,1,0) vibronic levels (see Table 4).

The situation in D_2O is quite similar. All bands, except those for which v_2' = 6, 7, 8 and 9 follow the alternating band shape criteria. The v_2' = 6, 1360.2 Å band is not broad, contrary to expectation, but possesses, at the lower-energy edge, a very sharp, intense maximum at 1365.0 Å. This foreign band yields n* = 1.958, in excellent agreement with H_2O and with higher-energy bands of D_2O which can be assigned as $4sa_1$; $^1B_1$ (n* = 2.934) and $5sa_1$; $^1B_1$ (n* = 3.948).

In summary, a considerable amount of evidence suggests the intervention of a new electronic state of H_2O at 1364.8 Å and of D_2O at 1365.0 Å. The observed vibrational frequencies (see Figure 3 and Table 4) suggest that the molecule in this excited state is bent, with ∢HOH essentially identical to that of the ground state. The associated vibronic frequencies also provide an interpretation of the anomalous shapes of bands v_2' = 7, 9, and 11 of H_2O and v_2' = 7, 8 and 9 of D_2O. The break in the slope of Figure 4, the continuing positive anharmonicity, and,

possibly, the difference of band shapes of the 1280 Å VUV feature and the $^2A_1$ PES band may well be explicable along these lines.

The polarized photoexcitation experiment on H_2O conducted by Chamberlain and Simon[44] confirmed the existence of a $^1B_1$ state in this region. We believe that the irregular band at 1365 Å is the state in question. Furthermore, because of the almost identical positions of these bands for H_2O and D_2O, the suggestion[44] of a $^1A_2$ vibronic state excited through coupling of the anti-symmetric vibrational mode (i.e., b_2) can be ruled out. If the $^1A_2$ assignment were correct, the resulting bands of H_2O and D_2O should exhibit an isotope shift of at least 400 cm^{-1} -- which they do not.

The K-shell excitation spectrum of H_2O (Fig. 5) by Wight and Brion[53] showed a strong peak between the first band (corresponding to the 1670 Å band in valence-shell excitation) and the bands corresponding to $3pa_1$; $^1B_1$ and $3pb_1$; $^1A_1$ of the valence-shell excitations (Table 9). This extra band has no equivalent in the valence-shell excitation spectrum and it yields $n^* = 1.89$. Since excitation of the oxygen 1s electron will not change the geometry of H_2O, we do not have the Renner-Teller effect to contend with

Figure 5. Electron-impact K-shell excitation spectrum of H_2O, measured by Wight and Brion (Ref. 53).

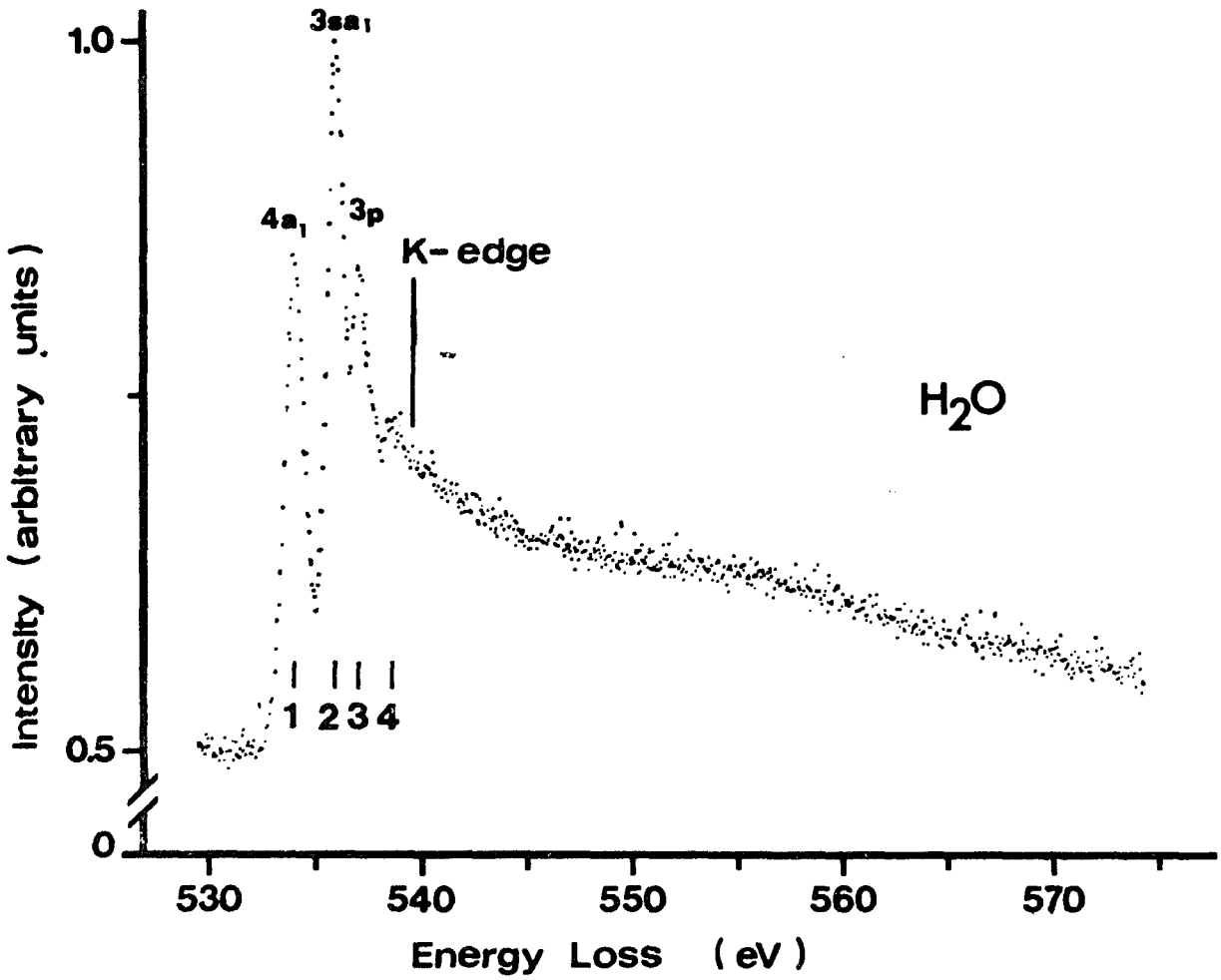
3sa1
4a1
3p
K-edge
H2O
1 2 3 4
1.0
0.5
0
Intensity (arbitrary units)
530
540
550
560
570
Energy Loss (eV)

TABLE 9

K-SHELL EXCITATION OF H_2O [a]

BAND	TERM VALUE (eV)	n^*	WIGHT ET AL.	THIS WORK
1	5.7	1.54	$3sa_1$	$4a_1$
2	3.8	1.89	$3pb_2$	$3sa_1$
3	2.6	2.29	$\begin{cases} 3pa_1 \\ 3pb_1 \end{cases}$	$\begin{cases} 3pa_1 \\ 3pb_1 \end{cases}$
4	1.2	3.37	$\begin{cases} 4s \\ 4p \end{cases}$	-

a) Ref. 53.

in the core excitation spectrum. Thus, all states observed in K-shell excitation can be considered to be "unperturbed" versions of the valence-shell excitations. Wight and Brion[53] assigned this extra band to either the $1a_1$; $\tilde{X}^1A_1 \rightarrow 3pb_2$; $^1B_2$ transition or the equivalent of the $1b_1$; $\tilde{X}^1A_1 \rightarrow 3pb_2$; $^1A_2$ forbidden transition of the valence-shell excitation spectrum. Again, we assign it as the $1a_1$; $\tilde{X}^1A_1 \rightarrow 3sa_1$; $^1A_1$ transition, which is the equivalent of the $1b_1$; $\tilde{X}^1A_1 \rightarrow 3sa_1$; $^1B_1$ transition of the valence-shell excitation spectrum.

D. The 1130 - 1250 Å Absorption Region

This region contains two major electronic transitions: The $1b_1$; $\tilde{X}\ ^1A_1 \rightarrow 3pa_1$; $^1B_1$ and $1b_1$; $\tilde{X}\ ^1A_1 \rightarrow 3pb_1$; $^1A_1$ excitations.[6,8] The tail of the $3a_1$; $\tilde{X}\ ^1A_1 \rightarrow 3sa_1$; $^1A_1$ transition also extends into this region but is obscured by the more intense $1b_1 \rightarrow 3p$ Rydberg transitions. Johns[10] has detected some other bands in this region which appear to be related to the $^2A_1$ core of H_2O^+. We do not know the nature of the state(s) to which these bands refer. We do note, however, that the $3a_1 \rightarrow 3p$ Rydberg transitions should exhibit origins

in this particular region. In specific, given the calculated vertical transition energy[32] for a $3a_1 \rightarrow 3pb_1$ Rydberg excitation at 1040 Å and the known difference of ~1 eV between the vertical and adiabatic ionization energies which produce the $^2A_1$ cation, the adiabatic $3a_1 \rightarrow 3pb_1$ event should occur at ~1135 Å.

Bell[8] observed bands at 1185, 1166 and 1144 Å which do not belong to the two $1b_1 \rightarrow 3p$ systems. He suggested the possibility that they might be $1b_1 \rightarrow 3d$ transitions. We do not know if these bands are identical to those discussed by Johns.[10] However, as mentioned by Bell, rotational analyses of these bands are possible; if so, it should then be possible to determine their excitation nature (i.e., whether they represent excitations from $1b_1$ or $3a_1$) and to assign them accordingly (i.e., $1b_1 \rightarrow 3d$ or $3a_1 \rightarrow 3p$, respectively). Our spectra for this region are given in Fig. 6.

E. The 1060 - 1130 Å Region

A synopsis of the assignments for this region is given in Table 10. We find an origin, which had not previously been so assigned, at 1122 Å in H_2O. The 1086 Å origin, assigned by Price[3] as 2B, is reassigned here as a (0,2,0) vibrational superposition on the 1122 Å origin. A detailed vibronic analysis is given in Table 11. The spectra are shown in Figure 7.

Figure 6(a) The absorption spectrum of H_2O in the 1150 Å region at various pressures: (a) ~95 μm; (b) ~230 μm; (c) ~400 μm; (d) pressure uncertain. The lower, outer O. D. scale is for spectrum (a) and the baseline. The inner O. D. scale is for spectrum (b). The upper, outer O. D. scale is for spectra (c) and (d).

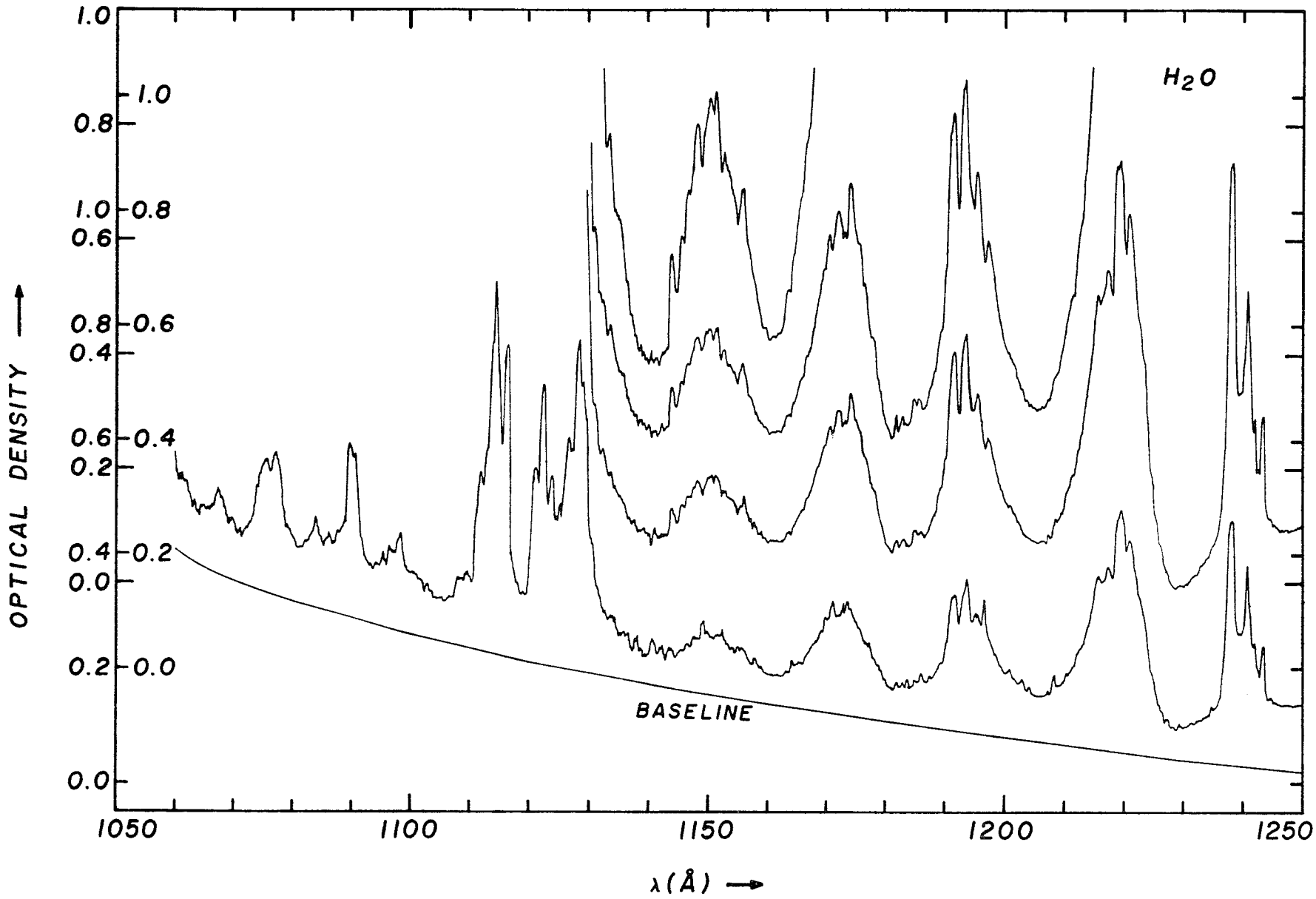
H_2O
BASELINE
OPTICAL DENSITY
λ(Å)
1050
1100
1150
1200
1250
1.0
0.8
0.6
0.4
0.2
0.0

Figure 6(b) The absorption spectrum of D_2O in the 1150 Å region at various pressures: (a) ~100 μm; (b) ~340 μm; (c) ~670 μm pressure. The lower, outer O. D. scale is for spectrum (a) and the baseline. The inner O. D. scale is for spectrum (b). The upper, outer O. D. scale is for spectrum (c).

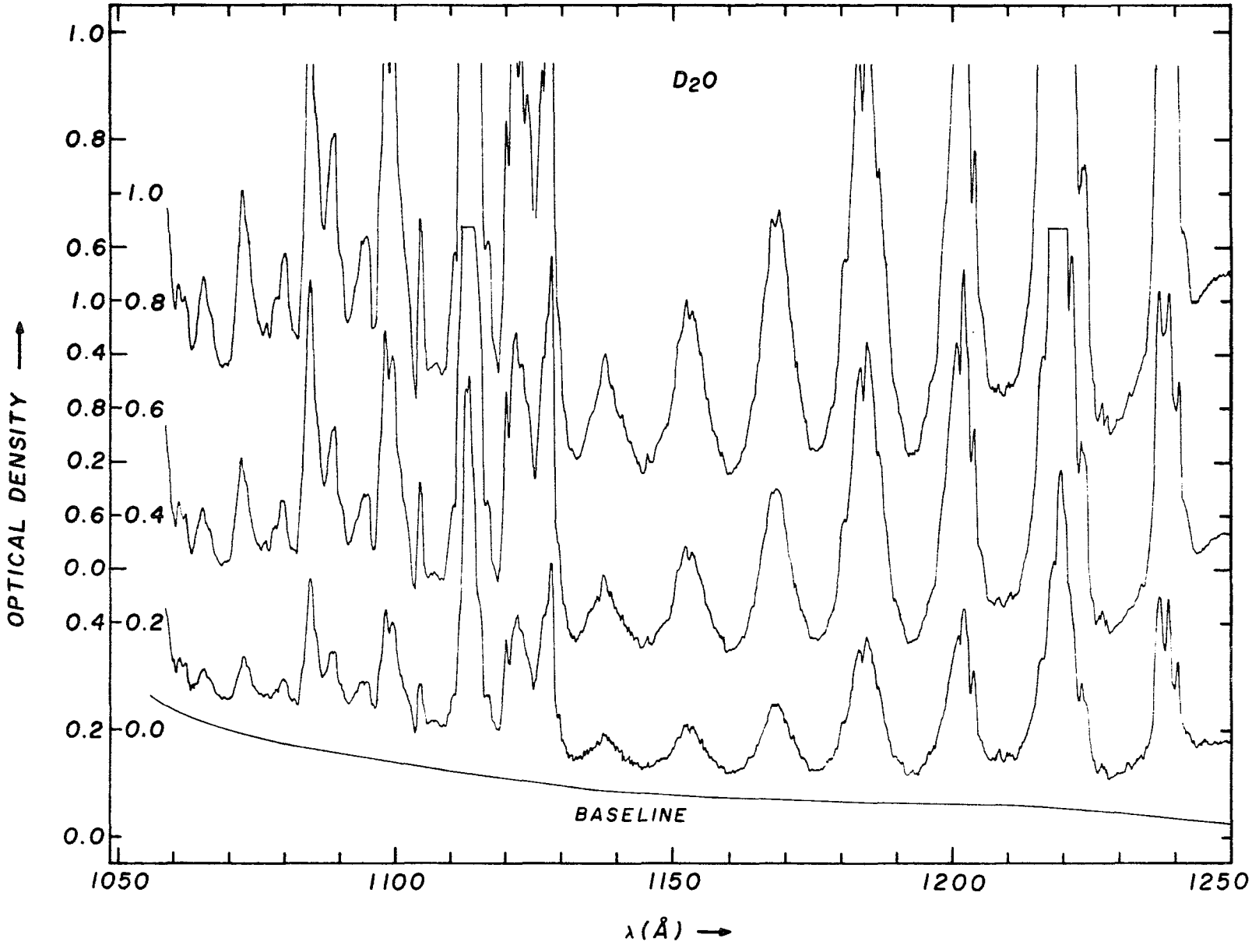
D2O
OPTICAL DENSITY
λ(Å)
BASELINE
1.0
0.8
0.6
0.4
0.2
0.0
1050
1100
1150
1200
1250

TABLE 10

ORIGIN ASSIGNMENTS IN THE 1060 - 1130 Å REGION OF H_2O

	THIS WORK			PRICE[b]		NOMENCLATURE[d]	
	λ (Å)	n*	Assignment	λ (Å)	Assignment	This Work	Price
1	- [a]	-	-	1086.4	$1b_1 \rightarrow 4pa_1$		2B
2	1090.8	3.301	$1b_1 \rightarrow 4pb_1$	1090.6	$1b_1 \rightarrow 4pb_1$	2B	2A
3	1114.5	3.021	$1b_1 \rightarrow 3db_1$	1115.0	$1b_1 \rightarrow 3d$	1D	1D
4	1122.4	2.945	$1b_1 \rightarrow 4sa_1$	c		2E	
5	1128.3	2.892	$1b_1 \rightarrow 3da_1$	1127.9	$1b_1 \rightarrow 4sa_1$	1C	1C

a) The 1086 Å band is assigned as the (0,2,0) vibrational band of the 1122.4 A origin

b) Ref. 3.

c) Unassigned previously.

d) Nomenclature for this work:

Transitions	Series
$1b_1 \rightarrow nsa_1$; $^1B_1$	mE
$\rightarrow npa_1$; $^1B_1$	mA
$\rightarrow npb_1$; $^1A_1$	mB
$\rightarrow nda_1$; $^1B_1$	mC
$\rightarrow ndb_1$; $^1A_1$	mD
$3a_1 \rightarrow nsa_1$; $^1A_1$	me

where

$n = 3,4,5,...$

$m = 1,2,3,...$

TABLE 11A

ABSORPTION SYSTEMS IN THE 1060 - 1130 Å REGION OF H_2O

λ(Å)	ν(cm^{-1})	Assignments[a] (v_1', v_2', v_3') ν_i (cm^{-1})			
1128.3	88629	1C(0,0,0)			
1122.4	89095		2E(0,0,0)		
1114.5	89726			1D(0,0,0)	
1109.6	90123	1C(0,1,0)1494			
1102.9	90670		2E(0,1,0)1575		
1098.3[b]	91050			1D(0,1,0)1490	
1096.3[b]	91216				
1090.8	91676				2B(0,0,0)
1089.7	91768	1C(1,0,0)3139			
1086.1	92072		2E(0,2,0)1402		
1083.9	92259		2E(1,0,0)3164		
1079.5	92635			1D(0,2,0)1419	
1077.2[b]	92833			1D(1,0,0)3107	
1075.5[b]	92980				
1067.2	93703		2E(1,1,0)1444		
1061.0	94251			1D(1,1,0)1418	

a) For nomenclature, see footnote to Table 10.

b) These two bands are indistinguishable.

TABLE 11B

ABSORPTION SYSTEMS IN THE 1060 - 1130 Å REGION OF D_2O

λ(Å)	ν(cm^{-1})	Assignments[a] $(v_1', v_2', v_3')\nu_i$ (cm^{-1})			
1127.8	88668	1C(0,0,0)			
1121.8[b]	89142		2E(0,0,0)		
1119.8	89302				
1114.7	89710	1C(0,1,0)1042			
1113.0[b]	89847			1D(0,0,0)	
1112.4	89896				
1106.7[b]	90359		2E(0,1,0)1217		
1104.3	90555		1253		
1101.7	90769	1C(0,2,0)1059			
1099.3	90967			1D(0,1,0)1120	
1098.1	91066	1C(1,0,0)2398			
1094.2	91391		2E(1,0,0)2249		
1088.4	91878				2B(0,0,0)
1085.4	92132	1C(1,1,0)1066			
1084.4	92217			1D(1,0,0)2370	
1079.6	92627		2E(1,1,0)1236		
1073.2	93179	1C(1,2,0)1047			
1072.3	93257			1D(1,1,0)1040	
1065.1	93888		2E(1,2,0)1261		
1062.0	94162	1C(1,3,0)983			
1060.7	94277			1D(1,2,0)1020	

a) For nomenclature, see footnote to Table 10.
b) These two bands are indistinguishable.

Figure 7. The absorption spectrum of H_2O (~95 μm pressure) and D_2O (~110 μm pressure) in the 1100 Å region.

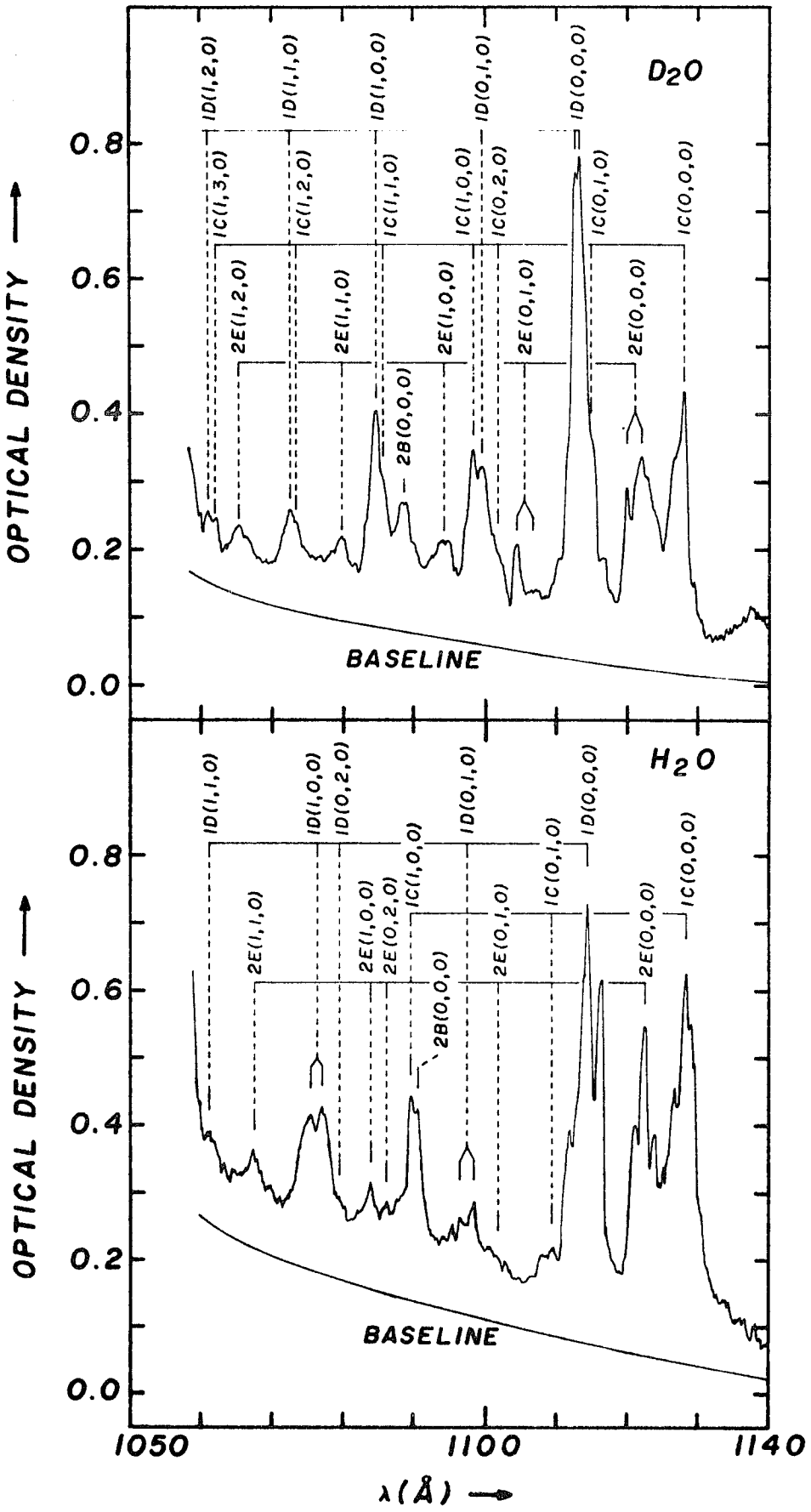
D2O
H2O
OPTICAL DENSITY
0.0
0.2
0.4
0.6
0.8
BASELINE
1050
1100
1140
λ(Å)
1D(1,2,0)
1D(1,1,0)
1D(1,0,0)
1D(0,1,0)
1D(0,0,0)
1C(1,3,0)
1C(1,2,0)
1C(1,1,0)
1C(1,0,0)
1C(0,2,0)
1C(0,1,0)
1C(0,0,0)
2E(1,2,0)
2E(1,1,0)
2E(1,0,0)
2E(0,1,0)
2E(0,0,0)
2B(0,0,0)
1D(1,1,0)
1D(1,0,0)
1D(0,2,0)
1D(0,1,0)
1D(0,0,0)
1C(1,0,0)
1C(0,1,0)
1C(0,0,0)
2E(1,1,0)
2E(1,0,0)
2E(0,2,0)
2E(0,1,0)
2E(0,0,0)
2B(0,0,0)

The vibrational analysis of this region yields vibrational frequencies which are not very different from those of the ground state. This, coupled with the coincidence of adiabatic and vertical energies for all four transitions, suggests that the initial MO is $1b_1$.

The 1122.4 Å origin is assigned as $1b_1 \rightarrow 4sa_1$ for two reasons, neither of them impressive. Firstly, we find $n^* = 2.945$, in nice accord with the value $n^* = 1.963$ for the band assigned as $1b_1 \rightarrow 3sa_1$. Secondly, the 1122.4 Å band is weaker than either of the two adjacent origins at 1128.3 Å and 1114.5 Å -- which would suggest[50] that these latter origins are best assigned as $1b_1 \rightarrow 3d$.

Of the five possible $1b_1 \rightarrow 3d$ transitions, four are allowed by electric dipole selection rules. The 1128.3 and 1114.5 Å origins may well be two of these. The intensity ratio I(1128 Å)/I(1114 Å) is ~1 for H_2O and ~2 for D_2O. The corresponding ratio of 3p Rydberg intensities, $I(1b_1 \rightarrow 3pb_1;\ ^1A_1)/I(1b_1 \rightarrow 3pa_1;\ ^1B_1)$, is also ~1 for H_2O and ~2 for D_2O. While such thinking is dangerous, we use this intensity analogy to assign the 1128 Å origin as one of the two $1b_1 \rightarrow 3da_1;\ ^1B_1$ and the 1114 Å origin as the $1b_1 \rightarrow 3db_1;\ ^1A_1$. These assignments have the added advantage of being in accord with the computational results of Goddard et al.[32] According to their calculation, one of the $1b_1 \rightarrow 3da_1;\ ^1B_1$ is degenerate with the 1114 Å $^1A_1$ transition, while the other $1b_1 \rightarrow 3da_1;\ ^1B_1$ lies ~800 cm^{-1} below the $^1A_1$ transition. In view of this, we may choose to assign two $1b_1 \rightarrow 3d$

transitions at 1114 Å, one being $3db_1$; $^1A_1$ and the other $3da_1$; $^1B_1$, while another $3da_1$; $^1B_1$ lies at 1128 Å.

The 1091 Å band is assigned to a 4p Rydberg excitation for reasons solely connected with the size of the effective quantum number. However, we do note that the intensity of this band, compared with the two 3p bands, is very much weaker than might be expected.

F. The 980 - 1060 Å Absorption Region

Due to the LiF cut-off at ~1060 Å, we now utilize the data of Katayama et al.[11] We will provide a vibronic analysis for this region, detect and assign some new origins, and reassign some older ones. This analysis is given in Table 12. The spectra for H_2O and D_2O are given in Fig. 8.

The 1050 - 1060 Å region contains three origins: 1057, 1055 and 1053 Å for H_2O with n* = 3.921, 3.960 and 4.024, respectively. These correspond well with the $1b_1 \rightarrow 3da_1$; $^1B_1$, the $1b_1 \rightarrow 4sa_1$; $^1B_1$ and the $1b_1 \rightarrow 3db_1$s; $^1A_1$ origin bands for which n* = 2.892, 2.945 and 3.021, respectively. Hence, we may assign the 1057, 1055 and 1053 Å bands as the $1b_1 \rightarrow 4da_1$; $^1B_1$, the $1b_1 \rightarrow 5sa_1$; $^1B_1$ and the $1b_1 \rightarrow 4db_1$; $^1A_1$ transitions, respectively.

The transitions from $1b_1$ to $5da_1$, $6sa_1$, and $5db_1$ (for which, by extrapolation, n* = 4.92, 4.96 and 5.02, respectively) should lie at 1028.7, 1027.9 and 1026.8 Å. The resolution available to Katayama et al. was adequate to

TABLE 12A

ANALYSIS OF THE 980 - 1060 Å ABSORPTION REGION OF H_2O

λ(Å)	ν(cm^{-1})	Assignment $(v_1', v_2', v_3')\nu_i$ (cm^{-1})			
1057.0*±0.2	94610	2C(0,0,0)			
1055.4	94750		3E(0,0,0)		
1053.0*	94970			2D(0,0,0)	
1048.2	95400		2E(2,0,0)3140		
1045.1	95680			1D(1,2,0)1429	
1042.6	95910			1D(2,0,0)3100	3B(0,0,0)[a]
1040.7	96090	2C(0,1,0)1480			
1039.0	96250		3E(0,1,0)1500		
1038.0	96340			2D(0,1,0)1370	
1027.5	97320			3D(0,0,0)	
1024.8	97580				
1022.6	97790	3C(1,0,0)3180			
1021.1	97930		3E(1,0,0)3180		
1018.6	98170			2D(1,0,0)3200	
1016.8[b]	98350				
1013.2	98700			4D(0,0,0)	
1011.2	98890			3D(0,1,0)1590	
1009.0	99110	2C(1,1,0)1320			5B(0,0,0)[a]
1006.3	99370		3E(1,1,0)1440		
1005.0	99500			5D(0,0,0)	

(continued on next page)

Table 12A (cont'd)

λ (Å)	ν (cm^{-1})	Assignment (v_1', v_2', v_3') ν_i (cm^{-1})
1003.5	99650	2D(1,1,0)1480
999.4	100060	6D(0,0,0)
998.2	100180	4D(0,1,0)1480
995.9	100410	7D(0,0,0)
994.7	100530	3D(1,0,0)3210
993.4	100660	8D(0,0,0)
991.6	100850	9D(0,0,0)
989.5	101060	5D(0,1,0)1560
985.1	101510	6D(0,1,0)1450
980.7	101970	4D(1,0,0)3270

* Price gave 1057.9 and 1051.6 Å instead (Ref. 3).

a) This is a possible assignment.

b) A shoulder.

TABLE 12B

ANALYSIS OF THE 980 - 1060 Å ABSORPTION REGION OF D_2O

λ(Å)	ν(cm^{-1})	Assignments $(v_1', v_2', v_3')\nu_i$ (cm^{-1})			
1057.5±0.2	94560			1D(2,0,0)2350	
1056.0	94700	2C(0,0,0)			
1054.3	94850		3E(0,0,0)		
1052.6	95000			2D(0,0,0)	
1045.7	95630			1D(2,1,0)1070	
1041.9	95980				3B(0,0,0)
1034.6	96660			1D(3,0,0)2090	
1031.5	96950	2C(1,0,0)2250			
1030.1	97080		3E(1,0,0)2230		
1027.0	97370			2D(1,0,0)2370	
1026.3	97440			3D(0,0,0)	
1019.2	98120				4B(0,0,0)
1016.0	98420			2D(1,1,0)1050	
1014.5	98570			3D(0,1,0)1130	
1011.8	98830			4D(0,0,0)	
1009.9[a]	99020				
1007.6	99250				5B(0,0,0)
1003.6	99640			5D(0,0,0)	
1002.4	99760			3D(1,0,0)2320	
998.2	100180			6D(0,0,0)	
994.5	100550			7D(0,0,0)	
993.5	100650			5D(0,1,0)1010	
992.3	100780			8D(0,0,0)	
989.0	100110			4D(1,0,0)2280	
981.0	101940			5D(1,0,0)2300	

a) A shoulder

Figure 8. Spectra measured by Katayama et al. (Ref. 11), a) for H_2O, b) for D_2O. Transitions are labeled by the upper orbitals only.

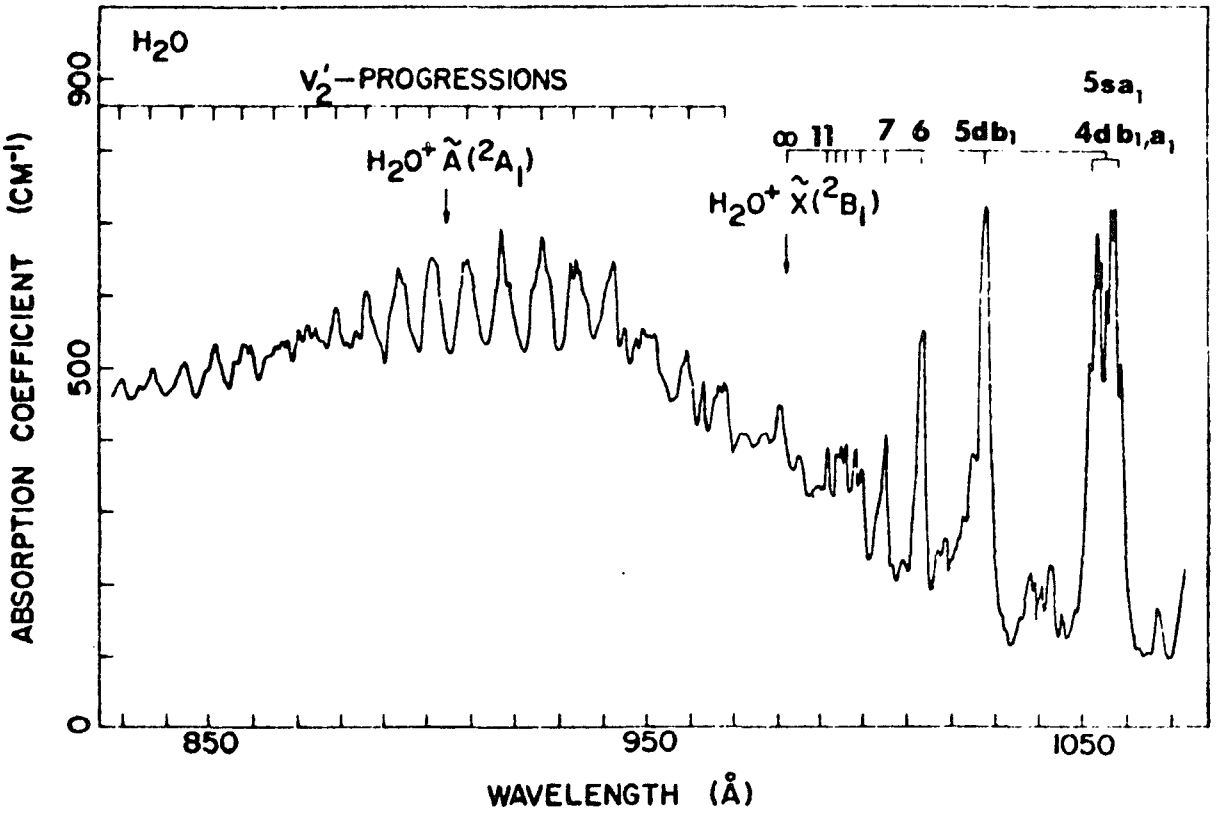
H2O
V2'—PROGRESSIONS
H2O+ Ã(2A1)
H2O+ X̃(2B1)
∞ 11
7 6
5db1
5sa1
4db1,a1
ABSORPTION COEFFICIENT (CM-1)
900
500
0
850
950
1050
WAVELENGTH (Å)

Figure 8(a)

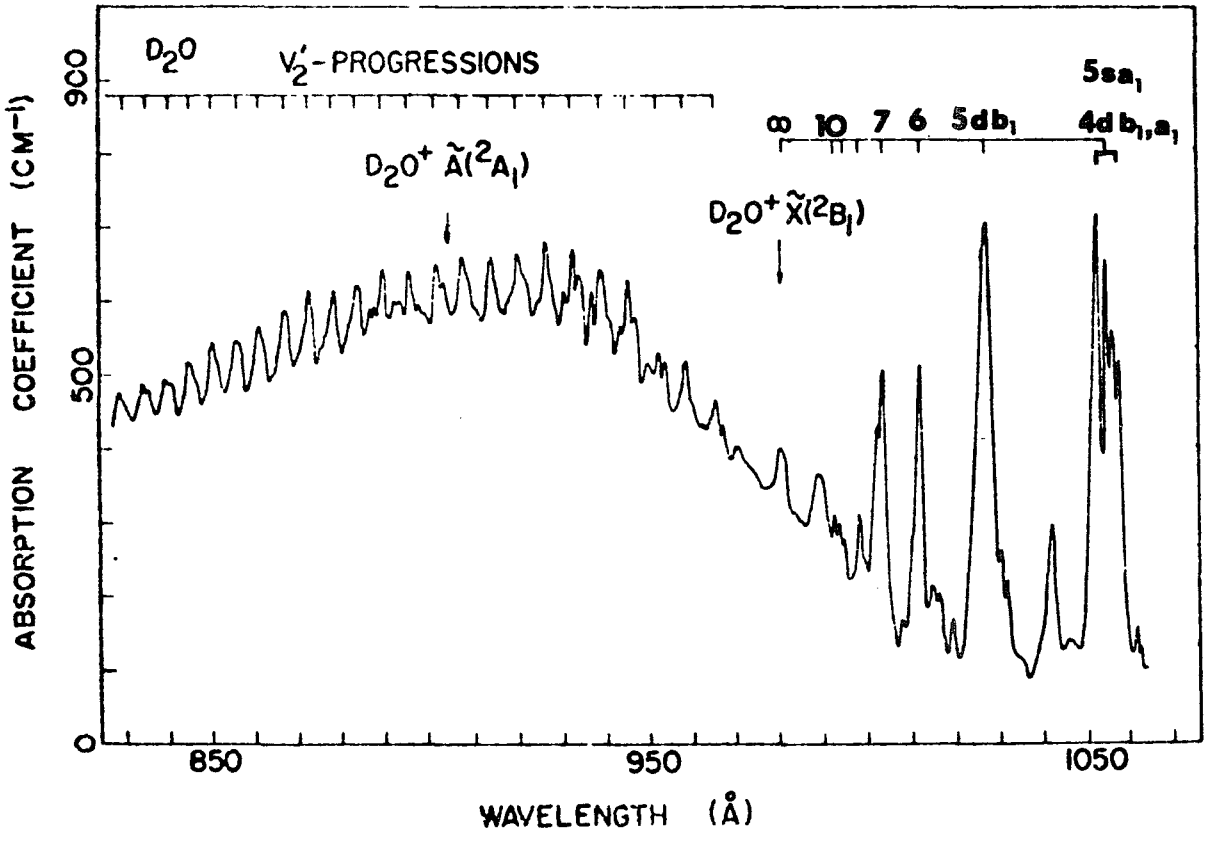
D2O
V2'-PROGRESSIONS
5sa1
∞ 10 7 6 5db1
4db1,a1
D2O+ Ã(2A1)
D2O+ X̃(2B1)
ABSORPTION COEFFICIENT (CM-1)
900
500
0
850
950
1050
WAVELENGTH (Å)

Figure 8(b)

resolve these three bands. Despite this, they found only one absorption band in the vicinity of 1027 Å. The appearance of only one band implies either a convergence of all three bands or a diminution of the intensity of two of them. The former is unreasonable because it requires co-directional and minimal adventitious band shifts of 180 cm^{-1} and 100 cm^{-1} for at least two of the three bands. The latter interpretation is preferable. Since the $1b_1 \rightarrow 3da_1$; $^1B_1$ and $1b_1 \rightarrow 4sa_1$; $^1B_1$ transitions are group-theoretically identical and possess very similar intensities, it may well be that higher members of these series lose intensity and drop into the background. Thus, the $1b_1 \rightarrow 4da_1$ and $1b_1 \rightarrow 5sa_1$ members are still recognizable but the $1b_1 \rightarrow 5da_1$ and $1b_1 \rightarrow 6sa_1$ members may be too weak to be detectable.

The remaining members of the series described by Katayama et al. may now be assigned as $1b_1 \rightarrow ndb_1$; $^1A_1$ with n = 5, 6, ..., 11. The effective quantum numbers are n* = 4.982, 5.999, 7.008, 8.068, 9.063, 10.052 and 11.067, respectively.

The vibrational analysis of Table 12 validates a number of points. These are: (i) All states observed in this region derive from excitation of a $1b_1$ electron. (ii) Vibronic coupling occurs, unmodified, out to and even beyond the first ionization limit (see Table 12). (iii) The vibronic analysis serves as a convenient filter

by means of which the residue of np Rydberg states may be sorted out and assigned.

G. The 968 Å Absorption Band

The vibrational progression found by Katayama et al.[54] in this region has its origin at 968.4 Å. This progression was analyzed in Section C from the point of view of anharmonicity, isotope effects, geometry of the excited state, etc. This origin at 968.4 Å corresponds to a Rydberg state converging to the 2nd ionization limit with $n^* = 3.624$ which, by comparison with $n^* = 1.621$ of the $3a_1$; $\tilde{X}\,{}^1A_1 \rightarrow 3sa_1$; $^1A_1$, can be assigned as $3a_1$; $\tilde{X}\,{}^1A_1 \rightarrow 5sa_1$; $^1A_1$. It has an equilibrium angle of $150^\circ \leq \measuredangle HOH \leq 180^\circ$, as established in Section C .

IV. SUMMARY AND CONCLUSIONS

Our investigation of the electronic absorption spectrum of the water molecule at energies less than ~14.0 eV has resulted in the following:

Revealed several electronic transitions which had previously been unobserved. They consist of the $1b_1$; $\tilde{X}\,^1A_1 \rightarrow 3sa_1$; $^1B_1$, $4sa_1$; $^1B_1$ and $5sa_1$; $^1B_1$ transitions at 1365, 1122 and 1055 Å, respectively. The possibility of a weak transition at 1530 Å has also been discussed.

Vibrational analyses have been given for the 1280 Å band system, the 1128, 1122 and 114 Å band complex, and the 980 Å - 1060 Å region.

New assignments have been provided for the 1670 Å absorption band, as well as for the 4.0 - 6.0 eV and the 7.0 eV electron-impact bands. Higher members of the $1b_1$; $\tilde{X}\,^1A_1 \rightarrow np$ series have been assigned with the aid of vibrational analyses. The 968 Å origin observed by Katayama et al. has been assigned as the $3a_1$; $\tilde{X}\,^1A_1 \rightarrow 5sa_1$; $^1A_1$ transition. Besides the above, a number of other important points merit further discussion.

A. Lower-Energy States

Our conclusions concerning the singlet states below 11 eV are summed up in the potential energy diagram of

Figure 9. The potential energy curves of Figure 9 are schematic, particularly with respect to curvatures. However, the energy levels and the equilibrium values of ∢HOH, which are either ~105° or ~180°, are experimentally determined. The degenerate states of the linear molecule are split by Renner-Teller effects in the manner shown in Figure 9. According to our assignments, the bent state at 1670 Å (6.81 eV) is an intravalence state, $4a_1$; $^1B_1$, which converges onto its partner, the $3sa_1$; $^1A_1$ state at 1432 Å (8.66 eV), as ∢HOH approaches 180°. This convergence implies a change of orbital character as a function of ∢HOH: The lowest-energy excited state at 180°, the $^1\Pi_u$ state, is predominantly 3s in nature. However, as ∢HOH deviates from 180°, two states result, the lower of which minimizes at ~105° and alters character from predominantly 3s to predominantly $4a_1$ whereas the upper remains predominantly 3s throughout its total angular extent.

The 1365 Å (9.08 eV) state has a bent equilibrium conformation and it is assigned as the predominantly $3sa_1$; $^1B_1$ Rydberg state. In this energy region, the character of all states must contain considerable 3s character, regardless of the magnitude of the equilibrium value of ∢HOH -- hence, the two 3s Rydberg states of equilibrium geometries 105° and 180° which coexist in this energy region.

Figure 9. The schematic potential diagram of H_2O with energy less than -11.0 eV. The potentials are plotted as functions of θHOH.

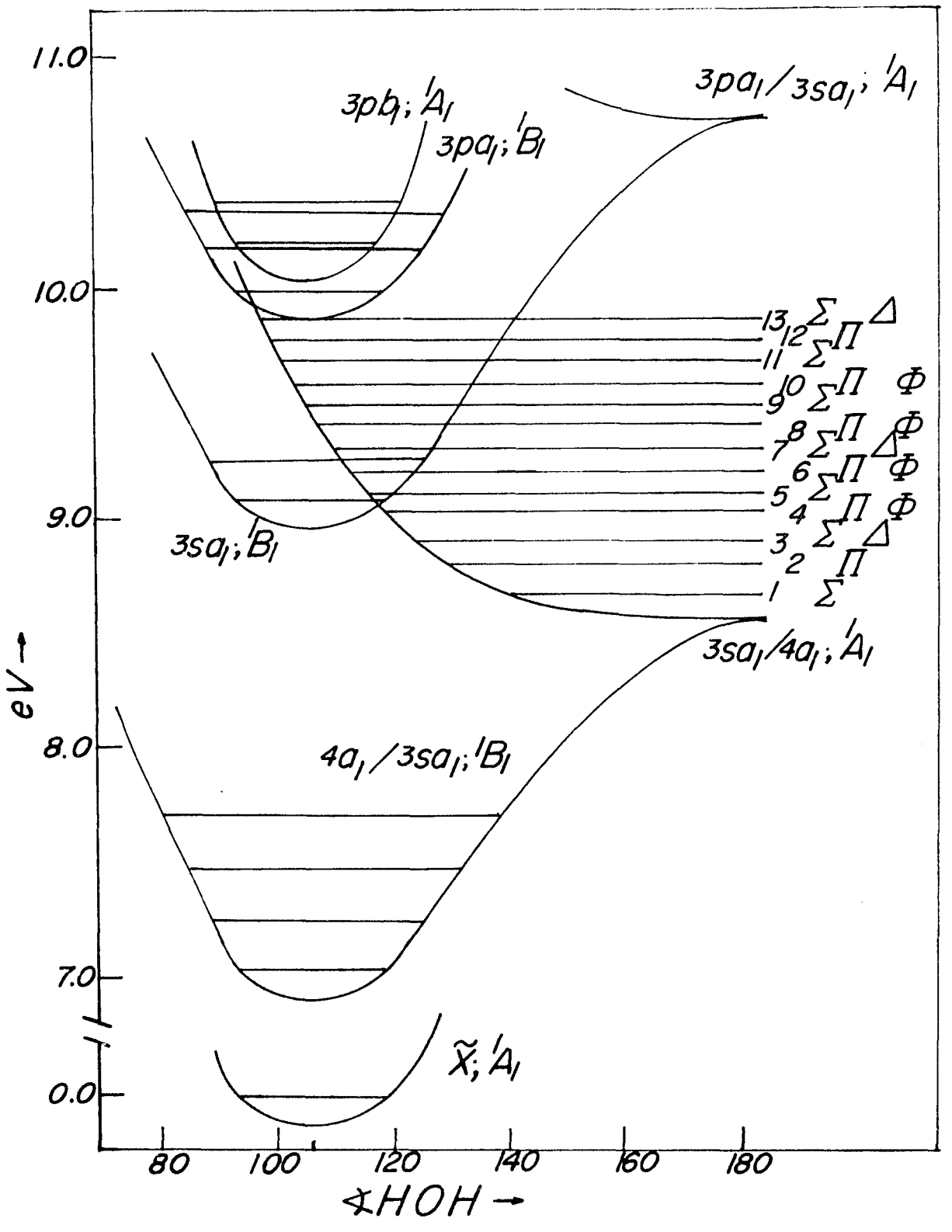
11.0
10.0
9.0
8.0
7.0
0.0
eV →
3pb1; 1A1
3pa1; 1B1
3pa1/3sa1; 1A1
13 12 11 10 9 8 7 6 5 4 3 2 1
Σ Π Δ Φ
3sa1; 1B1
3sa1/4a1; 1A1
4a1/3sa1; 1B1
X̃; 1A1
80 100 120 140 160 180
∠HOH →

The $3sa_1$; $^1B_1$ potential energy curve is shown to be convergent on a $^1\Pi_u$ state at 11 eV. This doubly-degenerate state is thought to possess considerable 3p character since the 3p energy region of the linear molecule should initiate at ~11 eV.

In sum, the four states which result from Renner-Teller splitting of the two $^1\Pi_u$ states of the linear conformation can be viewed as constituted of $4a_1$, $3sa_1$, and, to some extent, 3p terminal MO's. The orbital constitution of these Renner-Teller components is a function of ∢HOH and is, in our opinion, largely determined by energy. At lower energy, the intravalence $4a_1$ MO predominates; as energy increases, the $3sa_1$ Rydberg orbital begins to play a role; and, above ~11 eV, the 3p Rydberg orbitals may well be dominant.

The weak shoulder, which may well exist at ~1530 Å (8.1 eV), is tentatively assigned as the $3a_1$; $\tilde{X}^1A_1 \rightarrow 2b_2$; $^1B_2$ intravalence transition. If this assignment is correct, we will have accounted for all three possible dipole allowed intravalence transitions. The $3sa_1$; $^1A_1$ state at 1432 Å probably contains a certain amount of $4a_1$ in the upper state. In specific, the underlying "continuum" in the 1432 Å region may well refer to the same $3a_1$; $\tilde{X}^1A_1 \rightarrow 3sa_1$; $^1A_1$ transition, the broadness being caused by the mixing of $3sa_1$ and $4a_1$ orbitals in the upper state.

The $1b_1$; $\tilde{X}^1A_1 \rightarrow 2b_2$; $^1A_2$ transition is dipole forbidden and is not observed. It could well be the lower-energy Renner-Teller partner of the 1530 Å state and occurs at quite low energies. The triplet states which correspond to the various singlet states mentioned above can be assigned as follows: The 4.0 - 6.0 eV band is assigned as the $1b_1$; $\tilde{X}^1A_1 \rightarrow 4a$; $^3B_1$ transition; the 7.0 eV band is assigned either as $1b_1$; $\tilde{X}^1A_1 \rightarrow 2b_2$; $^3A_2$ or $3a_1$; $\tilde{X}^1A_1 \rightarrow 2b_2$; $^3B_2$ transitions; and the 9.0 eV electron-impact band is assigned as the $3a_1$; $\tilde{X}^1A_1 \rightarrow 3sa_1$; $^3A_1$ transition (see following).

Chutjian et al.[30] observed a band of triplet nature at ~9.0 eV with associated vibrational progressions of ~0.15 eV for H_2O and ~0.12 eV for D_2O. They assigned this band as the $\tilde{X}^1A_1 \rightarrow 3p\ b_2$, $^3A_2$ transition. We believe that this band corresponds to the excitation of a $3a_1$ electron: The highly non-vertical appearance of this band implies that either the upper state is dissociative (and, thus, intravalence) or Rydberg with almost linear geometry. The only candidate possible is the $3a_1$; $\tilde{X}^1A_1 \rightarrow 3sa_1$; $^3A_1$ transition as stated above.

As to the question of where the $^1b_1$; $X^1A_1 \rightarrow 3pb_2$; $^1A_2$ and $^3A_2$ transitions occur, we can only add that no evidence of their existence is available in the electron impact spectra. By this statement, we infer that these transitions should exhibit Franck-Condon patttern similar

to the corresponding singlets, $1b_1$; $\tilde{X}^1A_1 \rightarrow 3pb_1$; $^1A_1$ and $3pa_1$; $^1B_1$ at 1210 and 1240 Å, respectively.

B. Higher-Energy States

The higher members of the $1b_1$; $\tilde{X}^1A_1 \rightarrow npb_1$; $^1A_1$ series have intensities that are very low compared to those of the lower-energy $1b_1$; $\tilde{X}^1A_1 \rightarrow 3pa_1$; $^1B_1$ and $3pb_1$; $^1A_1$ series members. We may explain this observation using the atomic $\Delta\ell = \pm 1$ selection rule: Since the $1b_1$ MO is essentially a 2p AO on the oxygen atom, it is expected that transitions from $1b_1$ to higher np Rydberg states should be either totally forbidden or very weak. However, the $1b_1 \rightarrow 3p$ transitions show quite high intensities while higher $1b_1 \rightarrow np$ transitions, $n>3$, have very low intensities. The most plausible explanation is that the 3p orbitals, being very close to the molecular core, do not obey the atomic selection rules whereas the np orbitals, $n>3$, being nearly atomic, do obey the atomic selection rules.

In the region 980 Å - 1060 Å, vibrational analysis reveals not only the origins of the higher-energy npb_1; $^1A_1$ states but also the interference between vibrational levels of lower-energy Rydberg states with the electronic origins of higher-energy Rydberg states. For H_2O, the (1,0,0) band of the $5db_1$; $^1A_1$ state at 994.7 Å obscures the $10db_1$; $^1A_1$ band. As a result, Katayama et al.[11] cite 993.6 Å as the origin of the $10db_1$; $^1A_1$ state whereas we

conclude that 993.4 Å is the more likely. For D_2O, the (1,0,0) bands of the $4db_1$; $^1A_1$, $5sa_1$; $^1B_1$ and $4da_1$; $^1B_1$ states all overlap with the origin of the $5db_1$; $^1A_1$ state. Thus, we rewrite the true origin of the $5db_1$; $^1A_1$ state from 1026.5 Å to 1026.3 Å. The split bands at 1003.6 and 1002.4 Å are separately assigned as the origin of the $7db_1$; $^1A_1$ state and the (1,0,0) band of the $5d_1b_1$; $^1A_1$ state (whose origin lies at 1026.3 Å), respectively.

C. Ionization Potentials

The lowest-energy ionization potentials for H_2O and D_2O, as given by Katayama et al.[11]: 101784±50 cm^{-1} and 101920±50 cm^{-1} respectively, are less accurate than those given by Karlsson et al.[20]: 101746±8 cm^{-1} and 101890±8 cm^{-1} respectively. In particular, the latter values give very constant quantum defects for all higher members of the ndb_1; $^1A_1$ series.

The second ionization potentials are reported as 13.839±0.007 eV and 13.847±0.008 eV by Karlsson et al.[20] for H_2O and D_2O, respectively. However, Dixon et al.[21] later revised these values to 13.838 eV and 13.768 eV, respectively. In view of the very large isotope shift and its anomalous sign in the data of Dixon et al.[21], we prefer the values of Karlsson et al.[20] and it is these latter values which we use to evaluate the effective quantum numbers for the $3sa_1$; $^1A_1$ and $5sa_1$; $^1A_1$ states.

D. Interactions Between Bent and Linear States

The two Renner-Teller component states of Π parentage in $D_{\infty h}$, one bent and the other linear, exhibit considerable interactions of the vibrational levels of these two split components. These interactions account for the alternating band shapes of the vibrational levels of the linear state. It is suspected that similar interactions exist between bent states and linear states with different values of n but similar energies (i.e., dynamic Renner-Teller effects). An example is provided by the very low intensity of the $1b_1$; $\tilde{X}^1A_1 \rightarrow 3sa_1$; $^1B_1$ transition which happens to sit astride the $3a_1$; $\tilde{X}^1A_1 \rightarrow 3sa_1$; $^1A_1$ transition of the linear molecule. Similar situations exist also for the $1b_1$; $\tilde{X}^1A_1 \rightarrow 4pa_1$; $^1B_1$, $5pa_1$; $^1B_1$ and npa_1; $^1B_1$ ($n>5$) transitions of the same series. Furthermore, the transitions $1b_1$; $\tilde{X}^1A_1 \rightarrow nda_1$; $^1B_1$ ($n = 5,6,7,...$) and $1b_1$; $\tilde{X}^1A_1 \rightarrow nsa_1$; $^1B_1$ ($n = 6,7,8,...$) all exhibit the same "disappearance" of intensity.

Of all the possible linear states which converge to the $^2A_1$ cationic limit, we have observed only the $3sa_1$; $^1A_1$ and $5sa_1$; $^1A_1$ states whereas the $4sa_1$; $^1A_1$, $3pb_1$; $^1B_1$, $3pa_1$; $^1A_1$, $3pb_2$; $^1B_2$ and all the 3d states are not observed. These states must lie between ~1150 and ~980 Å and they may interact with the bent states which converge to the $^2B_1$ cationic limit. Though the nature of the

alleged interactions is uncertain, it is interesting to note that all of the "missing" states are of $^1B_1$ symmetry.

E. Summary of Assignments

Six Rydberg series have been assigned for H_2O and D_2O. The results are shown in Table 13. Of these six series, five converge to the first ionization limit and only one converges to the second ionization limit.

F. Future Work

We feel that the following studies will do much to solve the problems concerning the electronic structure of the water molecule.

-----A detailed Renner-Teller study of the 1280 Å band system should clarify the number of different electronic states involved in this band system and should prove (or disprove) our assignment of the 1365 Å irregular band as the $1b_1; \tilde{X}^1A_1 \rightarrow 3sa_1; {}^1B_1$ origin.

-----A high-resolution study of the 1060 - 1250 Å region should reveal the existence of other linear states which converge on the $^2A_1$ cationic state. Of particular interest are the 1185 and 1075 Å regions because these are the locations in which Chutjian et al.[30] assigned the $1b_1; \tilde{X}^1A_1 \rightarrow 4sa_1; {}^1B_1$ and $1b_1; \tilde{X}^1A_1 \rightarrow 5sa_1; {}^1B_1$, transitions, respectively. If the bands observed at 1185 and 1075 Å by

TABLE 13A

RYDBERG SERIES FOR H_2O [a]

	$1b_1 \rightarrow nsa_1; {}^1B_1$		$1b_1 \rightarrow npa_1; {}^1B_1$		$1b_1 \rightarrow npb_1; {}^1A_1$		$1b_1 \rightarrow nda_1; {}^1B_1$		$1b_1 \rightarrow ndb_1; {}^1A_1$		$3a_1 \rightarrow nsa_1; {}^1A_1$	
n	$\bar{\nu}(cm^{-1})$	n*	$\bar{\nu}(cm^{-1})$	n*	$\bar{\nu}(cm^{-1})$	n*	$\bar{\nu}(cm^{-1})$	n*	$\bar{\nu}(cm^{-1})$	n*	$\bar{\nu}(cm^{-1})$	n*
3	73271	1.963	80604	2.278	82038	2.360	88629	2.892	89726	3.021	69832	1.621
4	89095	2.945			91676	3.301	94610	3.921	94970	4.024	--	--
5	94750	3.960			95910	4.336			97324	4.982	103260	3.624
6					--	--			98697	5.999		
7					99110	6.452			99512	7.008		
8									100060	8.068		
9									100410	9.063		
10									100660	10.052		
11									100850	11.067		
∞ [b]	101746±8		101746±8		101746±8		101746±8		101746±8		111620±60	

a) For nomenclature, see footnote to Table 10.

b) From Ref. 20.

TABLE 13B

RYDBERG SERIES FOR D_2O [a]

	E $1b_1 \rightarrow nsa_1; {}^1B_1$		A $1b_1 \rightarrow npa_1; {}^1B_1$		B $1b_1 \rightarrow npb_1; {}^1A_1$		C $1b_1 \rightarrow nda_1; {}^1B_1$		D $1b_1 \rightarrow ndb_1; {}^1A_1$		E $3a_1 \rightarrow nsa_1; {}^1A_1$	
n	$\bar{\nu}(cm^{-1})$	n*	$\bar{\nu}(cm^{-1})$	n*	$\bar{\nu}(cm^{-1})$	n*	$\bar{\nu}(cm^{-1})$	n*	$\bar{\nu}(cm^{-1})$	n*	$\bar{\nu}(cm^{-1})$	n*
3	73260	1.958	80738	2.278	82061	3.352	88668	2.881	89847	3.018	69930	1.621
4	89142	2.934			91878	3.311	94697	3.906	95003	3.992	--	--
5	94850	3.948			95978	4.308			97437	4.964	103600	3.685
6					98116	5.392			98834	5.992		
7					99246	6.442			99641	6.985		
8									100180	8.011		
9									100550	9.049		
10									100780	9.943		
∞ [b]	101890±8		101890±8		101890±8		101890±8		101890±8		111680±60	

a) For nomenclature, see footnote to Table 10.

b) From Ref. 20.

Chutjian et al. can be resolved, then it should be easy to determine whether or not their assignments are correct. If the excited states are found to be linear, these states could not be either $4sa_1$; $^1B_1$ or $5sa_1$; $^1B_1$. If the excited states are found to be bent, the symmetry of the upper states being $^1B_1$ or not will provide the answer. Similarly, the symmetries of the 1128, 1122 and 1115 Å bands can also fixate the real identities of their corresponding upper states.

-----The 4.0 - 6.0 eV electron-impact band must be characterized unequivocally: Does it or does it not pertain to the neutral water molecule? If it does, its assignment as $1b_1$; $\tilde{X}^1A_1 \rightarrow 4a_1$; $^3B_1$ is quite conclusive.

-----Photodissociation studies of the 1280 Å band system may reveal the real identity of the 1365 Å irregular band. The polarized photoexcitation studies of Chamberlain and Simon[44] might be concentrated close to the 1365 Å region in order to determine the symmetry of the excited state at 1365 Å. A comparative study of D_2O should provide further evidence.

-----Any calculations on the Rydberg/intravalence character of excited states as a function of ∤HOH would be welcome. Any discussion of the possible interference interactions between bent and linear states of different n would also be very useful.

REFERENCES

1. H. J. Henning, Ann. Phys. 13 (1932) 599.
2. G. Rathenau, Z. Physik 87 (1933) 32.
3. W. C. Price, J. Chem. Phys. 4 (1936) 147.
4. P. G. Wilkinson and H. L. Johnston, J. Chem. Phys. 18 (1950) 190.
5. K. Watanabe and M. Zelikoff, J. Opt. Soc. Amer. 43 (1953) 753.
6. J. W. C. Johns, Can. J. Phys. 41 (1963) 209.
7. K. Watanabe and A. S. Jursa, J. Chem. Phys. 41 (1964) 1650.
8. S. Bell, J. Mol. Spec. 16 (1965) 205.
9. A. H. Laufer and J. R. McNesby, Can. J. Chem. 43 (1965) 3487.
10. J. W. C. Johns, Phys. Can. 27 (1971) 54.
11. D. H. Katayama, R. E. Huffman and C. L. O'Bryan, J. Chem. Phys. 59 (1973) 4309.
12. Ref. 11 and references therein.
13. K. H. Welge and F. Stuhl, J. Chem. Phys. 46 (1967) 2440.
14. I. Tanaka, T. Carrington and H. P. Broida, J. Chem. Phys. 35 (1961) 750.
15. T. Carrington, J. Chem. Phys. 41 (1964) 2012.
16. K. D. Byer and K. H. Welge, Z. Naturforsch. A22 (1967) 1161.
17. C. R. Brundle and D. W. Turner, Proc. Roy. Soc. Lond. A307 (1968) 27.

18. A. W. Potts and W. C. Price, Proc. Roy. Soc. Lond. A326 (1972) 181.

19. L. Åsbrink and J. W. Rabalais, Chem. Phys. Lett. 12 (1971) 182.

20. L. Karlsson, L. Mattsson, R. Jadrny, R. G. Albridge, S. Pinchas, T. Bergmark, and K. Siegbahn, J. Chem. Phys. 62 (1975) 4745.

21. R. N. Dixon, G. Duxbury, J. W. Rabalais and L. Åsbrink, Mol. Phys. 31 (1976) 423.

22. G. J. Schulz, J. Chem. Phys. 33 (1960) 1661.

23. A. Skerbele and E. N. Lassettre, J. Chem. Phys. 42 (1965) 395.

24. A. Skerbele, V. D. Meyer, and E. N. Lassettre, J. Chem. Phys. 43 (1965) 817.

25. A. Skerbele and E. N. Lassettre, J. Chem. Phys. 44 (1966) 4066.

26. R. N. Compton, R. H. Huebner, P. W. Reinhardt and L. G. Christophorou, J. Chem. Phys. 48 (1968) 901.

27. E. N. Lassettre, A. Skerbele, M. A. Dillion and K. J. Ross, J. Chem. Phys. 48 (1968) 5066.

28. F. W. E. Knoop, H. H. Brongersma and L. J. Oosterhoff, Chem. Phys. Lett. 13 (1972) 20.

29. S. Trajmar, W. Williams and A. Kuppermann, J. Chem. Phys. 54 (1971) 2274; 58 (1973) 2521.

30. A. Chutjian, R. I. Hall and S. Trajmar, J. Chem. Phys. 63 (1975) 892.

31. C. R. Clayton, G. A. Segal and H. S. Taylor, J. Chem. Phys. 54 (1971) 3799.

32. W. A. Goddard III and W. J. Hunt, Chem. Phys. Lett. 24 (1974) 464.

33. D. Yeager, V. McKoy and G. A. Segal, J. Chem. Phys. 61 (1974) 755.

34. R. J. Buenker and S. D. Peyerimhoff, Chem. Phys. Lett. 29 (1974) 253.

35. H. W. Winter, W. A. Goddard III and F. W. Bobrowicz, J. Chem. Phys. 62 (1975) 4325.

36. E. N. Lassettre and W. Huo, J. Chem. Phys. 61 (1974) 1703.

37. R. Azria and F. Fiquet-Fayard, C. R. Acad. Sci. Paris, B273 (1971) 944.

38. R. S. Mulliken, J. Chem. Phys. 3 (1935) 506.

39. K. J. Miller, S. R. Mielczarek and M. Krauss, J. Chem. Phys. 51 (1969) 26.

40. A. D. Walsh, "Advances in Molecular Spectroscopy", edited by A. Mangini, Pergamon, Oxford, 1962. Vol. I, p. 148.

41. F. Flouquet and J. A. Horsley, J. Chem. Phys. 60 (1974) 3767.

42. T. Horie, T. Nagura and M. Otsuka, J. Phys. Soc. Jap. 11 (1956) 1157; Phys. Rev. 104 (1956) 547.

43. S. Tsurubuchi, Chem. Phys. 10 (1975) 335.

44. G. A. Chamberlain and J. P. Simons, Chem. Phys. Lett. 32, (1975) 355.

45. G. R. Mohlmann, C. I. M. Beenakker and F. J. De Heer, Chem. Phys. 13 (1976) 375.

46. G. Herzberg, "Molecular Spectra and Molecular Structure" Vol. III, "Electronic Spectra and Electronic Structure of Polyatomic Molecules", Van Nostrand Reinhold, Princeton, New Jersey, 1966.

47. S. D. Thompson, D. G. Carroll, F. Watson, M. O'Donnell and S. P. McGlynn, J. Chem. Phys. 45 (1966) 1367.

48. From CNDO calculation

$$4a_1 = 0.4630(2sa_1)-0.4713(2p_z a_1)-0.5308(1s_H a_1+1s'_H a_1)$$

and

$$2K = 2\langle 2p_x(1)4a_1(2)\left|\frac{1}{r_{12}}\right|2p_x(2)4a_1(1)\rangle$$
$$\tilde{=} 1.8 \text{ eV}$$

49. a) J. K. Jacques and R. F. Barrow, Proc. Phys. Soc. 73 (1959) 538.

b) J. G. Stamper and R. F. Barrow, J. Phys. Chem. 65 (1961) 250.

c) G. Di Lonardo and A. E. Douglas, Can. J. Phys. 51 (1973) 434.

50. G. Herzberg, "Infrared and Raman Spectra of Polyatomic Molecules", Van Nostrand, New York, 1945, p. 169.

51. M. B. Robin, "Higher Excited States of Polyatomic Molecules", Academic Press, New York, 1974.

52. Ref. 46, p. 26.

53. G. R. Wight and C. E. Brion, J. Elect. Spec. and Related Phen. 4 (1974) 25.

54. Ref. 11. Katayama et al. established the geometry of the 968 Å band by considering isotope shifts between $H_2^{16}O$ and $H_2^{18}O$.

CHAPTER FIVE

CONCLUSIONS

A general correlative scheme for Rydberg states of atoms and molecules has been devised within the context of effective quantum numbers. The definition of an effective quantum number has been extended into the domain of valence- and inner-shells. We believe that differences of n* are the quantities which gauge the behavior of both atomic and molecular Rydberg states.

For atoms, differences of n* were used to define an "average atom" and to measure deviations from hydrogen-like behavior. They also served as a criterion in studying isoelectronic sequences and fine structures. For molecules, chemical shifts and substituent effects were expressed as differences of n* between the corresponding atomic and molecular valence- or inner-shells. The degree of bonding and the molecular geometry have been taken into consideration in correlating molecular Rydberg states among themselves.

A qualitative study of potentials for atoms and molecules enabled us to determine the repulsive or the attractive nature of the potentials and their relative range of effectiveness.

Some molecular data were presented in order to exemplify our correlative attitude. The detailed analysis of the water molecule provided an example of strategy and the problems of assigning molecular Rydberg states.

Further empirical studies of n* in the region of anti-bonding valence orbitals and in the field of inner-shell excitations should reveal regularities which should be very helpful in understanding the Rydberg states of molecules.

A theoretical attempt to generate characteristic n* differences for atoms is important to the elucidation of the physical meaning of the observed regularities. For substituent effects and chemical shifts of molecules, an investigation of model potentials should suffice to unveil the constancy of shifts in n*. The same type of model potentials should also be capable of describing regularities of molecular Rydberg states.

The regularities described in this work may have fundamental significance for a general understanding of the electronic structures of atoms and molecules. In any event, these n* differences are exceedingly helpful in making empirical spectroscopic assignments.

VITA

Hung-tai Wang was born on April 15, 1946 in Szechuan, China. In 1949, he and his family moved to Taiwan, Republic of China. He graduated from Provincial Kaohsiung High School in 1964. He received the degree of Bachelor of Science in Chemistry from Tunghai University, Taichung, Taiwan, in 1969. In September 1970, he came to the United States for post-graduate studies at Louisiana State University, Baton Rouge, Louisiana where he is presently a candidate for the degree of Doctor of Philosophy in the Department of Chemistry.

On June 5, 1971, he married the former Ching-ping Shih of Taipei, Taiwan.

EXAMINATION AND THESIS REPORT

Candidate: Hung-tai Wang

Major Field: Chemistry

Title of Thesis: Atomic and Molecular Rydberg States: A Correlative Approach.

Approved:

Sean P. McGlynn
Major Professor and Chairman

James G. Traynham
Dean of the Graduate School

EXAMINING COMMITTEE:

Sean P. McGlynn

Joseph Callaway

Neil R. Kestner

K. N. Houk

Robert M. Schwartz

Date of Examination:

July 9, 1976